Ultrafast Chemical Dynamics of Hydrogen Bonding Environments: From Alcohols to Crowded Proteins

by

John T. King

A dissertation submitted in partial fulfillment
of the requirements for the degree of
Doctor of Philosophy
(Chemistry)
in The University of Michigan
2013

Doctoral Committee:

Professor Kevin J. Kubarych, Chair
Professor Zhan Chen
Professor Eitan Geva
Professor Roberto D. Merlin
Professor Roseanne J. Sension

To my Father

Acknowledgements

I must start by thanking my advisor and friend Kevin Kubarych. His mentorship has trained me as a scientist, and his enthusiasm and passion for science is something I hope to carry with me.

I am also indebted to previous Kubarych lab members, namely Jessica Anna and Carlos Baiz, for training me and helping me become a productive member of the lab.

I thank my committee members, Professor Kevin Kubarych, Professor Roseanne Sension, Professor Eitan Geva, Professor Zhan Chen and Professor Roberto Merlin, for sitting on my committee and for providing insight into the research presented in this thesis.

Finally, I want to thank my family for their unconditional support and encouragement.

Table of Contents

List of Figures

List of Abbreviations

1D: one dimensional

2D: two dimensional

2DIR: two-dimensional infrared spectroscopy

CCD: charged coupled devise

CLS: center line slope

cm^{-1}: wavenumber

CO: carbonyl, $C \equiv O$

CORM: carbonyl monoxide releasing molecule

PI-CORM: photo-induced CORM

cP: centipoise

DFT: density functional theory

DMDC: dimanganese decacarbonyl, $Mn_2(CO)_{10}$

DRDC: dirhenium decacarbonyl, $Re_2(CO)_{10}$

EPR: electron paramagnetic resonance

ffcf: force-force correlation function

FFCF: frequency-frequency correlation function

FTIR: Fourier transform infrared (spectroscopy)

HEWL: hen egg white lysozyme

HEWL-RC: vibrationally labeled HEWL

HuLys: human lysozyme

HuLys-RC: vibrationally labeled HuLys

IR: infrared

IVR: intramolecular vibrational redistribution

LO: local oscillator

MD: molecular dynamics

NMR: nuclear magnetic resonance

PEG400: polyethylene glycol 400

P_n: participation ratio

t-2DIR: transient 2DIR

T_g: glass transition temperature

TFE: 2,2,2-trifluoroethanol

VER: vibrational energy relaxation

Abstract

Ultrafast two-dimensional infrared (2DIR) spectroscopy is used to study and characterize the hydrogen bonding dynamics of several systems including: linear alcohols, fragile glasses near the glass transition temperature, and hydration environments around small hydrophobes and proteins.

The hydrogen bonding dynamics of linear alcohols (methanol to 1-hexanol) are characterized using 2DIR spectroscopy. The spectral diffusion, a common 2DIR observable, of a metal carbonyl vibrational probe is measured for the series of alcohols and demonstrates a monotonic slowing of the hydrogen bond dynamics as the chain length of the alcohol increases. In addition, the influence of hydrogen bonding between the probe molecule and the solvent on intramolecular vibrational redistribution (IVR) is measured by monitoring the cross peak amplitude between two vibrational modes of the vibrational probe. The experimentally measured IVR time constants, coupled with molecular dynamics simulations, allowed a slower IVR time to be related to an increased number of hydrogen bonds, demonstrating solvent-hindered IVR.

Hydrogen bonding dynamics of a fragile glass former are studied as the system is cooled to a glass transition temperature. The spectral diffusion of dirhenium decacarbonyl (DRDC, $Re_2(CO)_{10}$) in 1,2-hexanediol is measured as the system is

cooled within a few degrees of T_g. Near the glass transition temperature the frequency-frequency correlation function shows non-exponential relaxation, illustrating the presence of ultrafast dynamic heterogeneity of fragile glasses near the glass transition. Additionally, a non-Arrhenius temperature dependence of the spectral diffusion is observed, suggesting that α-like relaxation (slow, cooperative motions found in fragile glasses near the glass transition temperature) are manifested on the ultrafast timescale.

The dynamics of water, in particular water near hydrophobic molecules and surfaces, is extensively studied using 2DIR. The dynamics associated with hydrophobic hydration are studied for small hydrophobic molecules as well as extended protein surfaces. In addition, the coupling between the protein dynamics and the hydration dynamics are observed using co-solvent additives. It is found that there is a measurable slowdown (factor of 2) of water around isolated protein surfaces that originates from an excluded volume effect, where limiting the number of possible hydrogen bond acceptors constrains the hydrogen bond rearrangements near hydrophobic surfaces. The collective nature of hydrogen bond rearrangements results in this perturbation extended several angstroms from the protein. This is measured through a crowding experiment, where a "dynamic transition" is observed when the extended hydration environments of neighboring proteins overlap.

Chapter 1

Introduction

1.1 Condensed Phase Dynamics

In the condensed phase, spontaneous fluctuations are of central importance to nearly all physical processes, from Brownian motion[1-7] to protein folding.[8-13] In liquids, the thermal energy available is on the same order as the intermolecular interactions strengths, such as van der Waals forces and hydrogen bonds, and thus these interactions are constantly broken and reformed. Hydrogen bonds are of particular importance to biological systems,[14-21] where these interactions not only help fold and stabilize proteins[15-18] and DNA,[14,19-21] but also are ubiquitous to the water surrounding the biomolecules.[14,22-24] A long standing goal of physical chemistry is to characterize these rapid fluctuations and to elucidate what role they play in molecular processes.

Ultrafast spectroscopy has proven to be extremely successful in characterizing the spontaneous fluctuations occurring in liquid systems.[25-32] In particular, multi-dimensional spectroscopy, which is capable of spreading out congested spectra onto multiple frequency axes, has been widely used to characterize the dynamics of liquids. Two-dimensional infrared (2DIR) spectroscopy has been successful in resolving the dynamics of hydrogen bond interactions, providing information on the lifetime of hydrogen bonds in liquid water[22-24,33-39] and the mechanism for hydrogen bond reorientation in water[23,24,36,40] and alcohols.[31,41] This

fundamental work has provided the platform for studying hydrogen bonding in complex systems, such as proteins,[8,42-47] DNA[48-50] and perhaps eventually cells.

This thesis focuses on the study of hydrogen bonding dynamics in several systems, beginning with simple alcohol environments and fragile glasses. We then extend this work into biologically relevant systems, including the dynamics of bulk water to the hydration dynamics of proteins in crowded, cell-like environments.

1.2 Two-Dimensional Infrared Spectroscopy

1.2.1 Experimental Implementation

Molecular vibrations provide an avenue for obtaining time-resolved information that can be combined with structural information afforded by the mapping of vibrational frequency to molecular structure. To further enhance the frequency resolution of traditional

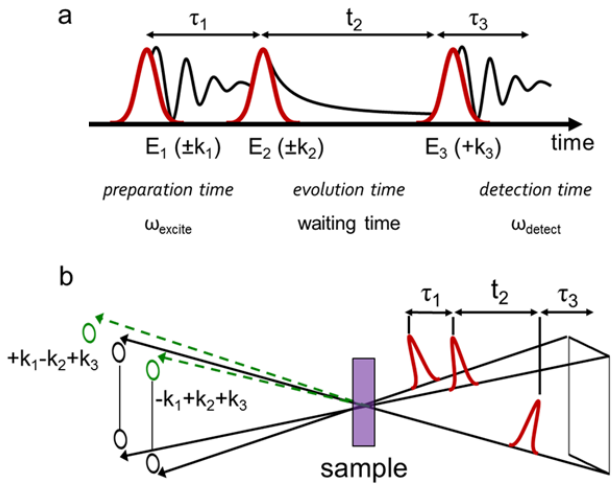

Figure 1.1 (a) Pulse sequence used in 2DIR consisting of three pulses with controlled time delays. The coherence period between E_1 and E_2 is Fourier transformed to provide the excitation axis, and an effective Fourier transform over the detection period is performed by a spectrometer. (b) Experimental set-up for 2DIR spectroscopy in the background free geometry, which allows the rephasing and nonrephasing signals to be emitted in a background free direction.

infrared spectroscopy, multidimensional spectroscopy spreads frequency information over two axes, making the coupling between vibrational modes and line shape information observable that are otherwise hidden in congested linear spectra.[28,51-53] 2DIR measures the third-order nonlinear response of a system using a series of three light-matter interactions.[54]

A series of three ultra-short IR pulses (<100 fs duration, 150 cm^{-1} bandwidth, centered at 2000 cm^{-1}) arrive at a sample in a background free geometry, where the signal is emitted in a unique direction (**Figure 1.1**). The initial excitation pulse pair, with a controllable time delay between the two pulses, excites the sample into a coherence period (pulse 1) followed by a population (pulse 2). A waiting time, t_2, is then set between the excitation of this population and the detection of the system using the final pulse. The dynamics of the system are typically analyzed as a function of t_2 by collecting a series of 2DIR spectra as the waiting time is systematically delayed.[28,53]

Implementing Fourier transform 2DIR, the detection axis is found by direct dispersion of the emitted third order signal onto an array detector, the excitation axis is achieved by collecting the detected spectrum for a series of time delays between the initial excitation pulse pair. Fourier transforming over this time delay, and therefore the coherence period between the first and second pulse, provides the excitation axis. The third order signal is emitted in a background free direction, and the vibrational echo signal is heterodyne detected by interfering the signal with a fully characterized local oscillator pulse that is not passed through the sample.[53]

In a 2D spectrum, the dynamics of single vibrational modes are studied using the time-dependent amplitudes and shapes of the diagonal peaks in the spectrum. Off-diagonal peaks provide information on the coupling of two or more modes, including possible coherent and incoherent energy transfer between modes.

1.2.2 Vibrational Lifetimes

The vibrational relaxation of a system is measured from the peak-amplitude of the diagonal peaks in the 2D spectrum. Though vibrational lifetime in condensed phase systems is a common observable that provides useful chemical information, it proves to be difficult to describe and predict by theory, despite decades of work.[26,55-57] Most of this difficulty comes from the complicated role that the solvent and other intermolecular interactions can play in modulating the relaxation events. A general framework for the relaxation between

two vibrational modes is provided by the Landau-Teller theory, which also serves as the basis for describing intramolecular vibrational redistribution processes (see section **1.3.3**).

The relaxation between two vibrational modes $|a\rangle$ and $|b\rangle$ can be described by second-order perturbation theory in the form of Landau-Teller theory,[26,55-57] where we start with the overall Hamiltonian

$$\hat{H} = \hat{H}_S + \hat{H}_B + \hat{H}_{SB} \qquad (1.1)$$

where $\hat{H}_{SB} = V(\hat{Q}, \hat{q})$ is the coupling between the bath and the relaxing mode. The potential can be expanded to first order around q= 0, assuming weak system-bath coupling where the displacement of the vibrational mode causes minimal perturbation to the environment.

$$\hat{V}(q, Q) = V|_{q=0}(Q) + \frac{\eth V}{\eth q}|_{q=0}\, q \qquad (1.2)$$

$$\hat{V}(q, Q) = V_B(Q) + \hat{F}(Q) \otimes q \qquad (1.3)$$

where $F_j(Q)$ is the time-dependent force exerted on the relaxing normal mode Q_j by the bath. Using a Fermi's Golden Rule formulism, the relaxation rate between two modes can be written in terms of the Fourier transform of a force-force correlation function.

$$k_{ab} = \frac{1-e^{-\beta\omega}}{2\hbar\omega} \int_{-\infty}^{\infty} d\tau e^{i\omega\tau} \langle F_j(t) F_j(0) \rangle \qquad (1.4)$$

From this equation it is seen that the vibrational energy relaxes exponentially to an equilibrium value. The bath acts to apply a fluctuating force on the relaxing mode that drives the vibrational relaxation. Additionally, anharmonic coupling between the solvent and the relaxing mode can act to increase the coupling between the solute's internal modes, and thus alter the relaxation and intramolecular vibrational redistribution.[26,58-60]

Though the presence of specific intermolecular interactions between the relaxing mode and the solvent can make predicting vibrational lifetimes difficult, it can also be leveraged to learn about such intermolecular interactions if studies are carried out in a systematic way.

1.2.3 Intramolecular Vibrational Energy Redistribution

The off-diagonal peaks of a 2D spectrum provide information on the coupling between vibrational modes, including the inherent anharmonic coupling between vibrational modes as well as coherent and incoherent energy transfer.[60-62] Upon vibrational excitation, energy deposited into a single vibrational mode will rapidly exchange with neighboring modes, provided there is sufficient coupling and energy overlap, through a process called intramolecular vibrational redistribution (IVR). The kinetics of IVR are observed through the time-dependent growth in cross-peak amplitude between two modes.

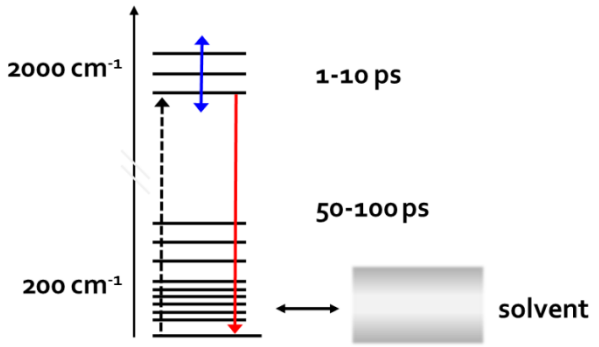

Figure 1.2 Energy level diagram showing initial excitation (dashed line) followed by intramolecular vibrational redistribution to nearby modes (blue line) followed by the slower vibrational relaxation into the lower frequency modes (red line) and eventually into the solvent.

In the condensed phase, the IVR process tends to compete with the vibrational relaxation of the system, though in most systems the IVR process occurs significantly faster than relaxation out of the excited state manifold (**Figure 1.2**).[26] In metal carbonyl probes in organic solvents, for instance, the IVR process typically occurs on a sub-10 ps timescale, whereas vibrational relaxation occurs on a longer 50-100 ps timescale.[60] Though the timescales are significantly different, IVR and vibrational relaxation are described by the same physics (see section **1.3.2** for the presentation of Landau-Teller Theory). Much like vibrational relaxation, it is very difficult to predict IVR times due to the complicated role that the solvent dynamics can play in modulating the timescale of these processes.

1.2.4 Spectral Diffusion

One of the most powerful pieces of information obtained from 2DIR spectroscopy is the frequency-frequency correlation function (FFCF), the decay of which results from spectral diffusion.[22,28,31,32,63-70] The FFCF provides information regarding the low-frequency motions of the solvent, in particular the timescale on which molecular fluctuations surrounding a probe vibration are occurring. We obtain the correlation function by monitoring the correlation between the initially excited ensemble of molecules and the final detected ensemble. Thus, the decay of the FFCF describes the amount of time it takes for an initially excited ensemble to lose frequency memory, and thus correlation with the detected

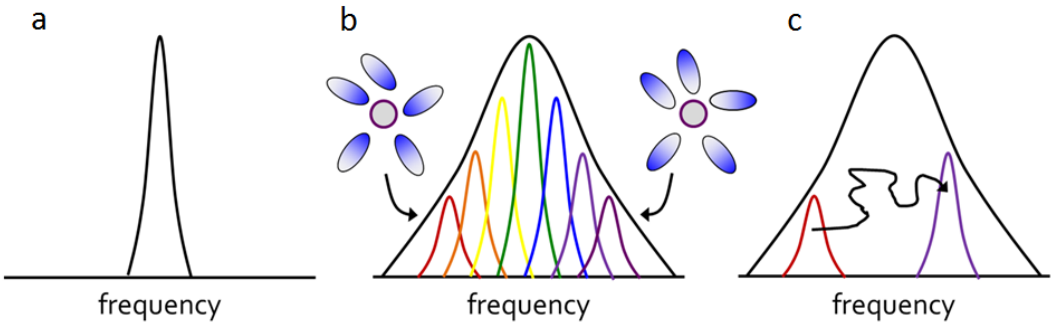

Figure 1.3 (a) Homogeneously broadened lineshape where an ensemble of molecules have the same transition frequency, but dephasing occurs through collisions with the solvent. (b) Inhomogeneously broadened lineshape, where distinct configurations of the solvent shift the transition frequency of each member of the ensemble. (c) Example trajectory of a single member of the ensemble that "spectrally diffuses" as the solvent fluctuates and exchanges configurations.

ensemble. This timescale is directly related to the fluctuations occurring in the solvent. The fluctuations that can be captured in the FFCF can range from hydrogen bond switching events in alcohols[31] or water[22,24,36,65,68,69] to global conformational dynamics of proteins.[8,47,70]

The measurement relies on a vibrational mode being sensitive to the structure of the solvation environment. In the linear spectrum this is observed as a broadening of the vibrational transition, commonly referred to as inhomogeneous broadening (whereas the broadening of transition in the absence of distinct microenvironments is referred to as homogeneous broadening).[71] The inhomogeneous broadening of a vibrational transition arises from polar solvents being able to present multiple solvation configurations that distinctly shift the transition frequency of the vibrational mode (**Figure 1.3**). Thus, the

linear spectrum provides a static snapshot of the solvation environments experienced by an ensemble to vibrational probes. However, because the solvent is constantly fluctuating, these configurations are not static but instead fluctuate. If you were able to select only one molecule from the ensemble and follow its trajectory, the transition frequency would

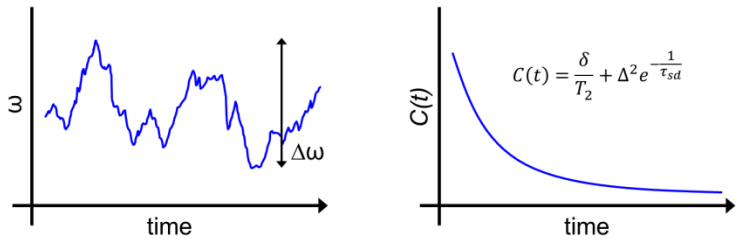

Figure 1.4 (left) Example of a frequency trajectory where the transition frequency is modulated by the motion of the solvent. Fast fluctuations (giving rise to homogeneous broadening) are seen on top of slower structural fluctuations (giving rise to inhomogenous broadening). (right) The value of *C(t=0)* provides information regarding the homogeneous dephasing which occurs "instantly", while the longer decay is indicative of the slower structural fluctuations.

randomly diffuse through frequency space as the solvent configurations exchanged, hence the term "spectral diffusion" (**Figure 1.4**). The FFCF is given by:[28,31]

$$C(t) = \langle \delta\omega_{01}(t) \cdot \delta\omega_{01}(0) \rangle \qquad (1.5)$$

Where $\delta\omega_{01}$ is the deviation of the 0 to 1 transition frequency. To measure the spectral diffusion, both the rephasing and nonrephasing 2DIR spectra are required.[53,63,72] As previously described, the coherence period between the initial pulse and the second pulse vibrational labels an ensemble of probes. The initially excited coherence dephases due to: 1) rapid solvent fluctuations, such as inertial fluctuations (termed homogeneous dephasing), and 2) the distribution of transition frequencies that leads to dephasing because the ensemble of transitions are oscillating at slightly different frequencies (termed inhomogeneous dephasing). While the homogeneous dephasing is irreversible, the inhomogeneous dephasing is reversible, provided the ensemble of transition frequencies do not change and the frequency information is not lost. This information is stored in a population during the waiting time, at which point the solvent fluctuates and reorganizes itself, thus randomizing the solvent configuration of each probe in the ensemble. The final

pulse then puts the system either into the conjugate coherence (rephasing), or the same coherence (non-rephasing), as the initial excitation period.[54]

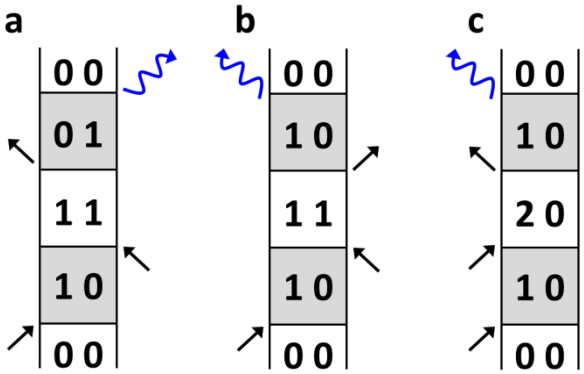

Figure 1.5 Example double-sided Feynman diagrams for rephasing (a), nonrephasing (b) and double-quantum (c) pathways.

In the rephasing spectrum, the two coherence periods are conjugates, thus the final coherence period evolves in a time-reversed manner and the dephasing that occurred due to a distribution of transition frequencies is undone, and a vibrational echo is emitted (**Figure 1.5**).[28,64] The FFCF then measures the ability to "rephase" an ensemble of oscillators as a function of waiting time, and the decay of the FFCF correlates to solvent reorganization dynamics that limit the rephasing ability. In the non-rephasing spectrum the initial and final coherence periods are identical, thus, the final pulse is only followed by further dephasing and no echo is generated. This spectrum essentially acts as a reference spectrum, allowing the evolution of the vibrational echo to be studied independently from other incoherent dynamics, such as vibrational relaxation and IVR.[31,64]

There are several ways to extract the FFCF from 2DIR data, all of which require both the rephasing and nonrephasing spectrum.[63,64,66] Ideally, the rephasing and nonrephasing spectra can be added in a manner well described in literature and the purely absorptive spectrum can be obtained.[53,72] In this spectrum, the uneven amplitude of the rephasing and nonrephasing spectra, which differ only by the vibrational echo amplitude in the rephasing spectrum, lead to a lineshape that is elongated along the diagonal at early times before spectral diffusion occurs.[28,53,64,66,72] This lineshape corresponds to a strong correlation between excitation and detection frequencies. As the waiting time is increased, the peak

becomes more symmetric and the initial correlation is lost. The center line slope method (CLS) can be used to monitor this evolution by fitting a straight line across the peak corresponding to maximum peak value, using the value of the slope to be the value of the FFCF at the given waiting time.[64,66]

The correlation function can also be extracting from the rephasing and nonrephasing spectra directly, without having the phase the purely absorptive spectrum (which requires an additional experiment to measure the pump-probe spectrum, then phasing of the absorptive spectrum is done by the projection slice theorem).[31,63] The inhomogeneity index has been shown to be equivalent to the CLS method in most cases, and easier to implement.[63] In this case the correlation function is obtained by:

$$C(t) \propto I(t) = \frac{A_{rephasing} - A_{nonrephasing}}{A_{rephasing} + A_{nonrephasing}} \qquad (1.6)$$

where A is the amplitude of the peak (typically peak volume) of the respective spectrum. This is also a preferable method when studying systems with limited signal strength, since it is not always possible/easy to obtain a pump-probe spectrum to use for the phasing. This method is widely used throughout the work presented in this thesis.

1.3 Thesis Outline

The remainder of this thesis focuses on using 2DIR spectroscopy to study hydrogen bonding dynamics in many systems, including alcohols, glasses and water in a biological setting. **Chapter 2** describes our initial work using metal carbonyl vibrational probes to study the hydrogen bonding dynamics in alcohols. We study the spectral diffusion of a metal carbonyl probe in a series of linear alcohols, finding an intuitive monotonic increase in the spectral diffusion timescale as the alkyl chain length is increased. We also observe the influence of intermolecular interactions (i.e. hydrogen bonds between the vibrational probe and the solvent) on the vibrational lifetime and IVR, generally considered intramolecular processes. While the vibrational lifetimes are found to be fairly insensitive to the solvent, the IVR timescale varies across the solvent series and is shown to be directly correlated to the degree of intermolecular hydrogen bonding.

Chapter 3 describes an ultrafast two-dimensional infrared (2DIR) spectroscopy study of the picosecond dynamics of a vibrational probe molecule dissolved in a fragile glass former. The spectral dynamics are observed as the system is cooled to within a few degrees of the glass transition temperature (T_g). We observe non-exponential relaxation of the frequency-frequency correlation function, similar to what has been reported for other dynamical correlation functions. In addition, we see evidence for α-like relaxation, typically associated with long-time, cooperative molecular motion, on the ultrafast timescale. The data suggests that the spectral dynamics are sensitive to cooperative motion occurring on timescales that are necessarily longer than the observation time.

Chapter 4 discusses our initial work at characterizing the dynamics of bulk H_2O and D_2O using various observables. Water is capable of assisting exceptionally rapid vibrational relaxation within dissolved solute species. Although ultrafast dynamics of metal carbonyl complexes have long served as models for vibrational relaxation, all reports to-date have investigated non-aqueous solutions due to the insolubility of the vast majority of metal carbonyl complexes in water. Using the water-soluble complex $[RuCl_2(CO)_3]_2$, which belongs to a class known as "carbon monoxide (CO) releasing molecules" (CORM), we report the first ultrafast vibrational relaxation measurements of a metal carbonyl complex in water, and compare this relaxation with the relaxation in polar organic solvents, namely methanol. The vibrational relaxation, measured by 2DIR spectroscopy, is an order of magnitude faster in H_2O (3.12±0.29 ps) than in methanol (42.25±3 ps). The accelerated relaxation times of the coupled CO units in H_2O and D_2O are interpreted as resulting from the enhancement of intramolecular relaxation pathways through additional coupling induced by the solvent. In addition, the vibrational lifetime shows a significant isotope dependence: in D_2O the relaxation time is 4.27±0.27 ps, a difference of roughly 30%. We interpret these measurements in terms of a non-resonant channel primarily arising from water's reorientational dynamics, which occur primarily through large angular jumps, as well as a resonant transfer of vibrational energy from the carbonyl bands to the libration-bend combination band. These measurements indicate that metal carbonyls, which are among the

strongest IR transitions, are exquisitely sensitive to the presence of water and hold promise as IR analogs of EPR spin labels.

Chapter 5 extends our studies of water into hydrophobic hydration, in particular the hydration dynamics of hydrophobes of different length scales. We begin by studying small hydrophobic molecules (which also serve as our vibrational probes) and demonstrate that the bulk-like dynamics of H_2O are measured in the solvation shell of small hydrophobes. The result is twofold, first demonstrating once again that the bulk-like dynamics of a liquid can be measured through the use of a vibrational probe, and second showing that the hydrogen bond switching events are unperturbed by small hydrophobic molecules. We then turn our attention to proteins, were a surface labeling protocol allows us to directly study the hydration environment of proteins. Using hen egg white lysozyme we are able to measure a factor of 1.8 retardation factor of the hydrogen bond dynamics near the hydrophobic protein, which is in quantitative agreement with independently performed MD simulations on lysozyme that predicted a retardation factor of 2. The slowdown in hydrogen bond switching events is consistent with measurements made on the isotope-dependent relaxation of the surface-probe, which showed bulk-like relaxation in particular regions of the protein and constrained relaxation in others. The origin of the slowdown is attributed to an excluded volume effect, where hydrogen bond switching events are hindered by presence of the non-hydrogen bonding protein surface, which acts to limit the number of hydrogen bonding partners available for a switching event.

Additionally, this chapter describes the role that constrained water can play in driving surface processes. By leveraging a simple surface process, dehydration of the protein surface and solvent exchange with 2,2,2-trifluoroethanol, we demonstrate that regions of constrained water readily dehydrate and exchange with the amphiphilic co-solvent, while regions of bulk-like water remain hydrated and show no signs of preferential solvent exchange. The results suggest that constrained water can play a critical thermodynamic role in driving surface processes, which can be more complex than solvent exchange, such as protein-protein recognition.

Chapter 6 describes experiments aimed at characterizing the coupling of protein dynamics to hydration dynamics and extent of the dynamical influence of a protein on the surrounding waters, as well as influence of crowding on the water and protein dynamics. Due to the location of the vibrational probe, the FFCF contains both the hydration water dynamics as well as the protein dynamics, which can be observed simultaneously without interference because of the large timescale difference between the two sets of dynamics. Using a small kosmotropic co-solvent, glycerol, we are able to slow the fluctuations of the bulk solvent while leaving the protein hydrated. We observe that the hydration dynamics are weakly coupled to the bulk solvent, while the protein dynamics and hydration dynamics are strongly coupled. Furthermore, using larger crowding agent we find that crowding induces a dynamical transition at a critical crowding value, where the protein and hydration dynamics undergo an abrupt slowdown. Similar behavior is seen in self-crowding, and the speculative explanation is the overlap between the extended hydration environments of neighboring macromolecules results in the transition. The distance of the extended hydration shells are estimated from the data to be upwards of 20 Å, which is on the order of the protein size itself.

The final chapter of this thesis describes the general conclusions provided by the work and details possible future directions.

References:

(1) Einstein, A.: The motion of elements suspended in static liquids as claimed in the molecular kinetic theory of heat. *Annalen Der Physik* **1905**, *17*, 549-560.

(2) Einstein, A.: The theory of the Brownian Motion. *Annalen Der Physik* **1906**, *19*, 371-381.

(3) Kramers, H. A.: Brownian motion in a field of force and the diffusion model of chemical reactions. *Physica* **1940**, *7*, 284-304.

(4) Metzler, R.; Klafter, J.: The random walk's guide to anomalous diffusion: a fractional dynamics approach. *Physics Reports-Review Section of Physics Letters* **2000**, *339*, 1-77.

(5) Mori, H.: Transport Collective Motion and Brownian Motion. *Progress of Theoretical Physics* **1965**, *33*, 423-&.

(6) Reimann, P.: Brownian motors: noisy transport far from equilibrium. *Physics Reports-Review Section of Physics Letters* **2002**, *361*, 57-265.

(7) Wang, B.; Kuo, J.; Bae, S. C.; Granick, S.: When Brownian diffusion is not Gaussian. *Nature Materials* **2012**, *11*, 481-485.

(8) Chung, H. S.; Khalil, M.; Smith, A. W.; Ganim, Z.; Tokmakoff, A.: Conformational changes during the nanosecond-to-millisecond unfolding of ubiquitin. *Proceedings of the National Academy of Sciences of the United States of America* **2005**, *102*, 612-617.

(9) Frauenfelder, H.; Fenimore, P. W.; Chen, G.; McMahon, B. H.: Protein folding is slaved to solvent motions. *Proceedings of the National Academy of Sciences of the United States of America* **2006**, *103*, 15469-15472.

(10) Nettels, D.; Gopich, I. V.; Hoffmann, A.; Schuler, B.: Ultrafast dynamics of protein collapse from single-molecule photon statistics. *Proceedings of the National Academy of Sciences of the United States of America* **2007**, *104*, 2655-2660.

(11) Giraud, G.; Karolin, J.; Wynne, K.: Low-frequency modes of peptides and globular proteins in solution observed by ultrafast OHD-RIKES Spectroscopy. *Biophysical Journal* **2003**, *85*, 1903-1913.

(12) Maisuradze, G. G.; Liwo, A.; Scheraga, H. A.: Principal Component Analysis for Protein Folding Dynamics. *Journal of Molecular Biology* **2009**, *385*, 312-329.

(13) Nettels, D.; Hoffmann, A.; Schuler, B.: Unfolded protein and peptide dynamics investigated with single-molecule FRET and correlation spectroscopy from picoseconds to seconds. *Journal of Physical Chemistry B* **2008**, *112*, 6137-6146.

(14) Ball, P.: Water as an active constituent in cell biology. *Chemical Reviews* **2008**, *108*, 74-108.

(15) Baker, E. N.; Hubbard, R. E.: Hydrogen-Bonding in Globular-Proteins. *Progress in Biophysics & Molecular Biology* **1984**, *44*, 97-179.

(16) Kabsch, W.; Sander, C.: Dictionary of Protein Secondary Structure - Pattern Recognition of Hydrogen-Bonded and Geometrical Features. *Biopolymers* **1983**, *22*, 2577-2637.

(17) McDonald, I. K.; Thornton, J. M.: Satisfying Hydrogen-Bonding Potential in Proteins. *Journal of Molecular Biology* **1994**, *238*, 777-793.

(18) Barlow, D. J.; Thornton, J. M.: Helix Geometry in Proteins. *Journal of Molecular Biology* **1988**, *201*, 601-619.

(19) Wang, A. H. J.; Quigley, G. J.; Kolpak, F. J.; Crawford, J. L.; Vanboom, J. H.; Vandermarel, G.; Rich, A.: Molecular-Structure of a Left-Handed Double Helical DNA Fragment at Atomic Resolution. *Nature* **1979**, *282*, 680-686.

(20) Watson, J. D.; Crick, F. H. C.: Molecular Structure of Nucleic Acids - A Structure fro Deoxyribose Nucleic Acid. *Nature* **1953**, *171*, 737-738.

(21) Watson, J. D.; Crick, F. H. C.: The Structure of DNA. *Cold Spring Harbor Symposia on Quantitative Biology* **1953**, *18*, 123-131.

(22) Cowan, M. L.; Bruner, B. D.; Huse, N.; Dwyer, J. R.; Chugh, B.; Nibbering, E. T. J.; Elsaesser, T.; Miller, R. J. D.: Ultrafast memory loss and energy redistribution in the hydrogen bond network of liquid H_2O. *Nature* **2005**, *434*, 199-202.

(23) Fecko, C. J.; Eaves, J. D.; Loparo, J. J.; Tokmakoff, A.; Geissler, P. L.: Ultrafast hydrogen-bond dynamics in the infrared spectroscopy of water. *Science* **2003**, *301*, 1698-1702.

(24) Fecko, C. J.; Loparo, J. J.; Roberts, S. T.; Tokmakoff, A.: Local hydrogen bonding dynamics and collective reorganization in water: Ultrafast infrared spectroscopy of HOD/D2O. *Journal of Chemical Physics* **2005**, *122*.

(25) Fayer, M. D.: Dynamics of Molecules in Condensed Phases - Picosecond Holographic Grating Experiments. *Annual Review of Physical Chemistry* **1982**, *33*, 63-87.

(26) Owrutsky, J. C.; Raftery, D.; Hochstrasser, R. M.: Vibrational-Relaxation Dynamics in Solutions. *Annual Review of Physical Chemistry* **1994**, *45*, 519-555.

(27) Hamm, P.; Lim, M.; Hochstrasser, R. M.: Non-Markovian dynamics of the vibrations of ions in water from femtosecond infrared three-pulse photon echoes. *Physical Review Letters* **1998**, *81*, 5326-5329.

(28) Khalil, M.; Demirdoven, N.; Tokmakoff, A.: Coherent 2D IR spectroscopy: Molecular structure and dynamics in solution. *Journal of Physical Chemistry A* **2003**, *107*, 5258-5279.

(29) Nibbering, E. T. J.; Elsaesser, T.: Ultrafast vibrational dynamics of hydrogen bonds in the condensed phase. *Chemical Reviews* **2004**, *104*, 1887-1914.

(30) Torre, R.; Bartolini, P.; Righini, R.: Structural relaxation in supercooled water by time-resolved spectroscopy. *Nature* **2004**, *428*, 296-299.

(31) King, J. T.; Baiz, C. R.; Kubarych, K. J.: Solvent-Dependent Spectral Diffusion in a Hydrogen Bonded "Vibrational Aggregate". *Journal of Physical Chemistry A* **2010**, *114*, 10590-10604.

(32) King, J. T.; Ross, M. R.; Kubarych, K. J.: Ultrafast alpha-Like Relaxation of a Fragile Glass-Forming Liquid Measured Using Two-Dimensional Infrared Spectroscopy. *Physical Review Letters* **2012**, *108*, 7401-7401.

(33) Asbury, J. B.; Steinel, T.; Stromberg, C.; Gaffney, K. J.; Piletic, I. R.; Goun, A.; Fayer, M. D.: Hydrogen bond dynamics probed with ultrafast infrared heterodyne-detected multidimensional vibrational stimulated echoes. *Physical Review Letters* **2003**, *91*.

(34) Asbury, J. B.; Steinel, T.; Kwak, K.; Corcelli, S. A.; Lawrence, C. P.; Skinner, J. L.; Fayer, M. D.: Dynamics of water probed with vibrational echo correlation spectroscopy. *Journal of Chemical Physics* **2004**, *121*, 12431-12446.

(35) Asbury, J. B.; Steinel, T.; Fayer, M. D.: Hydrogen bond networks: Structure and evolution after hydrogen bond breaking. *Journal of Physical Chemistry B* **2004**, *108*, 6544-6554.

(36) Eaves, J. D.; Loparo, J. J.; Fecko, C. J.; Roberts, S. T.; Tokmakoff, A.; Geissler, P. L.: Hydrogen bonds in liquid water are broken only fleetingly. *Proceedings of the National Academy of Sciences of the United States of America* **2005**, *102*, 13019-13022.

(37) Tokmakoff, A.: Shining light on the rapidly evolving structure of water. *Science* **2007**, *317*, 54-55.

(38) Elsaesser, T.: Two-Dimensional Infrared Spectroscopy of Intermolecular Hydrogen Bonds in the Condensed Phase. *Accounts of Chemical Research* **2009**, *42*, 1220-1228.

(39) Jansen, T. L. C.; Auer, B. M.; Yang, M.; Skinner, J. L.: Two-dimensional infrared spectroscopy and ultrafast anisotropy decay of water. *Journal of Chemical Physics* **2010**, *132*.

(40) Laage, D.; Hynes, J. T.: A molecular jump mechanism of water reorientation. *Science* **2006**, *311*, 832-835.

(41) Vartia, A. A.; Mitchell-Koch, K. R.; Stirnemann, G.; Laage, D.; Thompson, W. H.: On the Reorientation and Hydrogen-Bond Dynamics of Alcohols. *Journal of Physical Chemistry B* **2011**, *115*, 12173-12178.

(42) Backus, E. H. G.; Bloem, R.; Donaldson, P. M.; Ihalainen, J. A.; Pfister, R.; Paoli, B.; Caflisch, A.; Hamm, P.: 2D-IR Study of a Photoswitchable Isotope-Labeled alpha-Helix. *Journal of Physical Chemistry B* **2010**, *114*, 3735-3740.

(43) Ihalainen, J. A.; Paoli, B.; Muff, S.; Backus, E. H. G.; Bredenbeck, J.; Woolley, G. A.; Caflisch, A.; Hamm, P.: alpha-Helix folding in the presence of structural constraints. *Proceedings of the National Academy of Sciences of the United States of America* **2008**, *105*, 9588-9593.

(44) Ganim, Z.; Jones, K. C.; Tokmakoff, A.: Insulin dimer dissociation and unfolding revealed by amide I two-dimensional infrared spectroscopy. *Physical Chemistry Chemical Physics* **2010**, *12*, 3579-3588.

(45) Chung, J. K.; Thielges, M. C.; Fayer, M. D.: Dynamics of the folded and unfolded villin headpiece (HP35) measured with ultrafast 2D IR vibrational echo spectroscopy. *Proceedings of the National Academy of Sciences of the United States of America* **2011**, *108*, 3578-3583.

(46) King, J. T.; Arthur, E. J.; Brooks, C. L. I.; Kubarych, K. J.: Site-specific hydration dynamics of globular proteins and the role of constrained water in solvent exchange with amphiphilic cosolvents. *Journal of Physical Chemistry B* **2012**, *116*, 5604-5611.

(47) King, J. T.; Kubarych, K. J.: Site-Specific Coupling of Hydration Water and Protein Flexibility Studied in Solution with Ultrafast 2D-IR Spectroscopy. *Journal of the American Chemical Society* **2012**, *134*, 18705-12.

(48) Krummel, A. T.; Zanni, M. T.: DNA vibrational coupling revealed with two-dimensional infrared spectroscopy: Insight into why vibrational spectroscopy is sensitive to DNA structure. *Journal of Physical Chemistry B* **2006**, *110*, 13991-14000.

(49) Krummel, A. T.; Zanni, M. T.: Exposing the origins of vibrational coupling in DNA with 2-D infrared spectroscopy. *Abstracts of Papers of the American Chemical Society* **2007**, *233*.

(50) Krummel, A. T.; Zanni, M. T.: Evidence for coupling between nitrile groups using DNA templates: A promising new method for monitoring structures with infrared spectroscopy. *Journal of Physical Chemistry B* **2008**, *112*, 1336-1338.

(51) Jonas, D. M.: Two-dimensional femtosecond spectroscopy. *Annual Review of Physical Chemistry* **2003**, *54*, 425-463.

(52) Baiz, C. R.; McRobbie, P. L.; Anna, J. M.; Geva, E.; Kubarych, K. J.: Two-Dimensional Infrared Spectroscopy of Metal Carbonyls. *Accounts of Chemical Research* **2009**, *42*, 1395-1404.

(53) Anna, J. M.; Nee, M. J.; Baiz, C. R.; McCanne, R.; Kubarych, K. J.: Measuring absorptive two-dimensional infrared spectra using chirped-pulse upconversion detection. *Journal of the Optical Society of America B-Optical Physics* **2010**, *27*, 382-393.

(54) Mukamel, S.: Principles of Nonlinear Optical Spectroscopy. *Oxford University Press* **1995**.

(55) Elsaesser, T.; Kaiser, W.: Vibrational and Vibronic Relaxation of Large Polyatomic-Molecules in Liquids. *Annual Review of Physical Chemistry* **1991**, *42*, 83-107.

(56) Grote, R. F.; Hynes, J. T.: Energy Diffusion-Controlled Reactions in Solution. *Journal of Chemical Physics* **1982**, *77*, 3736-3743.

(57) Egorov, S. A.; Skinner, J. L.: A theory of vibrational energy relaxation in liquids. *Journal of Chemical Physics* **1996**, *105*, 7047-7058.

(58) Berg, M.; VandenBout, D. A.: Ultrafast Raman echo measurements of vibrational dephasing and the nature of solvent-solute interactions. *Accounts of Chemical Research* **1997**, *30*, 65-71.

(59) Bonner, G. M.; Ridley, A. R.; Ibrahim, S. K.; Pickett, C. J.; Hunt, N. T.: Probing the effect of the solution environment on the vibrational dynamics of an enzyme model system with ultrafast 2D-IR spectroscopy. *Faraday Discussions* **2010**, *145*, 429-442.

(60) King, J. T.; Anna, J. M.; Kubarych, K. J.: Solvent-hindered intramolecular vibrational redistribution. *Physical Chemistry Chemical Physics* **2011**, *13*, 5579-5583.

(61) Anna, J. M.; King, J. T.; Kubarych, K. J.: Multiple structures and dynamics of [CpRu(CO)2]2 and [CpFe(CO)2]2 in solution revealed with two-dimensional infrared spectroscopy. *Inorganic chemistry* **2011**, *50*, 9273-83.

(62) Nee, M. J.; Baiz, C. R.; Anna, J. M.; McCanne, R.; Kubarych, K. J.: Multilevel vibrational coherence transfer and wavepacket dynamics probed with multidimensional IR spectroscopy. *Journal of Chemical Physics* **2008**, *129*.

(63) Roberts, S. T.; Loparo, J. J.; Tokmakoff, A.: Characterization of spectral diffusion from two-dimensional line shapes. *Journal of Chemical Physics* **2006**, *125*.

(64) Kwak, K.; Park, S.; Finkelstein, I. J.; Fayer, M. D.: Frequency-frequency correlation functions and apodization in two-dimensional infrared vibrational echo spectroscopy: A new approach. *Journal of Chemical Physics* **2007**, *127*.

(65) Park, S.; Fayer, M. D.: Hydrogen bond dynamics in aqueous NaBr solutions. *Proceedings of the National Academy of Sciences of the United States of America* **2007**, *104*, 16731-16738.

(66) Kwak, K.; Rosenfeld, D. E.; Fayer, M. D.: Taking apart the two-dimensional infrared vibrational echo spectra: More information and elimination of distortions. *Journal of Chemical Physics* **2008**, *128*.

(67) Kim, Y. S.; Liu, L.; Axelsen, P. H.; Hochstrasser, R. M.: 2D IR provides evidence for mobile water molecules in beta-amyloid fibrils. *Proceedings of the National Academy of Sciences of the United States of America* **2009**, *106*, 17751-17756.

(68) Nicodemus, R. A.; Ramasesha, K.; Roberts, S. T.; Tokmakoff, A.: Hydrogen Bond Rearrangements in Water Probed with Temperature-Dependent 2D IR. *Journal of Physical Chemistry Letters* **2010**, *1*, 1068-1072.

(69) Jansen, T. I. C.; Cringus, D.; Pshenichnikov, M. S.: Dissimilar Dynamics of Coupled Water Vibrations. *Journal of Physical Chemistry A* **2009**, *113*, 6260-6265.

(70) Bandaria, J. N.; Dutta, S.; Nydegger, M. W.; Rock, W.; Kohen, A.; Cheatum, C. M.: Characterizing the dynamics of functionally relevant complexes of formate dehydrogenase. *Proceedings of the National Academy of Sciences of the United States of America* **2010**, *107*, 17974-17979.

(71) Piletic, I. R.; Moilanen, D. E.; Levinger, N. E.; Fayer, M. D.: What nonlinear-IR experiments can tell you about water that the IR spectrum cannot. *Journal of the American Chemical Society* **2006**, *128*, 10366-10367.

(72) Khalil, M.; Demirdoven, N.; Tokmakoff, A.: Obtaining absorptive line shapes in two-dimensional infrared vibrational correlation spectra. *Physical Review Letters* **2003**, *90*.

Chapter 2

Hydrogen Bond Dynamics in Linear Alcohols

The work presented in this chapter has been published in the following papers:

J. T. King, J. M. Anna, K. J. Kubarych "*Solvent-Hindered Intramolecular Vibrational Redistribution*" Physical Chemistry Chemical Physics, 13, 2011, 5579-5583. – Reproduced by permission of the PCCP owner Societies

J. T. King, C. R. Baiz, K. J. Kubarych "*Solvent Dependent Spectral Diffusion in a Hydrogen Bonded "Vibrational Aggregate"*", Journal of Physical Chemistry A, 114, 2010, 10590-10604.

2.1 Introduction

We leverage the observables provided by 2DIR (spectral diffusion, vibrational lifetime and IVR) to characterize the solvent dynamics as well as the solvents role in intramolecular processes. We systematically study this processes as in a series of linear alcohols, ranging from methanol to 1-hexanol. First, we find that bulk-like solvent dynamics can be measured through the use of vibrational probes, namely the hydrogen bond lifetime in methanol can be measured through the spectral diffusion of a vibrational probe dissolved in methanol. This provides confidence that the properties of the vibrational probe itself contribute little to

the measured spectral diffusion. This concept will occur several times throughout this thesis, as well as the observation that other observables, such as vibrational lifetime and IVR, are highly dependent on both the vibrational probe used and the solvent.

In addition to measuring the hydrogen bond lifetime in methanol we carry out the same measurement on the series of alcohols, finding an intuitive trend that the hydrogen bonding dynamics slow down as the alkyl-chain length of the alcohol is increased, going from 2.7 ps in methanol to 5.4 ps in 1-hexanol. A "vibrational aggregate" model is proposed using an excitonic Hamiltonian that is capable to capturing the majority of the spectral broadening effects seen in the linear spectrum.

Furthermore, we find that the vibrational lifetime of the vibrational probe is weakly dependent on the solvent, though the IVR process is extremely sensitive to the alcohol used and shows a non-monotonic trend in IVR timescales. Through the use of molecular dynamics (MD) simulations, we are able to reason the IVR timescale trend in terms of intermolecular hydrogen bonds, where the more hydrogen bonds formed between the probe and the solvent the slower the IVR process becomes, demonstrating that intermolecular interactions can strongly effect fast intramolecular dynamics.

2.2 Spectral Diffusion in Linear Alcohols

A solute in a hydrogen bonding solvent experiences rapid, discrete fluctuations in the number of hydrogen bonds it makes with the nearest solvent molecules. When those fluctuations induce appreciable changes in a spectroscopically observed transition frequency, multidimensional methods such as two-dimensional infrared (2DIR) spectroscopy are able to measure the correlation function of the frequency fluctuations.[1-12] A key challenge for visible and infrared spectroscopy is the link between actual molecular dynamics and accessible spectroscopic observables such as frequencies, transition moments and frequency correlation functions. For systems such as the amide I band of peptides and proteins,[13-17] and the OH (or OD) stretch of liquid water, it has become possible to predict 2DIR spectra using classical dynamics simulations.[18-23] Such simulations guide the atomistic interpretation that is otherwise lacking from the frequency correlation function, which necessarily confounds the actual molecular dynamics and how those dynamics modulate the probed transition. The

instances for which frequency mapping methods have been so successful are characterized by being either essentially local modes (e.g. OH/OD and nitrile[24-28]) or by having relatively weak coupling between local modes (e.g. amide I transition dipole coupling). Very recently extensive progress has been made in treating the complex coupled dynamics of pure liquid water using vibrational exciton models as well as electrostatic maps based on *ab initio* quantum chemistry.[23,29] There has been less extensive consideration of single, strongly coupled extended vibrational chromophores, which should also be sensitive to subtle long- and short-range interactions. It is a desirable feature of a dynamical probe to respond not only to local fluctuations, but also to be sensitive to correlated fluctuations as would be expected in a cooperative hydrogen bonded environment.

To assess the value of such a spatially distributed probe, we have undertaken a systematic study of the ultrafast vibrational dynamics of the metal carbonyl complex dimanganese decacarbonyl ($Mn_2(CO)_{10}$, DMDC) in a series of hydrogen bonding alcohol solvents. Due to their amphiphilic nature, alcohols exhibit complex liquid structure characterized by hydroxyl aggregation,[30-33] and given its ~1 nm length and extensive vibrational delocalization, DMDC is an attractive probe of the heterogeneous solvent environment. From Fourier transform IR (FTIR) and waiting-time dependent 2DIR spectra, we extract homogeneous and inhomogeneous spectral widths, as well as time constants for spectral diffusion. We find that with increased alkyl chain length the inhomogeneous width narrows and the time scale for spectral diffusion slows. With the aid of a vibrational exciton model incorporating Gaussian disorder, the data are interpreted in terms of the flexibility of the hydrogen bonded network responsible for the spectral inhomogeneity and its dynamical evolution. Based on the ability of the model to reproduce the solvent-dependent absorption spectra while identifying several features shared with electronic aggregates, we suggest that it is appropriate to view the extended delocalized complex as a "vibrational aggregate."[23,34,35] This analogy immediately facilitates identification of such phenomena as exchange narrowing[36,37] and exciton localization as characterized by measures such as the participation ratio.[37-39] The simple model, which only includes local site disorder, also correctly predicts that site energy disorder alone induces IR activity of otherwise IR-inactive modes. That is, the symmetry can

be sufficiently broken without explicit geometric distortion. Lastly, the model allows straightforward incorporation of site energy correlations in anticipation of the correlated

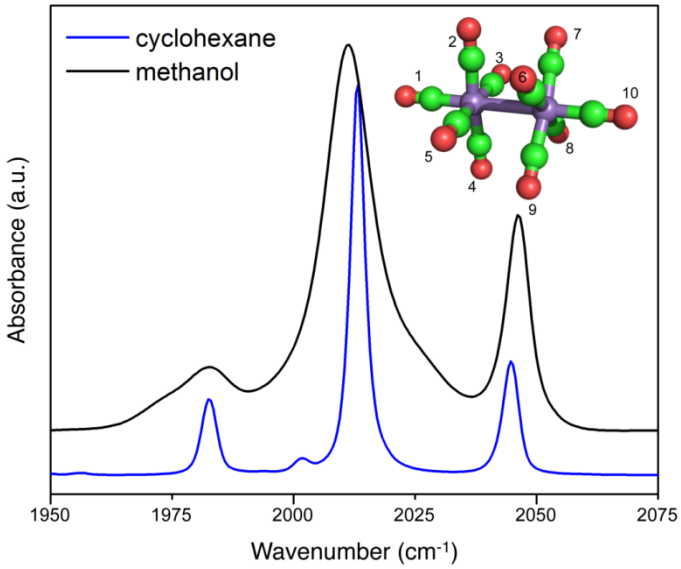

Figure 2.1. FTIR spectra of dimanganese decacarbonyl (structure shown in inset) in a polar solvent, methanol, and a nonpolar solvent, cyclohexane.

rearrangements of the hydrogen bonded network solvating the probe.[12,40] We find that the nature of the site energy correlations have signatures that, in principle, could be extracted from experimental 2DIR data and compared with atomistic simulations.

Delocalized Vibrational Probe: $Mn_2(CO)_{10}$. We have previously studied the photochemistry and coherent dynamics of dimanganese decacarbonyl using a variety of multidimensional IR methods.[41-44] In all of these studies, the solvent was chosen to yield an essentially homogeneously broadened set of coupled vibrations in order to maintain the maximum spectral resolution. DMDC (**Figure 2.1 inset**) is a highly symmetric molecule consisting of 10 strongly coupled carbonyl units, belonging to an uncommon symmetry point group of D_{4d}. For this particular point group, each vibrational mode of DMDC is either IR active or Raman active, with no vibrational modes that have both IR and Raman activity. The four IR active transitions (**Figure 2.1**) occurring at 1983, 2014, 2014 and 2045 cm^{-1} have B_2, E_1, E_1 and B_2 symmetry respectively. The modes of DMDC are highly delocalized vibrations involving the collective motion of eight (E_1 modes) and ten (B_2 modes) carbonyl units. The high and low frequency B_2 vibrational modes can be described by the symmetric and

antisymmetric stretches of the axial carbonyls with respect to the equatorial carbonyl units, with transition dipoles that are parallel to the Mn-Mn bond. The two E_1 modes involve the motion of only the equatorial carbonyls, with mutually perpendicular transition moments that are perpendicular to the Mn–Mn bond. The four IR transitions can be seen in the linear IR spectrum of DMDC in cyclohexane (**Figure 2.1**), where the small peak at 2005 cm^{-1} is a band due to natural abundance ^{13}C in the complex. The FTIR spectrum of DMDC in cyclohexane (**Figure 2.1**) shows transitions that are well characterized by homogeneously broadened Lorentzian lineshapes. In polar solvents the strong system-bath coupling results in inhomogeneous broadening, but several dark modes also gain significant IR activity. For metal carbonyl complexes it is common to observe broadening as well as new peaks emerging with increased solvent polarity, where the new bands often correspond to dark or Raman active vibrations. Below we introduce a vibrational exciton model that can account for the appearance of new spectral bands without any explicit geometric distortion or changes to the off-diagonal Hamiltonian matrix elements; instead they can be attributed to fluctuations that break the energetic symmetry of the molecule. The dynamic symmetry breaking results in Raman active modes (classified by no zero-disorder IR activity) gaining IR oscillator strength and becoming bright in the FTIR spectrum.

DMDC as a Vibrational Aggregate. For moderate to strong coupling, it is common to represent the system in a site basis, including the coupling between the sites as off-diagonal matrix elements of the Hamiltonian.[34] In the diagonal representation, the states are denoted excitons and generally exhibit some degree of delocalization among the sites. The incorporation of energetic disorder in those site energies (so-called "diagonal" disorder) often leads to localization of the resulting eigenstates. In coupled electronic aggregates, for example, such localization can significantly alter the rates and efficiencies of charge and energy transfer processes. Delocalized systems such as light-harvesting proteins,[45-47] J-aggregates[48-52] and conducting polymers[53] have been extensively studied due to the interest in long-distance charge separation and transport.

Although coupled vibrational systems are routinely described using excitonic Hamiltonians, DMDC displays striking manifestations of a range of phenomena that have

long been observed chiefly in coupled electronic chromophores. The highly delocalized vibrational modes of DMDC serve as a vibrational analogue of electronic chromophore aggregates, where delocalization across individual vibrational sites occurs as a function of the bath coordinates. Environmental fluctuations modulate the site energies, thus influencing the coupling and extent of vibrational delocalization. In general the bath causes disorder-induced localization,[54] where large fluctuations can dislodge a given site from the delocalized network. The extent to which an exciton is distributed over local chromophores can be quantified using the participation ratio, which provides the number of individual units that compose the eigenstate. Spectral lineshapes (either optical or vibrational) have been shown to be sensitive indicators of the participation ratio, where a higher degree of delocalization naturally leads to narrower lineshapes than would be expected for a given site energy distribution, a phenomenon known as exchange narrowing.[35,36,55] Effects identical to those seen in electronic systems, such as exchange narrowing and disorder-induced localization, are observed and modeled for DMDC in linear alcohol solvents.

Finally, the excitonic nature of the DMDC vibrations enables the molecule to sense nanometer-scale length correlations in the solvation shell, providing a perspective that extends beyond the vicinity of a single solvent molecule. Using the excitonic model, we find that correlations between site energy fluctuations have clear signatures in the inhomogeneous widths of the resulting exciton bands. Since the present model is non-dynamical and only considers the static ensemble of transitions, the full utility of this approach and its predictions will be realized once it is combined with a molecular dynamics simulation and a local mode frequency map. Nevertheless, as has been shown in numerous examples, a static description of the energy landscape and the correlations among structural units can provided key insight in applications ranging from peptides to molecular aggregates.

Spectral Diffusion. In linear and nonlinear infrared spectroscopy, the analysis of spectral features including peak position, shape, intensity, evolution, etc. provides insight into the underlying molecular structures and dynamics.[13,56,57] In the condensed phase, the analysis of spectral features in linear IR spectroscopy is particularly challenging due to constant fluctuations of an inhomogeneous environment leading to a distribution of transition

frequencies that depend on the bath coordinates. Time-resolved spectroscopies based on photon-echo experiments have allowed for the direct observation of the dynamic frequency fluctuations that underlie inhomogeneously broadened line shapes. The static distribution of transition frequencies in systems with strong system-bath coupling can easily be seen using linear IR spectroscopy, but the dynamic features are difficult to discern due to the lack of time resolution in frequency domain spectroscopies. Two-dimensional infrared spectroscopy (2DIR) monitors the correlation between excitation and detection frequencies as a function of waiting time as the system undergoes stochastic fluctuations that modulate the transition frequency. This correlation produces a signature lineshape in the 2D spectrum that evolves as the system undergoes environmental fluctuations. The purely absorptive 2DIR spectrum is the sum of real parts of the rephasing (echo) and nonrephasing spectra.[57-59] In the presence of inhomogeneous broadening the rephasing spectral amplitude is enhanced relative to the nonrephasing spectrum by strong correlation between excitation and detection frequencies. This imbalance in signal amplitudes relaxes as the system explores all the available microscopic environments. The time-dependent correlation of excitation and detection frequencies is described by the frequency-frequency correlation function, which can be extracted from 2DIR spectra through the inhomogeneity index $I(t)$:[60]

$$I(t) = \frac{A_{rephasing} - A_{nonrephasing}}{A_{rephasing} + A_{nonrephasing}} \qquad (2.1)$$

where A is the amplitude of the rephasing or nonrephasing peak amplitudes (for single transitions). Monitoring this ratio as a function of waiting time allows the frequency-frequency correlation function (FFCF) to be experimentally extracted for systems whose frequency correlations are slower than the dephasing time, a condition that is satisfied in the metal carbonyl system studied here. From the FFCF the homogeneous and inhomogeneous contributions to the total linewidth can be separated using the initial correlation function value combined with the full width at half maximum (FWHM) of the 1D IR spectrum.[1] Our goal in the present work is to investigate the correlation between translational diffusion—typically parameterized by the viscosity—and the rate of spectral diffusion. The viscosity of a linear alcohol increases monotonically with length, whereas the global hydrogen bond structure is much more weakly length dependent as discussed below.

A commonly used model for the FFCF consists of a motionally narrowed term as well as a sum of exponential terms:[1,61,62]

$$C_1(t) = \langle \delta\omega_{01}(t)\delta\omega_{01}(0)\rangle = \frac{\delta(t)}{T_2} + \sum_i \Delta_i^2 e^{-t/\tau_i} \qquad (2.2)$$

The first term in Eq. 2 describes the motionally narrowed portion of the correlation function, where T_2 incorporates pure dephasing, population relaxation and orientational relaxation into the correlation function, which are considered to be waiting time independent. This term, usually dominated by the dephasing of the system caused by extremely fast structural fluctuations, does not contribute to the time evolution of the 2D line shape or the ratio of magnitudes of the rephasing and nonrephasing signals. The second term is the sum over all inhomogeneous terms that contribute an exponential decay to the FFCF, where τ_i is the spectral diffusion time constant. For systems with no measurable inhomogeneous broadening, such as a vibrational probe in a weakly interacting solvent, there is no measurable spectral diffusion and the correlation function consists of only the delta function in the first term in Eq. 2, corresponding to the effectively constant transition frequency for the band. The correlation function $C_1(t)$ describes the 0 → 1 transition autocorrelation function, but note that the 1 → 2 autocorrelation function as well as the 0 → 1, 1 → 2 cross correlation function also contribute to the third order response function.

For systems that have inhomogeneous broadening, the homogeneous portion will not contribute to the observed exponential decay of the FFCF. By fully characterizing the inhomogeneous contributions to the correlation function, the dynamics of specific interactions can be isolated. In the case of DMDC in alcohol solvents there are two distinct limiting solvation environments, hydrogen bonded environments and non-interacting alkyl environments, though the sample is a complicated heterogeneous mixture of the two. Simple alkyl environments would contribute only to the motionally narrowed term of the correlation function, while the hydrogen bonded environments are responsible for the exponential decay. Because the inhomogeneous broadening is caused exclusively by the hydroxyl groups of the alcohol, the hydrogen bond dynamics of the system can be selectively studied despite the lack of preferential solvation. The high solubility of DMDC in both polar and non-polar solvents assures that the bulk solution will not be enhanced by phase separation upon

addition of the solute, making DMDC a non-perturbative probe to the natural solvent environment.

In this study we observe the spectral diffusion of a strongly coupled vibrational probe DMDC in a series of linear alcohol solvents. The hydrogen bonded environment leads to significant spectral broadening, the extent of which is dampened by exchange narrowing. In addition, large magnitude fluctuations of local coordinates that participate in the delocalization network cause dynamic vibrational exciton localization. This localization acts to break the energetic symmetry of the vibrational molecule, resulting in Raman active vibrational modes gaining IR intensity as well as the splitting of previously degenerate modes.

Experimental and Simulation Methods: 2DIR. The experimental implementation of chirped-pulse upconversion detected 2DIR spectroscopy has been described in detail elsewhere.[63-65] Briefly, a sequence of three fields E_1, E_2 and E_3 with wave vectors $\mathbf{k}_1$, $\mathbf{k}_2$ and $\mathbf{k}_3$, separated by times t_1 and t_2 arrive at the sample in a box geometry producing fields $E_\pm$ emitting during t_3 with wave vectors $k_\pm = \pm k_1 \mp k_2 + k_3$corresponding to rephasing (-) and nonrephasing (+) signals, respectively. The IR pulses are generated using a continuum seeded dual-frequency two-stage optical parametric amplifier based on β-barium borate. The collinear signal and reference local oscillator are upconverted to the visible by sum-frequency generation in a wedged 5% MgO:$LiNbO_3$ crystal with a highly chirped 800 nm pulse which is derived from the uncompressed amplifier output before entrance into the compressor. The upconverted light is detected using a silicon CCD camera with 1340 horizontal pixels (Roper, PIXIS). The detection frequency ω_3 axis conjugate to t_3 is obtained by the spectrometer, and the excitation axis ω_1 is obtained by Fourier transformation with respect to t_1. Recently we have demonstrated how to obtain purely absorptive spectra,[65] correcting the spectral phase of the signal using the known spectral phase of the chirped pulse.[66] The time delay between the first and second pulses is scanned using independent pairs of ZnSe wedges. The maximum scanned delay is 10 ps, corresponding to an experimental Fourier transform resolution of 3.3 cm^{-1}.

Simulation Methods. Both 1D and 2D spectra have been successfully modeled using a vibrational exciton treatment, coupling local modes to yield the vibrational eigenstates. Using semi-empirical transition dipole coupling between local mode units, and a fixed vibrational anharmonicity of the resulting eigenstates, it is possible to use MD simulations to generate an ensemble of structures from which the 2D spectrum at $t_2 = 0$ can be constructed from a sum of homogeneously broadened spectra. Although this approach does not provide information on the spectral diffusion of such an ensemble, it does aid in determining the inhomogeneous width as well as providing insight into the eigenstate energy landscape, including any pH, temperature or solvent dependence. The most complete spectral simulation uses the dynamic frequency trajectory to compute the full multi-time correlation function needed to predict the waiting time dependent 2DIR spectrum, capturing the spectral diffusion dynamics, and, in principle, vibrational redistribution and relaxation processes using, for example, a Redfield theory description of the dissipation.

Rather that constructing an electric field map for the metal carbonyl C≡O stretch, the model we have implemented simply imposes Gaussian distributed local mode energy disorder, as is commonly done for electronic aggregates.[34,50] This model provides insight into the signatures of site disorder in a highly coupled multi-vibrational chromophore system. The Hamiltonian (**Equation 2.3**)

$$H = \sum_{n=1}^{10} \varepsilon_n |n\rangle\langle n| + \sum_{n \neq m=1}^{10} J_{nm} |n\rangle\langle m| \qquad (2.3)$$

describes the 10 carbonyl units using diagonal site energies ε_n and off-diagonal coupling J_{nm} terms. The assignment of the 10 sites is shown in **Equation 2.4**. The values of the matrix elements are determined by a genetic algorithm multivariable fit to the 10 experimental terminal carbonyl stretching frequencies. Based on symmetry, the model has 7 coupling terms ($C_1 \ldots C_7$) and two different site energies (S_1 and S_2) as follows,

$$H = \begin{bmatrix} S_1 & C_1 & C_1 & C_1 & C_1 & C_2 & C_2 & C_2 & C_2 & C_3 \\ C_1 & S_2 & C_4 & C_5 & C_4 & C_6 & C_6 & C_7 & C_7 & C_2 \\ C_1 & C_4 & S_2 & C_4 & C_5 & C_7 & C_6 & C_6 & C_7 & C_2 \\ C_1 & C_5 & C_4 & S_2 & C_4 & C_7 & C_7 & C_6 & C_6 & C_2 \\ C_1 & C_4 & C_5 & C_4 & S_2 & C_6 & C_7 & C_7 & C_6 & C_2 \\ C_2 & C_6 & C_7 & C_7 & C_6 & S_2 & C_4 & C_5 & C_4 & C_1 \\ C_2 & C_6 & C_6 & C_7 & C_7 & C_4 & S_2 & C_4 & C_5 & C_1 \\ C_2 & C_7 & C_6 & C_6 & C_7 & C_5 & C_4 & S_2 & C_4 & C_1 \\ C_2 & C_7 & C_7 & C_6 & C_6 & C_4 & C_5 & C_4 & S_2 & C_1 \\ C_3 & C_2 & C_2 & C_2 & C_2 & C_1 & C_1 & C_1 & C_1 & S_1 \end{bmatrix} \tag{2.4}$$

The fit is also constrained to reproduce the experimental IR transition strengths, including the IR inactivity of the 6 dark modes. Agreement was found by setting the local mode transition dipole moment of the axial carbonyls μ_{ax} to have a magnitude 1.48 times that of the equatorial carbonyls μ_{eq}. Since the model considers only the excitations on each local unit, there is no information regarding the vibrational anharmonicity or the associated excited state absorption. However, it is possible to include multiple excitations either explicitly or by using perturbation theory[44] or the nonlinear exciton equations.[67] Using the present model, the two-exciton manifold was calculated using a fixed anharmonicity of 8 cm^{-1}, allowing the 2D spectrum of DMDC to be simulated in the presence of site disorder.

To simulate the hydrogen bonded solvent environment, we incorporate disorder into the model by allowing each diagonal site energy to vary according to a Gaussian random variable, $\delta\omega_n$, such that for each realization of the Hamiltonian, the n^{th} site energy is $\varepsilon_n = \varepsilon_n^{(0)} + \delta\omega_n$, where $\varepsilon_n^{(0)}$ corresponds to the perfectly ordered system. The $\delta\omega_n$ are uncorrelated (unless specified otherwise) with zero mean and we define the site inhomogeneous width $\Delta\Omega_{in}$ to be the standard deviation of $\delta\omega_n$. Using eigenstate frequencies and transition moments determined from diagonalization of 5000 realizations with varying degrees of inhomogeneity, we found no correlation between the two. The eigenstate transition moments are calculated using the approximation that the local carbonyl units have their transition moments parallel to the CO bond axis; the eigenstate transition moments are obtained by the coordinate transformation defined by the Hamiltonian

diagonalization. To compute the 1D spectrum, we used a Voigt profile, which takes as inputs the homogeneous (Lorentzian) and inhomogeneous (Gaussian) widths. The Voigt profile for each transition is then weighted by the square of the corresponding transition moment, and the sum of these is the linear spectrum. The Gaussian width for the Voigt profile corresponds to the standard deviation of the eigenstate frequency for each mode. We used an accurate analytical fit to a Voigt profile.[68]

In addition to the eigenstate frequencies, we also consider the eigenvectors in order to gain insight into the origin of the spectroscopic features exhibited by the model. As is common in analyses of J-aggregates and other excitonic systems, we consider the extent of delocalization via the participation ratio (PR).[35,69] In J-aggregates and in multi-chromophoric light-harvesting protein complexes the excitons are often delocalized over many nanometers, and the size of the exciton decreases with disorder. By comparison, DMDC is a very small molecule, but the vibrational eigenstates are nevertheless delocalized over at least half of the carbonyl units. Thus, from the perspective of the number of participating monomers, the extent of delocalization is comparable to what is observed in, for example, LH2 complexes.[39] Like these large scale electronic systems, as the site disorder is increased the excitons become localized. Indeed, all of the trends we have noted thus far can be correlated to disorder-induced exciton localization.

Using each eigenvector φ_n, we determine the degree of exciton localization resulting from site disorder. The participation ratio P_n given by Eq. 5 equals the number of local units (indexed by m) that contribute to the resulting delocalized eigenstate φ_n.[35]

$$P_n = \left[\sum_{m=1}^{10} \left(\phi_n \right)_m^4 \right]^{-1} \tag{2.5}$$

For the present system P_n ranges from 1 to 10. In addition to measuring the degree of localization, the participation ratio also allows us to discover any correlation between the localization tendency and the eigenstate frequency.

To illustrate the spectral signatures predicted by our exciton model for DMDC, we have simulated 2DIR spectra by including both the one- and two-exciton manifolds. Since our model treats only static disorder, we do not make any attempt to simulate the waiting time

dependence of the 2D spectra. The 2D spectra were simulated using the one-exciton transitions and transition dipoles, and a quasi-harmonic ansatz for the two-exciton states. Overtone and combination band energies were computed as the sum of the one-exciton energies with a constant anharmonicity for all of the excited states of 8 cm^{-1}. Harmonic oscillator scaling was assumed for all overtone transition dipole moments. The transition dipole moment direction for a transition between a given one-exciton state *a* and a given two-exciton state *ab* was taken to be parallel to the transition dipole moment for excitation of the one-exciton state *b*. Combination band transition moments were scaled by the moduli of the constituent one-exciton transitions to account for their degree of allowdness. With the set of 10 one-exciton states and 55 two-exciton states, as well as the transition dipole moments derived from the one-exciton Hamiltonian, we prepared multiple inputs for the SPECTRON package which we used to compute the 2D spectra.[70] The spectra were simulated using a constant exponential dephasing corresponding to a 2-cm^{-1} homogeneous width, and the response function was evaluated using the sum-over-states method (the "CGF" option in SPECTRON 2.4.0).

Experimental Results.

Linear and Nonlinear Spectroscopy. Linear IR spectra are often used to extract dynamic information using analysis of the linewidth. This approach can often produce ambiguous dynamic results, where multiple systems showing identical linear spectra exhibit different dynamics, such as orientational relaxation, population relaxation or spectral diffusion. This has been demonstrated clearly by Fayer and coworkers, where four proposed water systems having identical linear IR spectra displayed different orientational relaxation times.[71] As shown here, three systems, two different binary mixtures and a pure long chain alcohol, displaying identical linear IR spectra are shown to have significantly different spectral diffusion times.

Three solvent or solvent mixtures, 1-hexanol, propanol/hexane (65/35% v/v) and butanol/squalane (70/30% v/v), have viscosities ranging from roughly 1 to 6 cP at 25°C. In these solvents DMDC displays identical linear IR spectra, shown in **Figure 2.2**. Using the

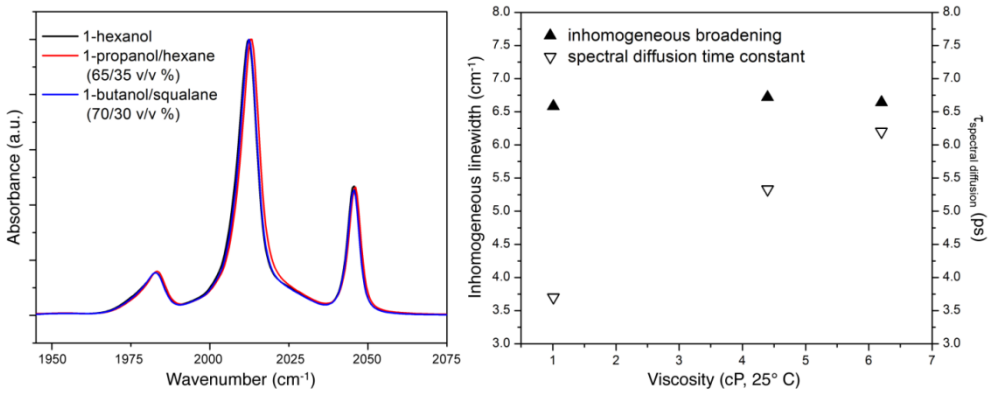

Figure 2.2 FTIR spectra of dimanganese decacarbonyl in 1-hexanol, as well as two solvent mixtures that show significant different viscosities, but identical bulk viscosities (b). While the inhomogeneous broadening is identical for the three solvent mixtures, the spectral diffusion shows a strong viscosity dependence, illustrating the disconnect between dynamics and broadening.

FFCF determined from the rephasing and nonrephasing 2DIR spectra (**Equation 2.1**), the spectral diffusion time constants as well as the inhomogeneous contributions to the lineshape were determined. The spectral diffusion time constants, which range from roughly 3.5 to 6 ps, were found to depend on the solvent's bulk viscosity. Despite the difference in the dynamical sampling of microenvironments, however, the inhomogeneous broadening of DMDC in these solvent mixtures is identical. The key observation from these data is that the time scale for spectral diffusion is independent of the magnitude of the microscopic fluctuations that produce the inhomogeneous width. The situation in the neat alcohols is markedly different, as shown below, where there is a pronounced correlation between inhomogeneous width and the time scale for spectral diffusion.

Heterogeneous Dynamics of Coupled Vibrations in DMDC. The four IR active modes are highly delocalized vibrations which have been described by DFT calculations. The linear FTIR spectrum of DMDC in methanol (**Figure 2.1**) shows significant broadening of the central and low frequency peaks compared to DMDC in cyclohexane, but little broadening is seen on the high frequency mode. This trend is common to the alcohol series shown below as well as several other polar solvents.

Figure 2.3a shows the absorptive spectrum of DMDC in methanol at a waiting time of 1 ps. Slices of the rephasing and nonrephasing spectra are shown in **Figure 2.3b and d** for the bands along the diagonal centered at 2045 cm^{-1} and 2013 cm^{-1}, respectively. Coherent

oscillations are evident in the 2045-cm^{-1} nonrephasing signal due to the coherence created between the low- and high-energy states in the first excited state manifold. These coherences have previously been described in detail for this system[41] as well as for $Co_2(CO)_8$,[72] and are the vibrational exciton analogues of similar coherences observed in electronic systems with excitonic coupling.[52,53,73,74] The slow dephasing is due to the narrow linewidth of the high-frequency band. Oscillations are not observed in the nonrephasing response for the central band. Such a feature would arise from a coherence between the broad central and low-energy bands, and their broad bandwidths lead to very rapid dephasing.

The FFCFs for the two bands are shown in **Figure 2.3c**. Although the large amplitude oscillations due to the intraband coherences obscure the FFCF at early times, the high frequency mode of DMDC in methanol shows little inhomogeneity, and exhibits little to no loss of correlation despite being in a polar solvent. Indeed, the fact that the coherences are

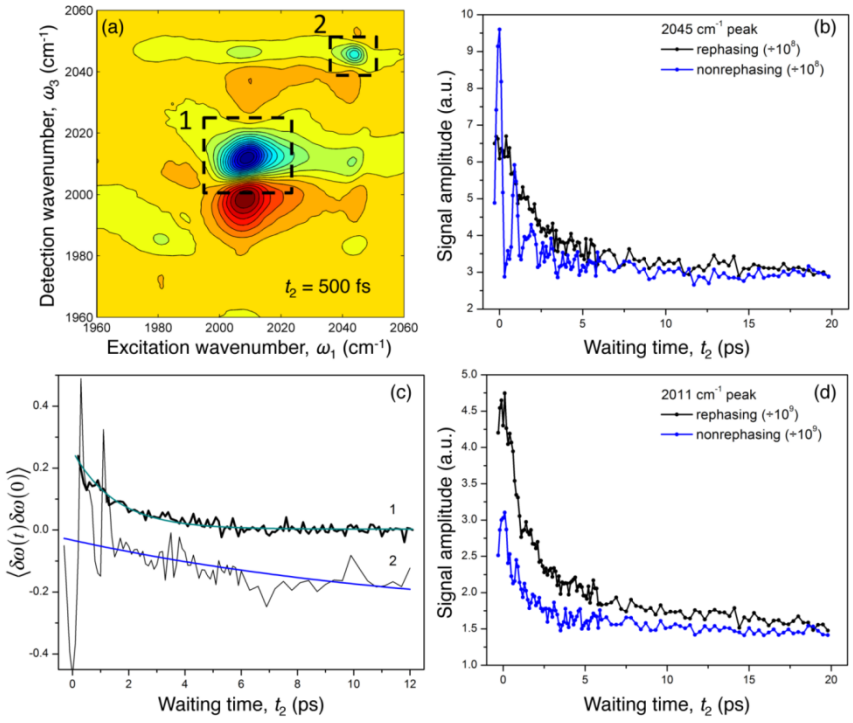

Figure 2.3 (a) 2D absorption spectrum of DMDC in methanol shown at a waiting time of 500 fs. Traces of the rephasing and nonrephasing spectra as a function of waiting time are shown for the mode highlighted as 1 (d) and 2 (b). (c) The frequency-frequency correlation functions obtained from the experimental data for these modes. The large oscillations seen in the correlation function of mode 2 are the result of coherent beats between the excited manifold that are observed in the nonrephasing spectrum.

so pronounced is a direct consequence of the comparable rephasing and nonrephasing signal amplitudes, a direct indication that the band is not significantly inhomogeneously broadened. Although there is additional information present in these low-frequency coherences, here we focus on the spectral diffusion, where it can be seen that there is little to no memory loss for this vibrational mode, as well as line broadening that differs significantly from the central band. The difference in line broadening can also be seen in the lineshape of the absorptive spectra, where the high frequency mode has a no peak elongation along the diagonal and a symmetric lineshape at t_2 = 1 ps. That two strongly coupled vibrational modes show different lineshapes suggests qualitatively distinct dynamics, and/or differences in each band's response to solvation structure and dynamics.[75]

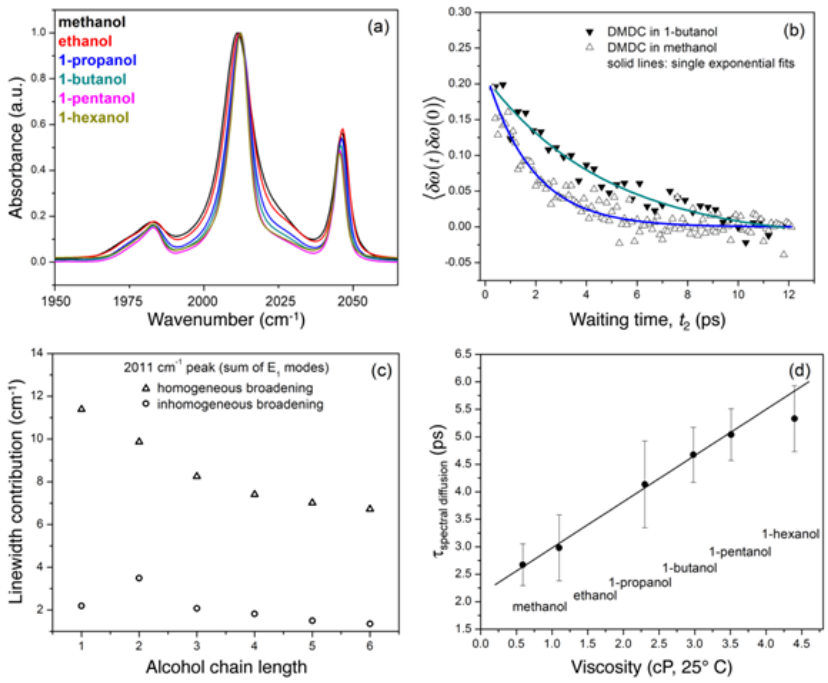

Figure 2.4 (a) FTIR spectra of dimanganese decacarbonyl in a series of alcohol solvents, ranging from methanol to 1-hexanol. (c) The inhomogeneous and homogeneous components to the line broadening extracted using the linear and 2D infrared spectrum. (b) FFCF of the main vibrational mode shown for methanol and 1-butanol, and the timescales for spectral diffusion obtained through single exponential fits to the correlation function (d).

Spectral Diffusion in Alcohol Series. The spectral diffusion timescale for DMDC in a series of alcohol solvents, ranging from methanol to 1-hexanol, were determined using the method previously described. **Figure 2.4** shows the FTIR spectra of DMDC in the series of alcohol solvents. The spectra become narrower with increased alkyl chain length. The central band

center remains largely constant, but the high frequency band shifts to the red with increased chain length. The presence of spectral amplitude at frequencies corresponding to IR-inactive modes also diminishes with increased chain length.

Figure 2.4b shows representative FFCFs for the solvents methanol and 1-butanol. The solid curves are single exponential fits to the data starting at t_2 = 100 fs. It is evident from the data that the loss of frequency correlation in methanol is considerably more rapid than it is in 1-butanol. The early waiting time value of the correlation function corresponds to the fraction of the 1D line width that is due to inhomogeneous broadening. Although the early time value for methanol (0.15) is smaller than that of 1-butanol (0.2), the overall spectral width of methanol is greater than that of 1-butanol. Combining the two observations—methanol's broader spectrum and comparable inhomogeneous contribution—indicates that methanol induces a broader inhomogeneous width. The full analysis described below is based on using a Voigt profile for the linear spectrum, and the two spectral width contributions are extracted using the method described by Kwak et al.[1]

Figure 2.4c shows the extracted homogeneous and inhomogeneous widths of the central band of DMDC in the alcohol series. The homogeneous widths decrease monotonically from 11 cm^{-1} for methanol to 7 cm^{-1} for 1-hexanol. Except for a slight exception in the case of ethanol, the inhomogeneous widths likewise decrease with increasing alcohol chain length, though the overall variation is less than 1 cm^{-1}. It is key to note here that this band is composed of two degenerate modes, and according to the model presented below these states are split by site disorder. Thus, the extracted width of the central band is actually the combined widths of two bands. From the model it is possible to deduce the width of the combined band, and this analysis is presented in the discussion.

Figure 2.4d shows the spectral diffusion time constants extracted using Eq. 2 as was also done for the case of the solvent mixtures. The spectral diffusion times depend monotonically on the solvent viscosity, ranging from 2. 7 ps in methanol to 5.33 ps in 1-hexanol. There is a linear dependence of spectral diffusion time on solvent viscosity from methanol to 1-pentanol, with some deviation for the longest chain solvent 1-hexanol.

Simulation Results

Analysis of the vibrational exciton model is broken into two parts: the first describes

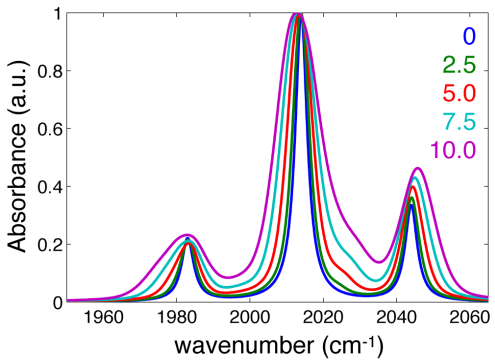

Figure 2.5 Simulated linear IR absorption spectrum of DMDC using the vibrational exciton Hamiltonian with site inhomogeneity $\Delta\omega_{in}$ varying from 0 to 10.0 cm^{-1}.

general aspects of the eigenstate distributions and the spectral lineshapes as a function of $\Delta\Omega_{in}$, the second compares the model to the measured data described above.

Figure 2.5 shows several spectra generated using the model exciton Hamiltonian with varying values of the site disorder frequency width $\Delta\Omega_{in}$. Besides the initial fit to the known experimental IR and Raman frequencies and IR transition moments, there are no further adjustable parameters. The model spectra reproduce the experimental 1D spectra remarkably

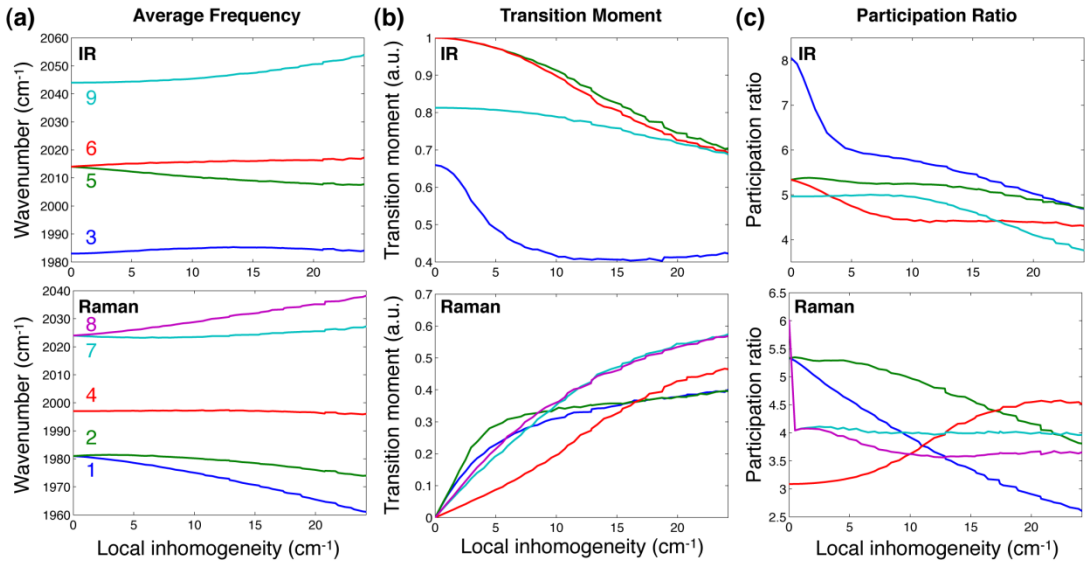

Figure 2.6 Eigenstate properties (a) average frequency, (b) transition moment, and (c) participation ratio (PR) for (top) the four IR active modes (modes 3, 5, 6 and 9) and (bottom) the five Raman modes (modes 1, 2, 4, 7 and 8) that acquire appreciable IR activity due to the site disorder.

well. In this section we analyze the model's results in order to deduce a molecular interpretation for the origin of the spectral changes.

For this simplified model of the vibrational Hamiltonian, we have only considered the effect of diagonal disorder since hydrogen bonding between the alcohol solvent and the carbonyl units is a local interaction. It should be noted, however, that the site energies and the coupling matrix elements are not independent parameters and future studies will need to include disorder in the full Hamiltonian. To sample a range of broadening that resembled the experiment, $\Delta\Omega_{in}$ ranged from 0 to 25 cm^{-1} and for each value of the local site inhomogeneity, 5000 realizations were evaluated. The resulting eigenvalues are enumerated from 1 to 10 in increasing energy, and are identified as either "IR" or "Raman" active according to their zero-disorder activity; hence modes 3, 5, 6, and 9 are the "IR modes", whereas 1, 2, 4, 7, 8, and 10 are the "Raman modes."

Figure 2.6a shows the average transition frequencies for each eigenstate as a function of the site disorder frequency width, $\Delta\Omega_{in}$. It is immediately clear that the two E modes—degenerate in the absence of disorder—split with increasing site disorder. Both B modes (3 and 9) increase in frequency initially, and then mode 3 starts to decrease when the site disorder becomes comparable to the large coupling terms in the Hamiltonian near $\Delta\Omega_{in}$ = 15 cm^{-1}. For the Raman modes a similar symmetry breaking is also clear: modes 1 and 2, are initially degenerate but become split by the increased disorder and shift to lower frequency. A similar trend is evident for modes 8 and 9 though they shift to higher frequency as they split. Mode 10 is not shown in these figures since it never acquires appreciable IR oscillator strength for the range of disorder considered here.

Along with the changes in the average eigenstate frequencies there is also a clear trend in the oscillator strengths. In general all of the IR active modes lose oscillator strength whereas all of the Raman modes gain oscillator strength. **Figure 2.6b** shows the IR and Raman mode transition moments as a function of $\Delta\Omega_{in}$. Among the IR modes, the principle difference is the rate at which the modes lose oscillator strength. Compared to the rather gradual decrease seen in the higher frequency modes (5, 6 and 9), mode 3 loses almost half of its oscillator strength by $\Delta\Omega_{in}$ = 10 cm^{-1}. This finding is consistent with our experimental observations,

and explains the much weaker diagonal and cross peaks seen in the 2D spectra for the lowest frequency band. The gradual increase in oscillator strength above $\Delta\Omega_{in} \approx 15$ cm^{-1} is likely due to the limited applicability of including only site disorder in our model. The Raman modes gain IR oscillator strength with increased disorder, with the lower frequency modes (1 and 2) growing at a somewhat faster rate than the higher frequency modes.

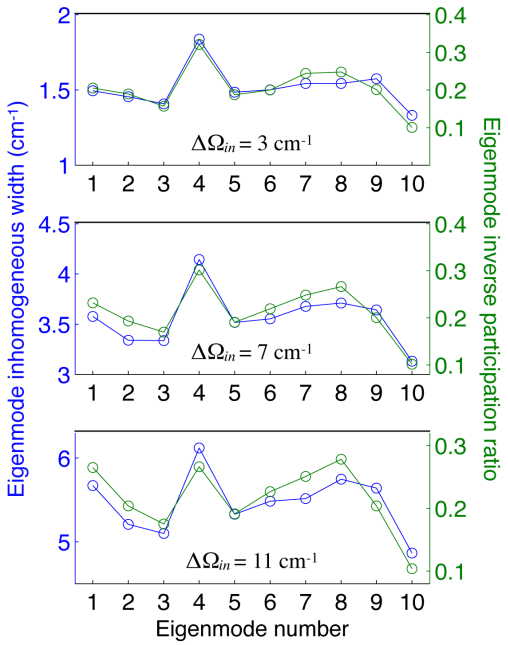

Figure 2.7 Correlation between the inhomo-geneous widths of each ensemble of eigenmode frequencies (left axis) and the eigenmode inverse participation ratio (right axis) for three representative values of the local site inhomogeneity, 3, 7 and 11 cm^{-1} (top to bottom).

Figure 2.6c shows the mean participation ratio (Eq. 5) as a function of the site energy inhomogeneity. The results clearly indicate that exciton localization is induced by disorder. All of the modes exhibit localization, with the more rapid and pronounced change seen in mode 3, which localizes by two carbonyl units with only about 3 cm^{-1} of disorder. The localization of mode 3 corresponds well to the loss of oscillator strength seen in **Figure 2.6c**. Modes 5 and 9 show the smallest degree of localization, whereas mode 6 contracts by about 20% with about 8 cm^{-1} of site disorder. The Raman modes also show varying degrees of localization, with the single exception of mode 4, which actually becomes more delocalized with increased disorder. Modes 7 and 8 abruptly collapse with the slightest

degree of disorder, reflecting their high symmetry. Modes 1 and 2 remain relatively delocalized, which again correlates with their rapid onset of oscillator strength.

Besides the average properties shown in **Figure 2.6**, we also examine the frequency widths of the eigenstates. For each value of $\Delta\Omega_{in}$ we take the standard deviation of each resulting eigenstate distribution as a measure of its inhomogeneous width. It is well known from molecular aggregates that in coupled systems the eigenstate width is narrower than the site width.[36] This exchange narrowing is a result of averaging over the site energy fluctuations. **Figure 2.7** shows the vibrational exciton inhomogeneous width together with the correlation with the inverse of the participation ratio. At three selected values of $\Delta\Omega_{in}$, we find that the eigenstate width tracks the participation ratio. Since the participation ratio is of the number of local modes units over which the exciton is delocalized, a larger inverse participation ratio indicates a higher degree of localization. Thus, the data show that the inhomogeneous width correlates with the degree of exciton localization, consistent with many studies of exchange narrowing in molecular aggregates. Note that in all cases, the eigenstate widths are narrower than the site widths. The relationship between site and exciton energy disorder allows us to associate a site energy distribution with the inhomogeneous widths determined from the FFCFs (**Figure 2.7**). Since the inhomogeneous and homogeneous broadening parameters shown in Fig. 4c are for the whole central band, where the two degenerate modes are split by the site disorder and thus increase the band's overall width, our estimate of the local site energy width is only an upper bound. Nevertheless, we can estimate the site energy full width at half maximum to be 31.5 cm^{-1} ($\mathrm{FWHM} = 2\Delta\Omega_{in}\sqrt{2\ln 2}$), for the case of methanol, which is substantially less than the 11.7 cm^{-1} inhomogeneous width. For the case of 1-hexanol, where the inhomogeneous width was measured to be 7 cm^{-1}, comparison with the model gives a site energy FWHM of 18.5 cm^{-1}.

Another informative measure that has been considered in molecular aggregates is the correlation between the participation ratio and the eigenstate frequency.[35] **Figure 2.8a-b** shows a summary of the results for $\Delta\Omega_{in}$ = 4.5 cm^{-1}. This figure combines several of the considerations above—frequency, PR, and inhomogeneous width—and illustrates that for the low-frequency modes, there is generally a positive correlation between frequency and PR

(i.e. delocalization), whereas for the highest frequency mode, the correlation is negative. In the middle of the band, the frequency and PR values are only weakly correlated. The results also indicate the lack of a clear trend in the absolute delocalization across the band, which differs from the trend in molecular aggregates where more delocalization has been observed in the band center relative to the band edges. When the degree of disorder is increased further, however, the expected trend is observed (**Figure 2.7**): the delocalization is greater in the center of the band relative to that in the wings, with the exception of mode 10 whose

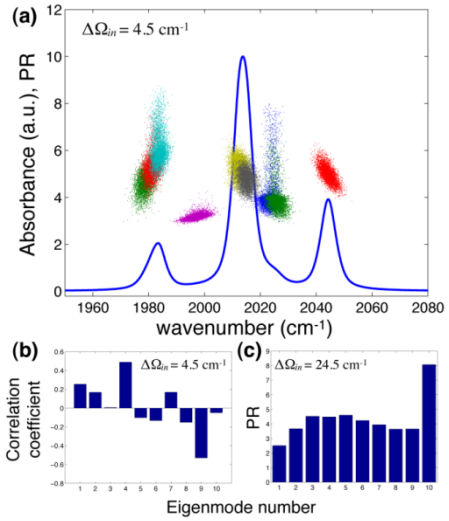

Figure 2.8 (a) Spectrum and ensemble of PR values plotted as a function of individual mode frequency. Each cluster of colored dots corresponds to a different eigenmode. (b) PR-frequency correlation coefficient of each eigenmode, showing generally positive correlation for the low-frequency modes and negative correlation for the high-frequency modes. (c) For the case of large site disorder, the PR versus mode number exhibits the trend that delocalization is greatest near the center of the spectrum, except for the highly symmetric mode 10.

high symmetry resists localization.

In addition to the 1D spectrum, the 2D absorptive spectrum of DMDC was simulated as described in the previous section. These simulations demonstrate the characteristic spectral signatures of the general trends we have described above. Figure 9 shows the 2D spectrum of DMDC calculated for $\Delta\Omega_{in}$ = 0, 3 and 7 cm^{-1}, with a fixed homogeneous width of 2 cm^{-1}. **Figure 2.9** shows the spectrum with no site disorder, and the simulation, which agrees well with our previous experimental results,[65] clearly displays no inhomogeneous broadening evident from the largely symmetric peak shapes. Some slants of the cross and

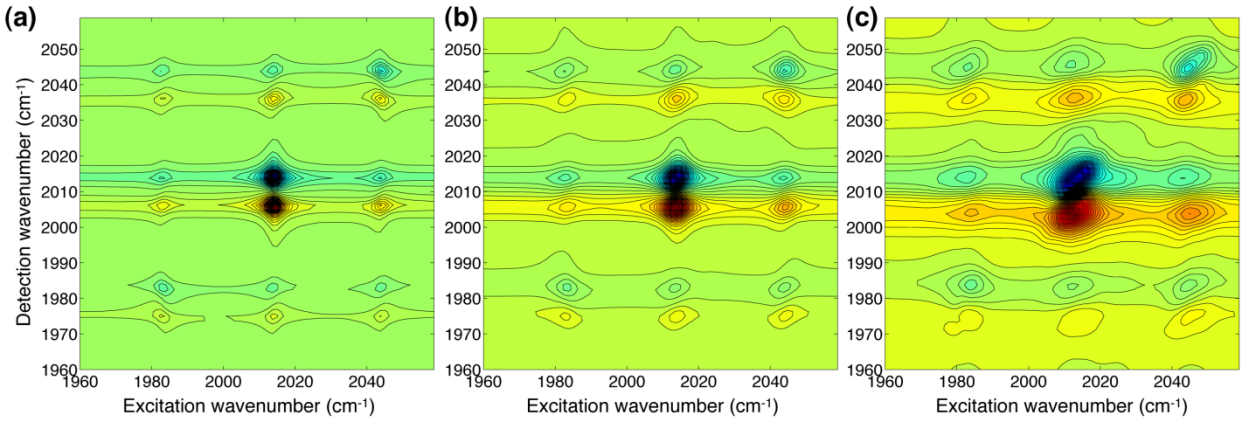

Figure 2.9 Simulated 2DIR spectra (t_2 = 0) of DMDC computed using the 10 one-exciton and 55 two-exciton states with local site disorder DW_{in} = 0 (a), 3 (b) and 7 cm^{-1} (c).

diagonal peaks are evident and are due to well-known Liouville path differences between rephasing and nonrephasing sequences previously observed in other metal carbonyl systems.[58,59] Upon the addition of 3 cm^{-1} of site disorder the spectrum becomes noticeably broader, the peak shapes begin to elongate along the diagonal (**Figure 2.7b**). Finally, with 7 cm^{-1} of site disorder the spectrum shows several dark transitions and significant spectral broadening (**Figure 2.7c**).

Site Disorder Correlation. So far we have only considered uncorrelated site disorder. Since recent simulation and experiment shows that hydrogen bond switching occurs largely by

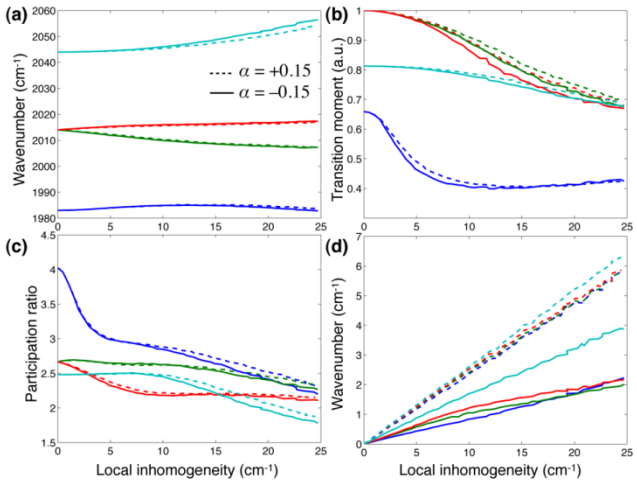

Figure 2.10 Simulations including correlation between sites—solid traces correspond to a = –0.15, and dashed traces to a = +0.15—of (a) average mode frequency, (b) average transition moment, (c) average PR and (d) the standard deviation of the eigenmode ensemble. Only the IR active modes are shown in this figure using the same color coding as in Fig. 6.

rapid angular jumps,[40,76] it is very likely that there will be site energy correlations as a hydroxyl hydrogen bond breaks from one carbonyl and forms with an adjacent carbonyl. Such a scenario could lead to a negative frequency correlation since the site of the broken bond would experience a blue shift accompanied by a red shift on the site gaining the hydrogen bond. Very recently hydrogen bond rearrangement around an anionic solute has been found to involve cooperative motion reminiscent of the Grotthuss mechanism for proton transport in liquid water.[76,77] Understanding the collective hydrogen bond network rearrangement is a general goal of condensed phase dynamics, and probes such as DMDC offer an attractive probe of these coordinated fluctuations.

Though it is difficult *a priori* to devise a site energy correlation scheme that is physically correct, we nevertheless consider what the effect of positive or negative correlation would be. We use the distances Δr_{ij} between pairs of oxygen atoms i and j to construct a covariance matrix M_{ij} according to the following scheme:

$$M_{ij} = \delta_{ij} + \alpha \frac{\left(1 - \delta_{ij}\right)}{\Delta r_{ij}^4} \tag{2.6}$$

where the amplitudes of the off diagonal elements ($1-\delta_{ij}$) are proportional to the inverse fourth power of the distance, which preferentially correlates those sites that are closest to each other. There is an overall scaling factor α. Multiplying the set of uncorrelated site energies by the Cholesky decomposition of M_{ij} produces Gaussian randomly distributed site energies with intersite correlation given by the covariance matrix elements. The sign and amplitude of the correlations are set by the parameter α. In our implementation, we first normalize the off-diagonal matrix elements to the maximum value, and then multiply all the values by α before adding the diagonal elements (all of which are equal to unity). This normalization ensures that the largest correlation coefficient is equal to α.

Figure 2.11 shows a summary of $|\alpha| = 0.15$ comparing positive and negative correlation. The sign of the correlation appears to have little effect on the values of PR,

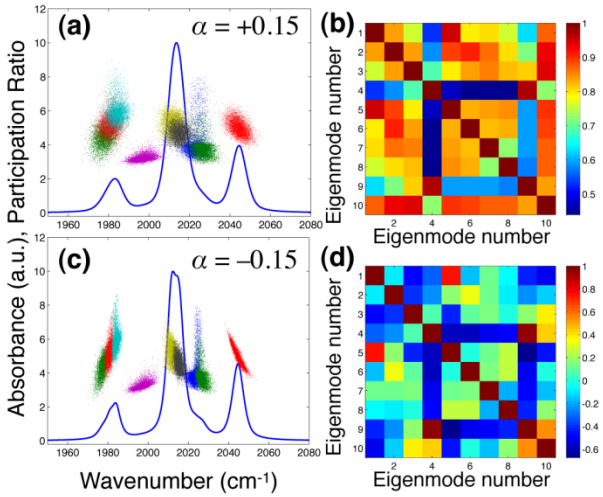

Figure 2.11 Spectra and eigenmode PR values for (a) positive and (c) negative site correlation. Maps of the correlation coefficients (indicated in the color bars) of eigenmode frequencies for (b) positive and (d) negative site correlation.

mean frequency, and the transition moments. On the other hand, the degree of exchange narrowing is more pronounced for the negatively correlated case. Indeed, negative correlation reduces the inhomogeneous width by roughly a factor of two relative to the case of positive correlation. Since the spectroscopy probes the eigenstates, it is instructive to consider their properties. One relationship among the eigenstates is their mutual eigenenergy correlation. It has been shown experimentally and through simulation that the extent and sign of correlation of two different exciton states is evident in the tilt of the cross peak connecting the two states.[59] For a fixed value of the site inhomogeneity ($\Delta\Omega_{in}$ = 6 cm^{-1}), we evaluate the matrix of correlation coefficients for both positive and negative site disorder correlation. **Figure 2.12** shows the predicted spectra with the superposed PR together with the matrix of eigenvalue correlation coefficients. The essential observation is that the correlation between the central band (modes 5 and 6) with the strong high-frequency band (mode 9) is positive with positive intersite correlation, whereas the bands are negatively correlated with negative intersite correlation.

This prediction can in principle be compared with the experiment, despite the fact that the presence of coherences complicates the clean extraction of the cross-peak tilt since it is

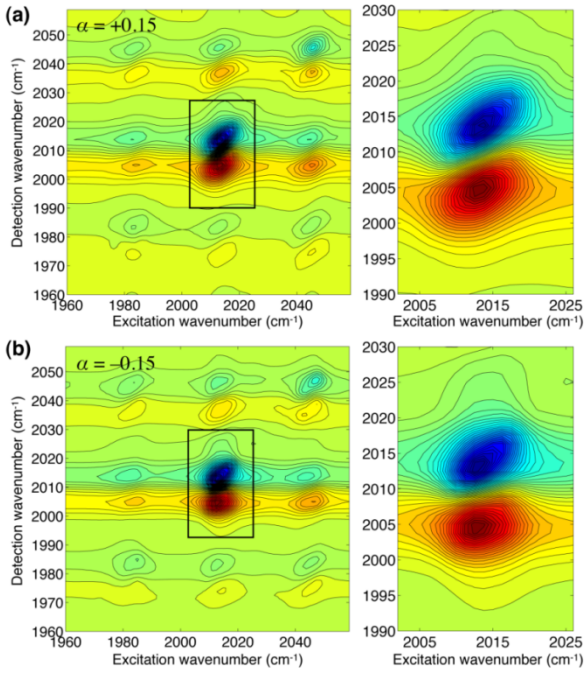

Figure 2.12 Simulated 2DIR spectra with positive (a = 0.15) (a) and negative (a = –0.15) (b) site energy correlation. The right panels are zooms of the central band involving modes 5 and 6. The site inhomogeneity is set at 6 cm^{-1}.

well known that coherent beating leads to cross peak tilt oscillations.[78,79] The simulated 2D absorptive spectra with intersite correlation are shown in **Figure 2.12b**, using $\alpha = \pm 0.15$. Due to the inherent tilt of the cross peak between mode 9 and modes 5 and 6, the predicted frequency cross correlation is not evident in the simulated 2D spectra. Instead a clear difference is observed in the degree of frequency correlation of the excited state absorption from modes 5 and 6, shown in the boxed region and zoomed. The spectrum simulated with positive correlation shows a more pronounced peak tilt in the spectrum parallel to the diagonal, whereas the spectrum simulated with negative correlation shows a reduced tilt angle as well as the narrower width expected from the simulated 1D spectra (**Figure 2.11**). To highlight the differences, we found the peak maximum along ω_3 for various values of ω_1 using the center of a Gaussian fit. **Figure 2.13a** shows the ω_3 maxima for the ground state bleach and stimulated emission band, and **Figure 2.13b** shows the ω_3 maxima for the excited state absorption bands. Negative correlation leads to both a narrower inhomogeneous width (~7 cm^{-1} vs. ~11 cm^{-1} for positive correlation) as indicated by the

region where the frequencies are correlated, and the degree of correlation is also reduced as indicated by the smaller slope of the correlation. This effect is most pronounced for the excited state absorption band, where the ratio of the slopes is roughly 2. Although it is difficult to extract the contribution due to intersite frequency correlation from measured 2D spectra, it is encouraging that such correlations do influence the observed 2D line shapes.

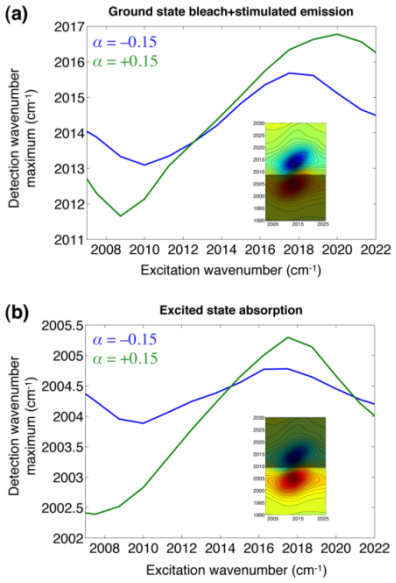

Figure 2.13 Plots of the correlation between ω_3 emission maximum versus excitation frequency ω_1 for (a) the peak due to ground state bleach and stimulated emission and (b) the peak due to excited state absorption. For each band the case of negative (blue) and positive (green) site energy correlation are shown.

Discussion

Spectral Diffusion in the Alcohol Series. The frequency correlation time is found to have a monotonic dependence on the solvent viscosity, where methanol shows the fastest spectral diffusion timescales and 1-hexanol the slowest. The dependence of spectral diffusion on solvent viscosity can be explained by the fluctuation rate, where motional diffusion throughout the first solvation shell is significantly hindered as the chain length is increased. The slowing of molecular motions leads to prolonged hydrogen bond interactions, and transition frequencies that are a function of these interactions stay correlated for longer periods of time. In the case of localized vibrations, spectral diffusion has been reliably

predicted using simple molecular diffusion models, such as the Stokes-Einstein relation to determine the diffusion constant of the solvent.[80] This relationship appears to break down when considering delocalized modes, where molecular diffusion models predict significantly longer spectral diffusion times. The spectral diffusion timescales predicted by the molecular diffusion model range from 1 ps in methanol to 27 ps in 1-hexanol. This disagreement suggests that the spectral diffusion of DMDC (and perhaps other delocalized systems) in alcohol solvents does not strongly depend on large scale solvent diffusion within or throughout the first solvation shell. However, the energetics and dynamics of the system could be affected by global structure in the liquid and local inhomogeneities that such a network could induce.

As seen in the FTIR spectra of DMDC in the alcohol series (**Figure 2.4a**), methanol leads to the broadest spectrum with additional contributions from otherwise IR inactive modes. Therefore the broadening seen in the IR spectrum of DMDC in methanol is not simply due to a distribution of transition frequencies, but instead has contributions from dark vibrational modes as well as degeneracy splitting. As the chain length is increased the fluctuations of the solvent are impeded and the extent of symmetry breaking is reduced. As the solvation environment is limited in its configurations the spectral broadening is reduced. The smaller magnitude fluctuations also lead to less dynamic exciton localization. Thus, in 1-hexanol the spectral features are relatively narrow and there are only small contributions from dark modes.

High Frequency Mode. Above we reported that the inhomogeneity in the transition frequency of the 2045 cm^{-1} mode does not follow the trend that is seen in the other vibrational modes. The 1D spectrum shows that the broadening of this mode throughout the alcohol series remains essentially constant, while other modes display greater inhomogeneous broadening in the more polar, short-chain alcohols. Even in methanol, the most polar alcohol solvent used in this study, the correlation function extracted from the 2D spectrum suggests that the vibrational mode is almost completely homogeneously broadened and shows no spectral diffusion. The simulated absorptive spectrum of DMDC with site disorder shows distinct peak elongation along the diagonal for the high frequency peak (**Figure 2.12a**), whereas the

experimental absorptive spectrum of DMDC in methanol shows no peak elongation (**Figure 2.3a**), even at early times. The vibrational exciton model used in this work accurately predicts the blue shift of this vibrational mode when site disorder is added, but does not accurately reproduce its resistance to inhomogeneous broadening.

The vibrational exciton model used in this work assumes a Gaussian distribution of transition frequencies to induce site disorder. This simple model of site disorder accurately predicts many aspects of the 1D and 2D spectrum of DMDC in alcohol solvents, but the Gaussian model for transition frequency distribution is not sufficient for predicting the full 1D and 2D spectrum of DMDC in systems that cause a large degree of inhomogeneous broadening. The simplest expression for the lineshape function uses the second order cumulant approximation, but recent work has suggested that non-Gaussian dynamics could influence the lineshape of systems that interact strongly with their environment.[75,81] Furthermore, it has been demonstrated that non-Gaussian fluctuations can lead to dissimilar dynamics of coupled vibrational modes.[81,82]

1D and 2D IR lineshapes and lineshape dynamics that are not accurately reproduced by Gaussian frequency fluctuations have been observed in hydrogen bonded environments, including the amide I transition in aqueous environments[81] and the OH transition of water in acetonitrile. In the case of the strongly coupled vibrational modes of the symmetric and asymmetric OH stretches of water in acetonitrile, the two coupled vibrational modes display significantly different frequency dynamics.[75] This effect was attributed to non-Gaussian statistics giving rise to non-zero odd-order correlation functions, which vanish in the case of Gaussian statistics. The non-Gaussian character of the hydrogen bond distance along the N–H coordinate leads to non-Gaussian frequency fluctuations, which are strongly dependent on the hydrogen bond coordinate.

The apparent non-Gaussian characteristic of the hydrogen bond dynamics occurring in DMDC in alcohol solvents could be the result of a non-Gaussian distribution of hydrogen bond distances between the carbonyl groups of DMDC and the hydroxyl groups of the alcohol solvent. Similar to the coupled vibrations of the water OH stretch in the H_2O/CH_3CN system, the strongly coupled vibrational modes of DMDC exhibit significantly

different dynamics as seen through the frequency-frequency correlation function. By coupling the current exciton model with MD simulations it will be possible to gain an atomistic view of the hydrogen bonding environment, including the distribution of hydrogen bond distances and angles. Whether non-Gaussian dynamics alone account for the large difference in lineshape and dynamics of the vibrational modes of DMDC will be the subject of a future study.

Nature of the Solvation Environment. Although it is established that alcohols contain some amount of polar/nonpolar structural segregation, the picture of alcohol structure that emerges from several simulation and experimental studies is that of a relatively well mixed hydrophobic and hydrophilic medium.[30,32,33] The smaller and more flexible solvents are able to present the DMDC probe with a larger range of hydrogen bonding configurations, while the lower viscosity facilitates rapid fluctuations of this solvation shell. On the other hand, the longer chain alcohols are sterically confined, while exhibiting slower dynamics.

Excellent agreement between experiment and the vibrational exciton Hamiltonian with site disorder enables us to deduce a molecular picture of the solvation environment probed by the 1D and waiting-time dependent 2DIR spectra reported above. Since DMDC is amphiphilic, both the 1D and 2D spectra contain both polar and nonpolar contributions, and it remains to be determined how the single site disorder parameter maps to the distinct solvation environments. If the DMDC solute were only present in a polar environment with a nearly complete hydrogen bonded solvation shell, we would conclude that as the solvent chain length is increased, the magnitude of the energetic fluctuations would decrease due to the increased stiffness of the more viscous solvents. From the spectral diffusion timescale, we would also conclude that the rate at which the frequencies are sampled decreases. Both conclusions are consistent with the 2DIR data, and the modeling explains why the frequencies shift with increased disorder and why the Raman modes become bright in the infrared.

Since the first implementations of liquid phase x-ray scattering, there has been interest in the structure of alcohols.[83,84] It is known that these liquids are structurally heterogeneous due to the need to balance hydroxyl hydrogen bonding and the hydrophobicity of the alkyl tails.

The result of these competing interactions is that linear alcohols adopt structures that to some degree segregate polar and nonpolar regions. Simulation and experimental studies have concluded that linear alcohols form aggregates of varying size corresponding to the alkyl chain length. A recent simulation study characterized the aggregate topology and found that from methanol to 1-octanol the aggregates were largely linear or branched, with only a small fraction (<5%) in ring or lasso aggregates. These authors also found the aggregate size to range from 1-5 nm throughout the series, with a trend toward larger diameter with increased alkyl chain length. The shift in the aggregate size distribution was found to be due largely to the increased size of the molecules rather than to the number of molecules in the aggregates. In fact, there was little variation in number density of the aggregates from methanol to 1-octanol, with roughly 4 molecules in linear aggregates and 15 molecules in branched aggregates (these values refer to maxima in the number density distributions). Thus despite the existence of aggregates, which certainly are responsible for rich structure and dynamics in alcohols, the solvent is nevertheless largely a well-mixed binary mixture of hydrophobic and hydrophilic components. We anticipate the framework described here to be instrumental in developing extended vibrational chromophores as probes of complex solvation environments such as alcohols, polymers and lipids.

We have reconsidered the delocalized coupled complex of carbonyl oscillators in $Mn_2(CO)_{10}$ as a vibrational aggregate, and have shown experimental and modeling results that indicate the complex can serve as a probe of large-scale hydrogen bonding solvation networks. Using an alcohol series to vary both the inhomogeneous broadening and the time scale for spectral diffusion, we find that DMDC is sensitive to local structure and dynamics in strongly interacting environments. With the alcohol series as a calibration, we identified several solvent systems consisting of pure solvents and solvent mixtures that result in identical linear FTIR spectra and inhomogeneous widths, but whose spectral diffusion time scales reflect the variation in solvent viscosity. To develop a predictive yet intuitive picture of the coupled vibrations in DMDC, we used an exciton model parameterized to reproduce the experimental transition frequencies and IR transition moments. With the simple addition of Gaussian site energy disorder, we found striking reproduction of several solvent dependent

spectral features observed experimentally. These included trends in the lineshape, reflecting the manifestation of pronounced exchange narrowing, and the appearance of IR inactive modes due to the disorder induced symmetry breaking. Correlations between sites also leads to testable signatures in the 2DIR spectrum in the form of correlated or anti-correlated cross peaks reflected in the tilts relative to the diagonal. Despite the many successes, the model fails to reproduce the lack of inhomogeneous broadening of the highest frequency IR mode, suggesting that qualitatively distinct dynamics or system-bath interactions influence that mode's transition energy. Beyond the 1D spectra and analysis of the one-exciton manifold, we computed the two-exciton manifold and used these states to simulate 2DIR spectra. These simulations largely confirm the observations of the analysis based only on the one-exciton manifold. The 2D simulations also demonstrated an effect of intersite frequency correlation on the 2D peak shapes, where negative site correlation was found to reduce the overall frequency correlation, particularly that probed in the excited state absorption band. This initial investigation prepares the groundwork for further computational studies using dynamical simulations in the place of static distributions, in order to extract the spectral diffusion dynamics as well as direct observation of coordinated hydrogen bonding solvation network rearrangements. Furthermore, DMDC can be incorporated into different complex environments providing a sensitive probe of local and global fluctuations with a high temporal dynamic range owing to the very long vibrational lifetime even in strongly interacting solvents.

2.3 Vibrational Lifetimes in Alcohols

We provide here a partial study of the vibrational lifetime of DMDC in two alcohol solvents, methanol and 1-hexanol. Through the data was collected to support the conclusions reached in **Section 2.4**, reviewing the results independently here will help provide a foundation for much of the work described in the coming chapters. The overall population relaxation could be influenced by the different hydrogen bonding environments presented from the alcohol solvents. To observe the influence of hydrogen bonds on T_1 relaxation we carried out T_1 relaxation measurements by analyzing the decay of the main vibrational mode of DMDC in the 2D rephasing spectra. In particular, we studied the two

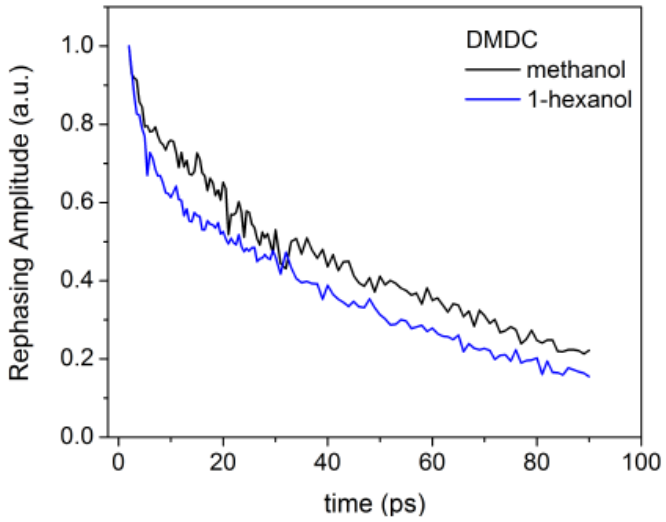

Figure 2.14 Vibrational relaxation of DMDC in two linear alcohols, methanol and 1-hexanol, that exhibited significantly different IVR timescales. From the data it is clear that the initial decay of the signal is different due to the fast IVR, but the slower T_1 relaxation is nearly identical in the two solvents.

solvents that showed significant differences in their IVR rates (**see Section 2.4**). **Figure 2.14** shows the decay in rephasing signal at waiting times approaching 100 ps, roughly the population relaxation time for DMDC in non-polar solvents like hexane. It is clearly seen that at early times DMDC in 1-hexanol shows a faster decay, reflecting the already observed trend that DMDC in 1-hexanol undergoes faster IVR on the 0-20 ps timescale. After the initial decay due to IVR, it is clear that the overall T_1 relaxation occurs not only on a much longer timescale, but is also not influenced to any significant amount by the change in solvent, recording values of 54 and 58 ps for methanol and 1-hexanol respectively. This data makes it clear that any small changes in the overall T_1 relaxation could not lead to large changes in IVR timescales that is seen through the alcohol series and presented in the next section.

2.4 Solvent-Hindered Intramolecular Vibrational Redistribution

The dissipation and transfer of vibrational energy is central to chemical reaction dynamics as a reactant approaches a barrier or descends from it to form a product.[85,86] In the gas phase, vibrational energy transfers through anharmonic coupling to the low-frequency modes of the molecule or via mechanisms involving, for example, a Fermi resonance.[87,88] In

solution, the increased low-frequency density of states provides ample degrees of freedom to accept or supply excess energy, generally accelerating the flow of vibrational energy relative to the case of an isolated gas-phase molecule.[89-97] This process, known as intramolecular vibrational redistribution (IVR), is traditionally considered a purely intramolecular process, though several experiments have made it evident that the solvent can indeed influence the IVR process through specific interactions.[90,97-99] Strong system bath coupling can lead to a higher density of states easily accessible to the system, and thus the IVR process is solvent-assisted. Here, we present an important counter example, and show that specific interactions arising from hydrogen bonding between solvent and solute can lead to solvent-hindered IVR. Adopting an exciton picture of delocalized vibrational modes, a hydrogen bond with the solvent introduces an energetic defect and traps the vibrational energy, thus slowing the rate of energy transfer. Aspects of this work have been seen by others,[100] but here we couple experimental data from a series of solvents with molecular dynamics simulations to show the remarkable influence on IVR caused by hydrogen bonding and solvation shell structure.

The standard treatment of IVR considers the energy gap ε_{ij} between two modes i and j and the density of states $\rho_B(\varepsilon_{ij})$ of the bath at that energy difference, which is generally modeled with an equilibrium Boltzmann distribution. Thus, for modes separated by an energy less than k_BT, both uphill and downhill energy transfer occurs,[101] and the temperature dependence of energy transfer can be easily predicted by the temperature dependence of $\rho_B(\varepsilon_{ij})$. In addition to this static energetic component is the dynamical fluctuation of the bath composed of all those degrees of freedom not directly probed spectroscopically.[98,102,103] The influence of the bath on relaxation processes such as IVR and homogeneous dephasing are related to the autocorrelation function of the force projected onto the transition dipole moment of the observed mode $\mathbf{q}$, such as $\langle F_{\mathbf{q}}(t)F_{\mathbf{q}}(0)\rangle$. Indeed, in the Landau-Teller description of vibrational relaxation, this correlation function is proportional to the friction felt by the classical oscillator.[102] Similar to the population relaxation, within the Redfield treatment of phase relaxation, the rate of homogeneous dephasing is also given in part by a time correlation function of the bath fluctuations, manifested as fluctuations of an interacting electric field.[104,105] Although the electric field and force fluctuations are distinct

physical manifestations of the bath, it is nevertheless reasonable to assume that they arise from the same underlying dynamics. Thus, one might expect a correlation between homogeneous dephasing and IVR rates.

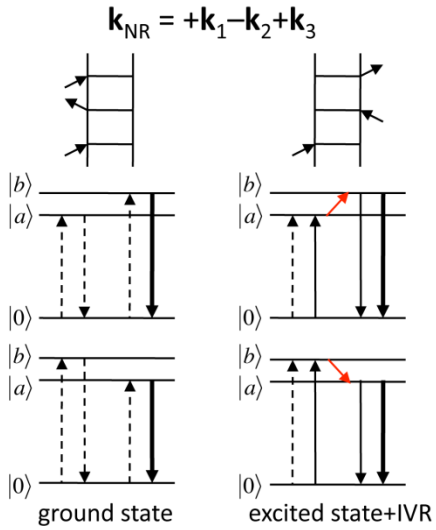

Figure 2.15 Double-sided Feynman diagrams for the cross peaks in a non-rephasing spectrum($k_{NR} = +k_1 - k_2 + k_3$,) with wave-matching energy level diagrams showing the ket (dashed) and bra (solid) sides of the density matrix as well as the emitted signal (bold solid). The red arrow indicates vibrational energy transfer due to IVR

This conventional treatment of IVR generally neglects specific interactions between the solute and solvent that may become significant when it is possible to form hydrogen bonds or other directional contacts. We have used a vibrational probe, the metal carbonyl complex $Mn_2(CO)_{10}$ (DMDC), to investigate the solvation environment in a series of linear alcohols ranging from methanol to 1-hexanol, and we have extracted time constants for IVR using two-dimensional infrared spectroscopy (2DIR). The terminal carbonyl stretches of DMDC are highly delocalized and thus are able to act as distributed sensors of the hydrogen bonded solvation shell dynamics. Using a series of linear alcohols allows a systematic variation of the hydrogen bonding environment as well as the solvation shell structure. It is important to stress that the frequencies of the system are not resonant with any Raman or IR fundamental transitions of the solvent bath; such resonances can significantly accelerate vibrational energy relaxation to the solvent. In previous work we analyzed the solvent influence on the frequency fluctuations of the vibrational eigenstates.[106] In the present study we investigate a

remarkable trend in the IVR time constants, for which we have developed a microscopic explanation by comparison to molecular dynamics simulations of DMDC in the full solvent series. In all the solvents investigated we find that the time constant for IVR is directly proportional to the average number of hydrogen bonds formed between the solute and solvent. That is, the more hydrogen bonds between the probe solute and the solvent bath, the slower the IVR process becomes. It is both noteworthy and surprising that an essentially geometrical factor such as hydrogen bond number determines the inherently dynamical IVR

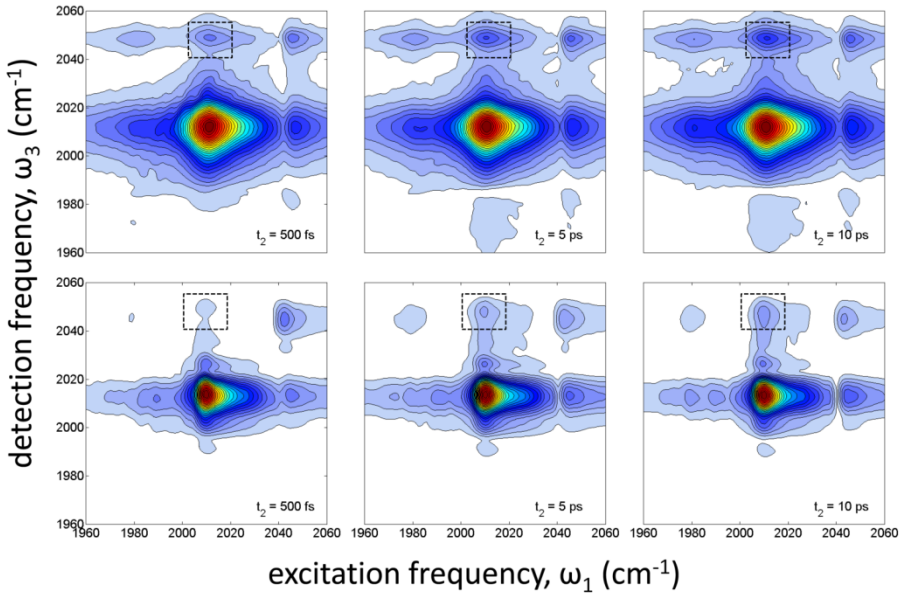

Figure 2.16 Absolute value non-rephasing spectra of DMDC in methanol (top panels) and 1-hexanol (bottom panels) shown at t_2 = 0.5, 5, 10 ps. The crosspeak that is analyzed for IVR timescales appears between main vibrational mode (excitation) and the high frequency mode (detection), highlighted with a dashed box.

process. These observations indicate the importance of structurally-specific solvent-hindered IVR, a phenomenon that would be expected to be significant in vibrational energy transfer in structured systems such as surfaces, interfaces, proteins and nucleic acids. We use an exciton picture of the delocalized vibrations to explain the observed IVR retardation caused by the formation of hydrogen bonds with the solvent.

The experimental data for this study consist of a series of 2DIR spectra recorded in methanol, ethanol, 1-propanol, 1-butanol, 1-pentanol, and 1-hexanol. The spectral aspects of DMDC in this series have been analyzed elsewhere (**see section 2.2**), and it was found for the central band (~2010 cm^{-1}) that the timescale for spectral diffusion—which describes the

loss of vibrational frequency memory—is a monotonically increasing function of solvent viscosity (i.e. chain length), whereas the inhomogeneous spectral width decreases monotonically with increased chain length. That study also measured ~2 cm^{-1} homogeneous line widths in all solvents except in ethanol where the observed with was 4 cm^{-1}.

Here, we analyzed specifically the non-rephasing 2DIR spectra which offer a clean probe of vibrational redistribution. Due to pulse ordering and phase matching of a non-rephasing sequence, any coherent vibrational dynamics that occur during the waiting time are contained in the diagonal peaks, whereas they appear at the cross peak locations in a rephasing spectrum.[41,64,107] We have analyzed these kinds of vibrational coherences in DMDC and other metal carbonyl systems, and while sometimes informative, for the purposes of isolating IVR they complicate the fitting and analysis.[41] In a non-rephasing 2D spectrum, the cross peak signal amplitude—in the absence of IVR—arises only from paths

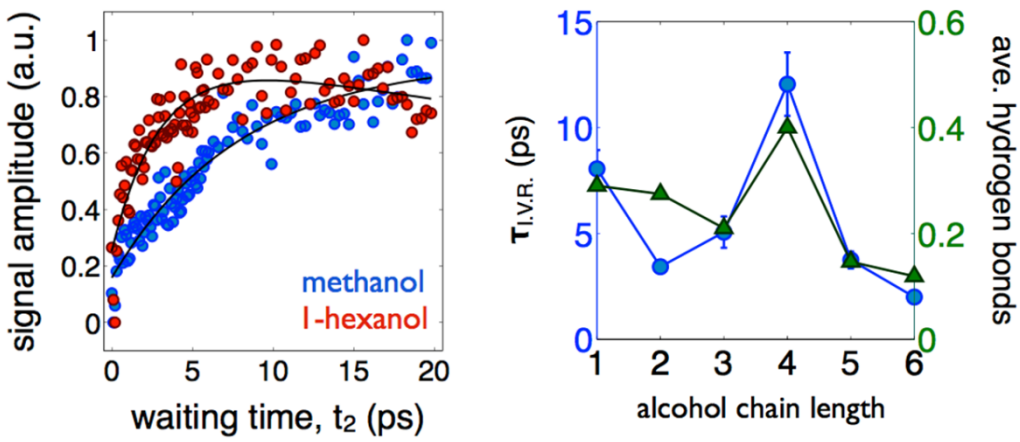

Figure 2.17 (left) Crosspeak traces for DMDC in two alcohol solvents, methanol and 1-hexanol. The traces illustrate a difference in the IVR rates between coupled vibrationally excited modes that is a function of the solvent. (right) The IVR timescales for the complete alcohol series, showing no clear trend with alkyl chain length, plotted with the average number of hydrogen bonds formed between the system and the bath determined from MD simulations.

that evolve as ground state populations during the waiting time (t_2). A rise in the non-rephasing cross peak amplitude requires IVR, which transfers energy from one eigenstate to another during t_2, as depicted in **Figure 2.15**. The time evolution of these cross peaks is thus due to vibrational relaxation, orientational relaxation and IVR. Because nanometer scale molecules in alcohols orientationally diffuse on >100 ps time scales,[108-111] our measurements are free from the complications of molecular orientational relaxation. Moreover, simple

inspection of molecular dynamics trajectories show minimal orientational diffusion on the <50 ps time scale for all the solvents considered (**see Section 2.2**). Our IVR measurements are also free from population relaxation effects.The T_1 vibrational lifetime of DMDC (i.e. the time to vibrationally relax to the ground state) is longer than 50 ps even in alcohol solvents. Furthermore, for the two solvents that exhibit the largest differences in IVR time constants—methanol and 1-hexanol—we find theT_1 vibrational energy relaxation (VER) to be identical (**see Section 2.2**). This solvent invariance of the lifetime allows us to extract the IVR timescales without interference from other relaxation processes.

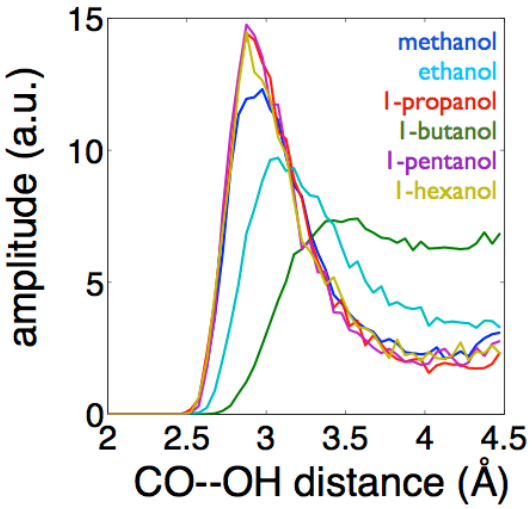

Figure 2.18 Hydrogen bond distances between the CO units of DMDC and the hydroxyl groups of the alcohol solvent obtained from MD simulations. It is clear that particular alcohol solvents, namely ethanol and 1-butanol, form solvation shells that are structurally different from the other alcohol solvents.

Figure 2.16 shows non-rephasing 2DIR spectra of DMDC in methanol and 1-hexanol at three different waiting times t_2, with a dashed box indicating the cross peak between the central 2010 cm^{-1} band and the high-frequency 2045 cm^{-1} mode used for the IVR analysis. It should be noted that the central band consists of contributions from two modes that are degenerate in the gas phase as well as in non-polar solvents. In the hydrogen bonding solvents, the two modes are split due to the site disorder which lowers the overall energetic symmetry of the molecule. The appearance of Raman active vibrations in the IR spectrum is

another manifestation of this disorder-induced symmetry breaking, an observation discussed in detail in previous work.[106]

Figure 2.17a shows time dependent traces of the highlighted cross peak with single exponential fits. Time constants extracted from single-exponential fits to waiting time dependent cross peak amplitudes in all six solvents are shown in **Figure 2.17b**. At first glance, it is not apparent that the time constants—which correspond directly to IVR—follow any obvious trend, a fact that is in stark contrast to our previous observations of the inhomogeneous widths and spectral diffusion time constants that tracked alkyl chain length. Also plotted in the same figure, however, is the average number of hydrogen bonds between the DMDC solute and each alcohol solvent determined by equilibrium molecular dynamics simulations (see details in the supporting information, SI). There is a clear correspondence

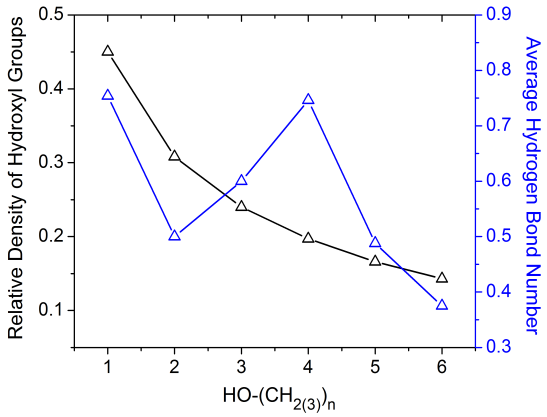

Figure 2.19 Plot of the hydroxyl group density as a function of the alcohol solvent (black). It shows the expected trend, as the alkyl chain of the solvent is increased, there is a lower relative volume of OH groups and thus less hydrogen bonds. Plotted with this is again the average hydrogen bond number calculated from MD simulations (blue). It appears that both ethanol and 1-butanol deviate from the expected trend, which are the two solvents that have unique solvation shell structures.

between the *average* number of hydrogen bonds and the IVR time constants across the solvent series. Again, the *more* hydrogen bonds the solute forms with the solvent, the *slower* the IVR process becomes. Thus, it is clear that the solvent significantly influences the rate of vibrational energy transfer, but that the relevant parameter seems to be neither energetic (i.e. $\rho_B(\varepsilon_{ij})$) nor dynamic (i.e. $\langle F_q(t)F_q(0)\rangle$), but rather structural in nature.

To explain the observation of solvent-hindered IVR, the first traditional component

of IVR that can be ruled out is the dynamical fluctuation of the bath. As discussed above, the underlying physical origins of the frequency and electric field fluctuations that enter the Landau-Teller and Redfield models of population and phase relaxation reflect common molecular dynamics. Our previous study of the solvent-dependent spectral diffusion of DMDC in the same solvent series yielded homogeneous and inhomogeneous contributions to the vibrational lineshape as well as the time scale for spectral diffusion. That work found a roughly constant 2 cm^{-1} homogeneous line width for all the solvents except ethanol. The inhomogeneous widths and spectral diffusion time constants, however, showed a simple solvent viscosity dependence, indicating that both the structural diversity of the solvation environment and its fluctuations were linked to the alkyl chain length and solvent dynamics. These observations indicate that the fast bath dynamics responsible for the motionally-narrowed (homogeneous) line width are relatively insensitive to solvent viscosity, and that the slower dynamics leading to loss of frequency correlation tracked viscosity. Thus, should the IVR time scale be determined by either of these two dynamical factors, we would have expected to see either no solvent dependence, or one that followed the solvent viscosity.

The energetic component is more subtle because of the complex role the solvent can play in assisting IVR through anharmonic coupling to the solute's degrees of freedom. In general, however, most investigations have found that solvent assistance leads to IVR that is faster than observed in solvents that do not assist IVR.[90,95,97,100] This acceleration is due to the increased number of transfer pathways available in a strongly interacting solvent. In our study, we find that the solvent is also capable of playing the opposite role, slowing the rate of IVR through specific interactions. Our system shows that the strong coupling between the system and the bath through hydrogen bonds hinders the IVR rate. This is an important counter example illustrating the complexity of the solvent's influence on intramolecular processes when the system states are delocalized and the solvation environment is structured.

It is interesting that the homogeneous dynamics of DMDC in ethanol are so much faster than in the other solvents. MD simulations enable an interpretation of this dynamical difference from the perspective of the average solvation shell structure. **Figure 2.18** shows

radial distribution functions derived from the MD simulations between the DMDC oxygen hydrogen bond acceptors and the oxygen atoms of the alcohol solvents which have the potential to participate in a hydrogen bond. While most of the solvents show a similar solvation shell density, ethanol clearly deviates. The fact that the solvation shell in ethanol is much less tightly packed than it is in the other solvents implies that the DMDC carbonyls are less constrained and thus are able to exhibit more rapid motion.

Similar observations have been made in the heterogeneous spectrum of the OH stretch of water and in the isotopic variants, where the "homogeneous" line widths of OH oscillators on the blue edge of the band are broader than those on the red edge.[10,112,113] The higher-frequency OH stretches correspond to longer and weaker hydrogen bonds, whereas the lower-frequency region is composed of shorter and stronger hydrogen bonds. Indeed, our earlier experiments found the homogeneous width of DMDC's central band in ethanol to be nearly a factor of two broader than in the other alcohols studied.

The solvation structure of 1-butanol also deviates from the structures of the other four solvents. It is interesting to compare the solvation structures of these solvents with the hydrogen bond statistics. If we consider the number of hydrogen bonds formed between the solute and the solvent to be a function of the percent composition of hydroxyl groups compared to the complete volume, then the relative number of hydrogen bonds can be estimated based on molar volumes. A simple calculation was carried out to estimate the percent of the total solvent volume that is comprised of hydroxyl groups (**Figure 2.19)**. Viewed from this perspective, the extracted average numbers of hydrogen bonds generally follow the continuum-like trend, with the exception of ethanol and 1-butanol. This observation is mirrored by the computed radial distribution functions that also show marked deviations for ethanol and 1-butanol relative to the other liquids. We thus propose that the unique solvation structure is responsible for the unexpected solvent specificity of solute-solvent hydrogen bonding. Radial distribution functions and average hydrogen bond numbers are clearly not dynamic quantities, and it is most certainly the case that to predict the absolute magnitude of the IVR time constant it will be necessary to evaluate the force autocorrelation function. Nevertheless, here we are focused primarily on the trend with

respect to solvent chain length that is clearly observed in experiment. A full computational treatment of spectral and vibrational dynamics is beyond the scope of this communication and will be the subject of a future manuscript.

Why do hydrogen bonds trap vibrational excitation, thus hindering IVR? To answer this question, we combine our recently implemented "vibrational aggregate" picture of the many coupled carbonyl oscillators of DMDC and the well-known empirical correlation between metal carbonyl site energies and the coupling between sites. We have found a 10-site excitonic Hamiltonian to be capable of reproducing features of the 1D and 2DIR spectra of DMDC upon incorporation of gaussian site energy disorder uniformly to all 10 sites. The experimental and simulation data indicate, however, that IVR is controlled by directional hydrogen bonding. In metal carbonyl complexes a hydrogen bond formed with a single CO site has a non-local effect due to the alteration of the π back bonding between the metal and both the hydrogen bonded site and the remaining sites.[114-116] For a dicarbonyl the consequence is straightforward: electron density shifts from the carbonyl to the hydrogen bond, reducing electron density on the metal that was previously available due to back bonding. The reduced metal electron density weakens the π back bonding with the non-hydrogen bonded carbonyl, which blue shifts that site's frequency. The anti-correlated site energy shifts serve to reduce the coupling between the sites, and viewed from the perspective of the molecular eigenstates, the resulting exciton becomes localized. Although the non-local nature of the hydrogen bonded carbonyl complicates a detailed microscopic picture, it magnifies the degree of exciton localization and supports the interpretation that in these extended, coupled vibrational systems hydrogen bonds spatially trap vibrational excitation, inhibiting IVR. Since the hydrogen bonding that traps the vibrational excitons and hinders IVR is also responsible to some degree for the vibrational frequency fluctuations, we would expect some link between the two dynamical observables. Future work using MD simulation will implement a frequency mapping approach for site energies combined with the empirical force-field to predict 2DIR spectra as well as energy transfer and spectral dynamics. These simulations will help to explain why the spectral diffusion and IVR time scales appear to be decoupled.

The experimental results presented here, in conjunction with the analysis of a series of molecular dynamics simulations, shows that solvent-hindered IVR in condensed phase molecules can be viewed as an exciton transport subject to the presence of local traps. Since the hydrogen bonding environment constantly fluctuates, these traps are transient in nature, and thus mix the spatial overlap and energy matching with the bath dynamics contributions to the IVR rate. There are clear analogies with vibrational energy flow in peptides and proteins, where the amide I carbonyl band is similarly excitonic and subject to defects due to variations in local hydrogen bonding. Distortions in the secondary structure could induce changes in the location of traps, which in turn may influence the flow of vibrational energy. Such vibrational energy transfer is one of the proposed origins of long-range communication required for allosteric regulation. In the context of smaller transition metal organic complexes, the efficient flow of excess vibrational energy may play a role in the dynamics of selective catalysis, which is a largely unexplored aspect of condensed phase reaction dynamics.

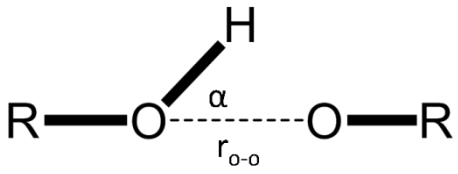

Figure 2.20. Criteria used for counting hydrogen bonds. $\alpha \leq 30^{o}$, $r_{o-o} \leq 3.5$ Å.

Molecular Dynamics (MD) simulations were used to determine the average number of hydrogen bonds between the vibrational probe and the solvent. For each simulation, DMDC was placed in a cubic box containing between 500 and 520 solvent molecules, with periodic boundary conditions in all directions. The simulations were carried out using the NPT ensemble, where temperature and pressure where held constant at 298 K and 1 bar using the Berendsen coupling scheme. The particle-mesh Ewald summation method was used to account for long range electrostatic interactions. Simulations were carried out for 50 ps with 1 fs step sizes. The force field of DMDC was constructed using DFT calculations, carried out using the B3LYP functional and the 6-31+G(d) basis set for the oxygen and carbon atoms and the LANL2DZ pseudopotential for the manganese atoms. The general AMBER

force field was used to describe the solvent molecules, ranging from methanol to 1-hexanol, where optimized structures were found from DFT calculations using the B3LYP functional and the 6-31+G(d) basis.

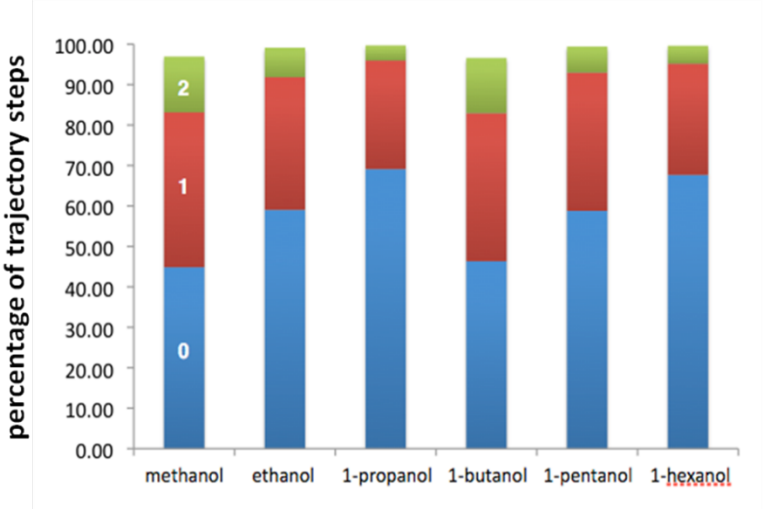

Figure 2.21 Breakdown of the hydrogen bond statistics for this system. The number of hydrogen bonds formed between solute and solvent, shown are 0-2, and the percentage of steps in the MD simulation in which this number of hydrogen bonds is found.

The hydrogen bonding statistics were determined using the g_hbond function of the GROMACS package, where the default and most commonly implemented criteria for a hydrogen bond were used. These criteria are an oxygen to oxygen distance ($r_{o\text{-}o}$) of 3.5 Å or less, and an angle (α) between the oxygen-oxygen bond and the oxygen-hydrogen bond of 30^{o} or less (**Figure 2.20**). The g_hbond function will characterize the hydrogen bonding environment based on these criteria, where the presence of hydrogen bonds between selected groups (in this case the solute and the solvent) are counted during each time step of the simulation. Therefore, for each step in the simulation, the g_hbond function counts the number of solvent molecules that satisfy the hydrogen bond criterion described above and shown in **Figure 2.20**. For this study, we used a simple measure of the total number of hydrogen bonds between bath and solute per time step, averaged over the entire MD trajectory.

Figure 2.21 shows the percentage of steps in the molecular dynamics simulation where the corresponding number of hydrogen bonds is observed. It can be seen that for all of the solvents, the solute is only participating in a hydrogen bond with a solvent molecule for

roughly half of the steps. The steps in which the solute is hydrogen bonding with the solvent are further broken down into percentage of the steps in which one hydrogen bond is formed and the percentage of the steps in which two hydrogen bonds are formed. The differences in hydrogen bonding number can also be seen from this graph, where methanol and 1-butanol clearly show the largest degree of hydrogen bonding.

2.5 Conclusions

We have reconsidered the delocalized coupled complex of carbonyl oscillators in $Mn_2(CO)_{10}$ as a vibrational aggregate, and have shown experimental and modeling results that indicate the complex can serve as a probe of large-scale hydrogen bonding solvation networks. Using an alcohol series to vary both the inhomogeneous broadening and the time scale for spectral diffusion, we find that DMDC is sensitive to local structure and dynamics in strongly interacting environments. With the alcohol series as a calibration, we identified several solvent systems consisting of pure solvents and solvent mixtures that result in identical linear FTIR spectra and inhomogeneous widths, but whose spectral diffusion time scales reflect the variation in solvent viscosity. To develop a predictive yet intuitive picture of the coupled vibrations in DMDC, we used an exciton model parameterized to reproduce the experimental transition frequencies and IR transition moments. With the simple addition of Gaussian site energy disorder, we found striking reproduction of several solvent dependent spectral features observed experimentally. These included trends in the lineshape, reflecting the manifestation of pronounced exchange narrowing, and the appearance of IR inactive modes due to the disorder induced symmetry breaking. Correlations between sites also leads to testable signatures in the 2DIR spectrum in the form of correlated or anti-correlated cross peaks reflected in the tilts relative to the diagonal. Despite the many successes, the model fails to reproduce the lack of inhomogeneous broadening of the highest frequency IR mode, suggesting that qualitatively distinct dynamics or system-bath interactions influence that mode's transition energy. Beyond the 1D spectra and analysis of the one-exciton manifold, we computed the two-exciton manifold and used these states to simulate 2DIR spectra. These simulations largely confirm the observations of the analysis based only on the one-exciton manifold. The 2D simulations also demonstrated an effect of intersite frequency

correlation on the 2D peak shapes, where negative site correlation was found to reduce the overall frequency correlation, particularly that probed in the excited state absorption band. This initial investigation prepares the groundwork for further computational studies using dynamical simulations in the place of static distributions, in order to extract the spectral diffusion dynamics as well as direct observation of coordinated hydrogen bonding solvation network rearrangements.

In addition, the experimental results presented here, in conjunction with the analysis of a series of molecular dynamics simulations, shows that solvent-hindered IVR in condensed phase molecules can be viewed as an exciton transport subject to the presence of local traps. Since the hydrogen bonding environment constantly fluctuates, these traps are transient in nature, and thus mix the spatial overlap and energy matching with the bath dynamics contributions to the IVR rate. There are clear analogies with vibrational energy flow in peptides and proteins, where the amide I carbonyl band is similarly excitonic and subject to defects due to variations in local hydrogen bonding. Distortions in the secondary structure could induce changes in the location of traps, which in turn may influence the flow of vibrational energy. Such vibrational energy transfer is one of the proposed origins of long-range communication required for allosteric regulation. In the context of smaller transition metal organic complexes, the efficient flow of excess vibrational energy may play a role in the dynamics of selective catalysis, which is a largely unexplored aspect of condensed phase reaction dynamics.

References:

(1) Kwak, K.; Park, S.; Finkelstein, I. J.; Fayer, M. D.: Frequency-frequency correlation functions and apodization in two-dimensional infrared vibrational echo spectroscopy: A new approach. *Journal of Chemical Physics* **2007**, *127*.

(2) Elsaesser, T.: Two-Dimensional Infrared Spectroscopy of Intermolecular Hydrogen Bonds in the Condensed Phase. *Accounts of Chemical Research* **2009**, *42*, 1220-1228.

(3) Kim, Y. S.; Hochstrasser, R. M.: Chemical exchange 2D IR of hydrogen-bond making and breaking. *Proceedings of the National Academy of Sciences of the United States of America* **2005**, *102*, 11185-11190.

(4) Asbury, J. B.; Steinel, T.; Stromberg, C.; Corcelli, S. A.; Lawrence, C. P.; Skinner, J. L.; Fayer, M. D.: Water dynamics: Vibrational echo correlation spectroscopy and comparison to molecular dynamics simulations. *Journal of Physical Chemistry A* **2004**, *108*, 1107-1119.

(5) Asbury, J. B.; Steinel, T.; Fayer, M. D.: Hydrogen bond networks: Structure and evolution after hydrogen bond breaking. *Journal of Physical Chemistry B* **2004**, *108*, 6544-6554.

(6) Zheng, J. R.; Fayer, M. D.: Hydrogen bond lifetimes and energetics for solute/solvent complexes studied with 2D-IR vibrational echo spectroscopy. *Journal of the American Chemical Society* **2007**, *129*, 4328-4335.

(7) Fecko, C. J.; Eaves, J. D.; Loparo, J. J.; Tokmakoff, A.; Geissler, P. L.: Ultrafast hydrogen-bond dynamics in the infrared spectroscopy of water. *Science* **2003**, *301*, 1698-1702.

(8) Fecko, C. J.; Loparo, J. J.; Roberts, S. T.; Tokmakoff, A.: Local hydrogen bonding dynamics and collective reorganization in water: Ultrafast infrared spectroscopy of HOD/D2O. *Journal of Chemical Physics* **2005**, *122*.

(9) Nicodemus, R. A.; Ramasesha, K.; Roberts, S. T.; Tokmakoff, A.: Hydrogen Bond Rearrangements in Water Probed with Temperature-Dependent 2D IR. *Journal of Physical Chemistry Letters* **2010**, *1*, 1068-1072.

(10) Roberts, S. T.; Ramasesha, K.; Tokmakoff, A.: Structural Rearrangements in Water Viewed Through Two-Dimensional Infrared Spectroscopy. *Accounts of Chemical Research* **2009**, *42*, 1239-1249.

(11) Bakker, H. J.; Skinner, J. L.: Vibrational Spectroscopy as a Probe of Structure and Dynamics in Liquid Water. *Chemical Reviews* **2010**, *110*, 1498-1517.

(12) Stirnemann, G.; Laage, D.: Direct Evidence of Angular Jumps During Water Reorientation Through Two-Dimensional Infrared Anisotropy. *Journal of Physical Chemistry Letters* **2010**, *1*, 1511-1516.

(13) Cho, M.: Coherent two-dimensional optical spectroscopy. *Chemical Reviews* **2008**, *108*, 1331-1418.

(14) Woys, A. M.; Lin, Y.-S.; Reddy, A. S.; Xiong, W.; de Pablo, J. J.; Skinner, J. L.; Zanni, M. T.: 2D IR Line Shapes Probe Ovispirin Peptide Conformation and Depth in Lipid Bilayers. *Journal of the American Chemical Society* **2010**, *132*, 2832-2838.

(15) Sengupta, N.; Maekawa, H.; Zhuang, W.; Toniolo, C.; Mukamel, S.; Tobias, D. J.; Ge, N.-H.: Sensitivity of 2D IR Spectra to Peptide Helicity: A Concerted Experimental and Simulation Study of an Octapeptide. *Journal of Physical Chemistry B* **2009**, *113*, 12037-12049.

(16) Ganim, Z.; Chung, H. S.; Smith, A. W.; Deflores, L. P.; Jones, K. C.; Tokmakoff, A.: Amide I two-dimensional infrared Spectroscopy of proteins. *Accounts of Chemical Research* **2008**, *41*, 432-441.

(17) Ihalainen, J. A.; Paoli, B.; Muff, S.; Backus, E. H. G.; Bredenbeck, J.; Woolley, G. A.; Caflisch, A.; Hamm, P.: alpha-Helix folding in the presence of structural constraints. *Proceedings of the National Academy of Sciences of the United States of America* **2008**, *105*, 9588-9593.

(18) Zhuang, W.; Hayashi, T.; Mukamel, S.: Coherent Multidimensional Vibrational Spectroscopy of Biomolecules: Concepts, Simulations, and Challenges. *Angewandte Chemie-International Edition* **2009**, *48*, 3750-3781.

(19) Schmidt, J. R.; Corcelli, S. A.; Skinner, J. L.: Pronounced non-Condon effects in the ultrafast infrared spectroscopy of water. *Journal of Chemical Physics* **2005**, *123*.

(20) DeCamp, M. F.; DeFlores, L.; McCracken, J. M.; Tokmakoff, A.; Kwac, K.; Cho, M.: Amide I vibrational dynamics of N-methylacetamide in polar solvents: The role of electrostatic interactions. *Journal of Physical Chemistry B* **2005**, *109*, 11016-11026.

(21) Jansen, T. L.; Hayashi, T.; Zhuang, W.; Mukamel, S.: Stochastic Liouville equations for hydrogen-bonding fluctuations and their signatures in two-dimensional vibrational spectroscopy of water. *Journal of Chemical Physics* **2005**, *123*.

(22) Skinner, J. L.; Auer, B. M.; Lin, Y.-S.: Vibrational Line Shapes, Spectral Diffusion, and Hydrogen Bonding in Liquid Water. *Advances in Chemical Physics, Vol 142*; Rice, S. A., Ed., 2009; Vol. 142; pp 59-103.

(23) Paarmann, A.; Hayashi, T.; Mukamel, S.; Miller, R. J. D.: Nonlinear response of vibrational excitons: Simulating the two-dimensional infrared spectrum of liquid water. *Journal of Chemical Physics* **2009**, *130*.

(24) Choi, J.-H.; Oh, K.-I.; Cho, M.: Azido-derivatized compounds as IR probes of local electrostatic environment: Theoretical studies. *Journal of Chemical Physics* **2008**, *129*.

(25) Choi, J.-H.; Oh, K.-I.; Lee, H.; Lee, C.; Cho, M.: Nitrile and thiocyanate IR probes: Quantum chemistry calculation studies and multivariate least-square fitting analysis. *Journal of Chemical Physics* **2008**, *128*.

(26) Oh, K.-I.; Choi, J.-H.; Lee, J.-H.; Han, J.-B.; Lee, H.; Cho, M.: Nitrile and thiocyanate IR probes: Molecular dynamics simulation studies. *Journal of Chemical Physics* **2008**, *128*.

(27) Lindquist, B. A.; Haws, R. T.; Corcelli, S. A.: Optimized Quantum Mechanics/Molecular Mechanics Strategies for Nitrile Vibrational Probes: Acetonitrile and para-Tolunitrile in Water and Tetrahydrofuran. *Journal of Physical Chemistry B* **2008**, *112*, 13991-14001.

(28) Lindquist, B. A.; Corcelli, S. A.: Nitrile groups as vibrational probes: Calculations of the C N infrared absorption line shape of acetonitrile in water and tetrahydrofuran. *Journal of Physical Chemistry B* **2008**, *112*, 6301-6303.

(29) Jansen, T. L. C.; Auer, B. M.; Yang, M.; Skinner, J. L.: Two-dimensional infrared spectroscopy and ultrafast anisotropy decay of water. *Journal of Chemical Physics* **2010**, *132*.

(30) Lehtola, J.; Hakala, M.; Hamalainen, K.: Structure of Liquid Linear Alcohols. *Journal of Physical Chemistry B* **2010**, *114*, 6426-6436.

(31) Tomsic, M.; Jamnik, A.; Fritz-Popovski, G.; Glatter, O.; Vlcek, L.: Structural properties of pure simple alcohols from ethanol, propanol, butanol, pentanol, to hexanol: Comparing Monte Carlo simulations with experimental SAXS data. *Journal of Physical Chemistry B* **2007**, *111*, 1738-1751.

(32) Vahvaselka, K. S.; Serimaa, R.; Torkkeli, M.: Determination of Liquid Structures of the Primary Alcohols Methanol, Ethanol, 1-Propanol, 1-Butanol and 1-Octanol by X-Ray-Scattering. *J. Appl. Crystallogr.* **1995**, *28*, 189-195.

(33) Wilson, K. R.; Cavalleri, M.; Rude, B. S.; Schaller, R. D.; Catalano, T.; Nilsson, A.; Saykally, R. J.; Pettersson, L. G. M.: X-ray absorption spectroscopy of liquid methanol microjets: Bulk electronic structure and hydrogen bonding network. *Journal of Physical Chemistry B* **2005**, *109*, 10194-10203.

(34) Abramavicius, D.; Palmieri, B.; Voronine, D. V.; Sanda, F.; Mukamel, S.: Coherent Multidimensional Optical Spectroscopy of Excitons in Molecular Aggregates; Quasiparticle versus Supermolecule Perspectives. *Chemical Reviews* **2009**, *109*, 2350-2408.

(35) Bakalis, L. D.; Knoester, J.: Pump-probe spectroscopy and the exciton delocalization length in molecular aggregates. *Journal of Physical Chemistry B* **1999**, *103*, 6620-6628.

(36) Knapp, E. W.: Lineshapes of Molecular Aggregates - Exchange Narrowing and Intersite Correlation. *Chemical Physics* **1984**, *85*, 73-82.

(37) Didraga, C.; Knoester, J.: Exchange narrowing in circular and cylindrical molecular aggregates: degenerate versus nondegenerate states. *Chemical Physics* **2002**, *275*, 307-318.

(38) Mukamel, S.; Tretiak, S.; Wagersreiter, T.; Chernyak, V.: Electronic coherence and collective optical excitations of conjugated molecules. *Science* **1997**, *277*, 781-787.

(39) Dahlbom, M.; Pullerits, T.; Mukamel, S.; Sandstrom, V.: Exciton delocalization in the B850 light-harvesting complex: Comparison of different measures. *Journal of Physical Chemistry B* **2001**, *105*, 5515-5524.

(40) Laage, D.; Hynes, J. T.: A molecular jump mechanism of water reorientation. *Science* **2006**, *311*, 832-835.

(41) Nee, M. J.; Baiz, C. R.; Anna, J. M.; McCanne, R.; Kubarych, K. J.: Multilevel vibrational coherence transfer and wavepacket dynamics probed with multidimensional IR spectroscopy. *Journal of Chemical Physics* **2008**, *129*.

(42) Baiz, C. R.; Nee, M. J.; McCanne, R.; Kubarych, K. J.: Ultrafast nonequilibrium Fourier-transform two-dimensional infrared spectroscopy. *Optics Letters* **2008**, *33*, 2533-2535.

(43) Baiz, C. R.; McRobbie, P. L.; Anna, J. M.; Geva, E.; Kubarych, K. J.: Two-Dimensional Infrared Spectroscopy of Metal Carbonyls. *Accounts of Chemical Research* **2009**, *42*, 1395-1404.

(44) Baiz, C. R.; McRobbie, P. L.; Preketes, N. K.; Kubarych, K. J.; Geva, E.: Two-Dimensional Infrared Spectroscopy of Dimanganese Decacarbonyl and Its Photoproducts: An Ab Initio Study. *Journal of Physical Chemistry A* **2009**, *113*, 9617-9623.

(45) Pullerits, T.; Chachisvilis, M.; Sundstrom, V.: Exciton delocalization length in the B850 antenna of Rhodobacter sphaeroides. *Journal of Physical Chemistry* **1996**, *100*, 10787-10792.

(46) Krueger, B. P.; Scholes, G. D.; Fleming, G. R.: Calculation of couplings and energy-transfer pathways between the pigments of LH2 by the ab initio transition density cube method (vol 102B, pg 5384, 1998). *Journal of Physical Chemistry B* **1998**, *102*, 9603-9603.

(47) van Amerongen, H.; van Grondelle, R.: Understanding the energy transfer function of LHCII, the major light-harvesting complex of green plants. *Journal of Physical Chemistry B* **2001**, *105*, 604-617.

(48) Durrant, J. R.; Knoester, J.; Wiersma, D. A.: Local Energetic Disorder in Molecular Aggregates Probed by the One-Exciton to 2-Exciton Transition. *Chemical Physics Letters* **1994**, *222*, 450-456.

(49) Kano, H.; Kobayashi, T.: Real-time spectroscopy of the excited-state excitons in porphyrin J-aggregates. *Bulletin of the Chemical Society of Japan* **2002**, *75*, 1071-1074.

(50) Dijkstra, A. G.; Jansen, T. L. C.; Knoester, J.: Localization and coherent dynamics of excitons in the two-dimensional optical spectrum of molecular J-aggregates. *Journal of Chemical Physics* **2008**, *128*.

(51) Milota, F.; Sperling, J.; Nemeth, A.; Mancal, T.; Kauffmann, H. F.: Two-Dimensional Electronic Spectroscopy of Molecular Excitons. *Accounts of Chemical Research* **2009**, *42*, 1364-1374.

(52) Womick, J. M.; Miller, S. A.; Moran, A. M.: Probing the Dynamics of Intraband Electronic Coherences in Cylindrical Molecular Aggregates. *Journal of Physical Chemistry A* **2009**, *113*, 6587-6598.

(53) Collini, E.; Scholes, G. D.: Coherent Intrachain Energy Migration in a Conjugated Polymer at Room Temperature. *Science* **2009**, *323*, 369-373.

(54) Anderson, P. W.: Absense of Diffusion in Certain Random Lattices. *Physical Review* **1958**, *109*, 1492-1505.

(55) Knoester, J.: Nonlinear Optical Susceptibilities of Disordered Agggregates - A Comparison of Schemes to Account for Intermolecular Interactions. *Physical Review A* **1993**, *47*, 2083-2098.

(56) Faeder, S. M. G.; Jonas, D. M.: Two-dimensional electronic correlation and relaxation spectra: Theory and model calculations. *Journal of Physical Chemistry A* **1999**, *103*, 10489-10505.

(57) Hybl, J. D.; Ferro, A. A.; Jonas, D. M.: Two-dimensional Fourier transform electronic spectroscopy. *Journal of Chemical Physics* **2001**, *115*, 6606-6622.

(58) Khalil, M.; Demirdoven, N.; Tokmakoff, A.: Obtaining absorptive line shapes in two-dimensional infrared vibrational correlation spectra. *Physical Review Letters* **2003**, *90*.

(59) Khalil, M.; Demirdoven, N.; Tokmakoff, A.: Coherent 2D IR spectroscopy: Molecular structure and dynamics in solution. *Journal of Physical Chemistry A* **2003**, *107*, 5258-5279.

(60) Roberts, S. T.; Loparo, J. J.; Tokmakoff, A.: Characterization of spectral diffusion from two-dimensional line shapes. *Journal of Chemical Physics* **2006**, *125*.

(61) Kwak, K.; Rosenfeld, D. E.; Fayer, M. D.: Taking apart the two-dimensional infrared vibrational echo spectra: More information and elimination of distortions. *Journal of Chemical Physics* **2008**, *128*.

(62) Kuroda, D. G.; Vorobyev, D. Y.; Hochstrasser, R. M.: Ultrafast relaxation and 2D IR of the aqueous trifluorocarboxylate ion. *Journal of Chemical Physics* **2010**, *132*.

(63) Nee, M. J.; McCanne, R.; Kubarych, K. J.; Joffre, M.: Two-dimensional infrared spectroscopy detected by chirped pulse upconversion. *Optics Letters* **2007**, *32*, 713-715.

(64) Ogilvie, J. P.; Kubarych, K. J.: Multidimensional Electronic and Vibrational Spectroscopy: An Ultrafast Probe of Molecular Relaxation and Reaction Dynamics. *Advances in Atomic, Molecular, and Optical Physics, Vol 57* **2009**, *57*, 249-321.

(65) Anna, J. M.; Nee, M. J.; Baiz, C. R.; McCanne, R.; Kubarych, K. J.: Measuring absorptive two-dimensional infrared spectra using chirped-pulse upconversion detection. *Journal of the Optical Society of America B-Optical Physics* **2010**, *27*, 382-393.

(66) Lee, K. F.; Nuernberger, P.; Bonvalet, A.; Joffre, M.: Removing cross-phase modulation from midinfrared chirped-pulse upconversion spectra. *Optics Express* **2009**, *17*, 18738-18744.

(67) Chernyak, V.; Zhang, W. M.; Mukamel, S.: Multidimensional femtosecond spectroscopies of molecular aggregates and semiconductor nanostructures: The nonlinear exciton equations. *Journal of Chemical Physics* **1998**, *109*, 9587-9601.

(68) Gharavi, M.; Buckley, S. G.: Single diode laser sensor for wide-range H2O temperature measurements. *Applied Spectroscopy* **2004**, *58*, 468-473.

(69) Vlaming, S. M.; Malyshev, V. A.; Knoester, J.: Localization properties of one-dimensional Frenkel excitons: Gaussian versus Lorentzian diagonal disorder. *Physical Review B* **2009**, *79*.

(70) Zhuang, W.; Abramavicius, D.; Hayashi, T.; Mukamel, S.: Simulation protocols for coherent femtosecond vibrational spectra of peptides. *Journal of Physical Chemistry B* **2006**, *110*, 3362-3374.

(71) Piletic, I. R.; Moilanen, D. E.; Levinger, N. E.; Fayer, M. D.: What nonlinear-IR experiments can tell you about water that the IR spectrum cannot. *Journal of the American Chemical Society* **2006**, *128*, 10366-10367.

(72) Anna, J. M.; Ross, M. R.; Kubarych, K. J.: Dissecting Enthalpic and Entropic Barriers to Ultrafast Equilibrium Isomerization of a Flexible Molecule Using 2DIR Chemical Exchange Spectroscopy. *Journal of Physical Chemistry A* **2009**, *113*, 6544-6547.

(73) Engel, G. S.; Calhoun, T. R.; Read, E. L.; Ahn, T.-K.; Mancal, T.; Cheng, Y.-C.; Blankenship, R. E.; Fleming, G. R.: Evidence for wavelike energy transfer through quantum coherence in photosynthetic systems. *Nature* **2007**, *446*, 782-786.

(74) Collini, E.; Wong, C. Y.; Wilk, K. E.; Curmi, P. M. G.; Brumer, P.; Scholes, G. D.: Coherently wired light-harvesting in photosynthetic marine algae at ambient temperature. *Nature* **2010**, *463*, 644-U69.

(75) Jansen, T. I. C.; Cringus, D.; Pshenichnikov, M. S.: Dissimilar Dynamics of Coupled Water Vibrations. *Journal of Physical Chemistry A* **2009**, *113*, 6260-6265.

(76) Ji, M.; Odelius, M.; Gaffney, K. J.: Large Angular Jump Mechanism Observed for Hydrogen Bond Exchange in Aqueous Perchlorate Solution. *Science* **2010**, *328*, 1003-1005.

(77) Tielrooij, K. J.; Garcia-Araez, N.; Bonn, M.; Bakker, H. J.: Cooperativity in Ion Hydration. *Science* **2010**, *328*, 1006-1009.

(78) Tekavec, P. E.; Myers, J. A.; Lewis, K. L. M.; Ogilvie, J. P.: Two-dimensional electronic spectroscopy with a continuum probe. *Optics Letters* **2009**, *34*, 1390-1392.

(79) Cho, B.; Yetzbacher, M. K.; Kitney, K. A.; Smith, E. R.; Jonas, D. M.: Propagation and Beam Geometry Effects on Two-Dimensional Fourier Transform Spectra of Multilevel Systems. *Journal of Physical Chemistry A* **2009**, *113*, 13287-13299.

(80) Kwak, K. W.; Park, S.; Fayer, M. D.: Dynamics around solutes and solute-solvent complexes in mixed solvents. *Proceedings of the National Academy of Sciences of the United States of America* **2007**, *104*, 14221-14226.

(81) Kim, Y. S.; Hochstrasser, R. M.: The 2D IR responses of amide and carbonyl modes in water cannot be described by Gaussian frequency fluctuations. *Journal of Physical Chemistry B* **2007**, *111*, 9697-9701.

(82) Garrett-Roe, S.; Hamm, P.: What Can We Learn from Three-Dimensional Infrared Spectroscopy? *Accounts of Chemical Research* **2009**, *42*, 1412-1422.

(83) Stewart, G. W.; Morrow, R. M.: X-ray diffraction in liquids primary normal alcohols. *Physical Review* **1927**, *30*, 232-244.

(84) Stewart, G. W.; Skinner, E. W.: X-ray diffraction in liquids - A comparison of certain primary normal alcohols and their isomers. *Physical Review* **1928**, *31*, 1-9.

(85) Crim, F. F.: Bond-selected chemistry: Vibrational state control of photodissociation and bimolecular reaction. *Journal of Physical Chemistry* **1996**, *100*, 12725-12734.

(86) Voth, G. A.; Hochstrasser, R. M.: Transition state dynamics and relaxation processes in solutions: A Frontier of physical chemistry. *Journal of Physical Chemistry* **1996**, *100*, 13034-13049.

(87) Felker, P. M.; Zewail, A. H.: Dynamics of Intramolecular Vibrational-Energy Redistribution (Ivr) .1. Coherence Effects. *Journal of Chemical Physics* **1985**, *82*, 2961-2974.

(88) Nesbitt, D. J.; Field, R. W.: Vibrational energy flow in highly excited molecules: Role of intramolecular vibrational redistribution. *Journal of Physical Chemistry* **1996**, *100*, 12735-12756.

(89) Stratt, R. M.; Maroncelli, M.: Nonreactive dynamics in solution: The emerging molecular view of solvation dynamics and vibrational relaxation. *Journal of Physical Chemistry* **1996**, *100*, 12981-12996.

(90) Berg, M.; VandenBout, D. A.: Ultrafast Raman echo measurements of vibrational dephasing and the nature of solvent-solute interactions. *Accounts of Chemical Research* **1997**, *30*, 65-71.

(91) Deak, J. C.; Iwaki, L. K.; Dlott, D. D.: Vibrational energy redistribution in polyatomic liquids: Ultrafast IR-Raman spectroscopy of acetonitrile. *Journal of Physical Chemistry A* **1998**, *102*, 8193-8201.

(92) Deak, J. C.; Iwaki, L. K.; Rhea, S. T.; Dlott, D. D.: Ultrafast infrared-Raman studies of vibrational energy redistribution in polyatomic liquids. *Journal of Raman Spectroscopy* **2000**, *31*, 263-274.

(93) Dlott, D. D.: Vibrational energy redistribution in polyatomic liquids: 3D infrared-Raman spectroscopy. *Chemical Physics* **2001**, *266*, 149-166.

(94) Elles, C. G.; Cox, M. J.; Crim, F. F.: Vibrational relaxation of CH3I in the gas phase and in solution. *Journal of Chemical Physics* **2004**, *120*, 6973-6979.

(95) Iwaki, L. K.; Dlott, D. D.: Three-dimensional spectroscopy of vibrational energy relaxation in liquid methanol. *Journal of Physical Chemistry A* **2000**, *104*, 9101-9112.

(96) Wang, Z. H.; Pakoulev, A.; Dlott, D. D.: Watching vibrational energy transfer in liquids with atomic spatial resolution. *Science* **2002**, *296*, 2201-2203.

(97) Kiba, T.; Sato, S.; Akimoto, S.; Kasajima, T.; Yamazaki, I.: Solvent-assisted intramolecular vibrational energy redistribution of S-1 perylene in ketone solvents. *Journal of Photochemistry and Photobiology a-Chemistry* **2006**, *178*, 201-207.

(98) Owrutsky, J. C.; Raftery, D.; Hochstrasser, R. M.: Vibrational-Relaxation Dynamics in Solutions. *Annual Review of Physical Chemistry* **1994**, *45*, 519-555.

(99) Charvat, A.; Assmann, J.; Abel, B.; Schwarzer, D.; Henning, K.; Luther, K.; Troe, J.: Direct observation of intramolecular vibrational energy redistribution of selectively excited

CH2I2 and C3H5I molecules in solution. *Physical Chemistry Chemical Physics* **2001**, *3*, 2230-2240.

(100) Bonner, G. M.; Ridley, A. R.; Ibrahim, S. K.; Pickett, C. J.; Hunt, N. T.: Probing the effect of the solution environment on the vibrational dynamics of an enzyme model system with ultrafast 2D-IR spectroscopy. *Faraday Discussions* **2010**, *145*, 429-442.

(101) Kenkre, V. M.; Tokmakoff, A.; Fayer, M. D.: Theory of Vibrational-Relaxation of Polyatomic-Molecules in Liquids. *Journal of Chemical Physics* **1994**, *101*, 10618-10629.

(102) Grote, R. F.; Hynes, J. T.: Energy Diffusion-Controlled Reactions in Solution. *Journal of Chemical Physics* **1982**, *77*, 3736-3743.

(103) Lawrence, C. P.; Skinner, J. L.: Vibrational spectroscopy of HOD in liquid D_2O. VI. Intramolecular and intermolecular vibrational energy flow. *Journal of Chemical Physics* **2003**, *119*, 1623-1633.

(104) Jean, J. M.; Friesner, R. A.; Fleming, G. R.: Application of a Multilevel Redfield Theory to Electron-Transfer in Condensed Phases. *Journal of Chemical Physics* **1992**, *96*, 5827-5842.

(105) Pollard, W. T.; Friesner, R. A.: Solution of the Redfield Equation for the Dissipative Quantum Dynamics of Multilevel Systems. *Journal of Chemical Physics* **1994**, *100*, 5054-5065.

(106) King, J. T.; Baiz, C. R.; Kubarych, K. J.: Solvent-Dependent Spectral Diffusion in a Hydrogen Bonded "Vibrational Aggregate". *Journal of Physical Chemistry A* **2010**, *114*, 10590-10604.

(107) Khalil, M.; Demirdoven, N.; Tokmakoff, A.: Vibrational coherence transfer characterized with Fourier-transform 2D IR spectroscopy. *Journal of Chemical Physics* **2004**, *121*, 362-373.

(108) Spears, K. G.; Cramer, L. E.: Rotational Diffusion in Aprotic and Protic Solvents. *Chemical Physics* **1978**, *30*, 1-8.

(109) Benamotz, D.; Scott, T. W.: Microscopic Frictional Forces on Molecular-Motion in Liquids - Picosecond Rotational Diffusion in Alkanes and Alcohols. *Journal of Chemical Physics* **1987**, *87*, 3739-3748.

(110) Blanchard, G. J.; Cihal, C. A.: Orientational Relaxation Dynamics of Oxazine-118 and Resorufin in the Butanols - Valence-Dependent and State-Dependent Solvation Effects. *Journal of Physical Chemistry* **1988**, *92*, 5950-5954.

(111) Gaab, K. M.; Bardeen, C. J.: Nonstationary rotational diffusion in room temperature liquids measured by femtosecond three-pulse transient anisotropy. *Physical Review Letters* **2004**, *93*.

(112) Nibbering, E. T. J.; Elsaesser, T.: Ultrafast vibrational dynamics of hydrogen bonds in the condensed phase. *Chemical Reviews* **2004**, *104*, 1887-1914.

(113) Asbury, J. B.; Steinel, T.; Kwak, K.; Corcelli, S. A.; Lawrence, C. P.; Skinner, J. L.; Fayer, M. D.: Dynamics of water probed with vibrational echo correlation spectroscopy. *Journal of Chemical Physics* **2004**, *121*, 12431-12446.

(114) Timney, J. A.: Ligand Effect Constants - New Method for Predicting the Carbonyl Stretching Frequencies in Transition-Metal Compounds. *Inorganic Chemistry* **1979**, *18*, 2502-2506.

(115) Lokshin, B. V.; Kazarian, S. G.; Ginzburg, A. G.: Ir Study of Hydrogen-Bonds Formed by Pi-Complexes of Transition-Metals in Liquid Xenon Solution. *Journal of Molecular Structure* **1988**, *174*, 29-34.

(116) Lokshin, B. V.; Kazaryan, S. G.; Ginzburg, A. G.: Hydrogen-Bond of Transition-Metal Carbonyl-Complexes with Perfluoro-Tert-Butanol. *Bulletin of the Academy of Sciences of the Ussr Division of Chemical Science* **1988**, *37*, 470-475.

Chapter 3

Hydrogen Bond Dynamics Approaching the Glass Transition

The work presented in this chapter has been published in the following paper:

J. T. King, M. R. Ross, K. J. Kubarych "*Ultrafast Alpha-Like Relaxation of a Fragile Glass-Forming Liquid Measured using Two-Dimensional Infrared Spectroscopy*" Physical Review Letters, 108, 2012, 157401.

3.1 Introduction

Chapter 3 describes a temperature-dependent study of the hydrogen bond dynamics of a fragile glass former as the system is cooled towards the glass transition temperature, T_g. Though people have known how to utalize glasses for hundreds of years, and researched intensely for decades, the process of glass formation is still not well understood.[1-10] Glasses are formed when a liquid is cooled below its melting temperature without undergoing a proper phase transition to form a solid crystal, forming what is known as a supercooled liquid.[1,2] This can occur if the temperature is rapidly dropped, thus trapping the molecules in their liquid like structure, or if the molecular reorganization energy is high enough that the timescale for a liquid to solid structural change is not feasible. Once trapped in this supercooled state there is not enough thermal energy to reorganize the molecules, thus creating a long-lived non-equilibrium state of the system that continues to flow and evolve,

but the transition into a solid state is impossible long. Fragile glasses, which are glasses that have a high configurational entropy in the supercooled state, tend to form highly heterogeneous systems where the dynamics acquire a strong spatial dependence. These glasses are of particular interest because of their complexity, forming dynamically distinct regimes that undergo cooperative domain rearrangements, thus given rise to a relaxation phenomenon known as α-relaxation. The persisting local fluctuations are generally referred to as β-relaxation.

Upon further cooling the system undergoes a transition unique to disordered liquids, the glass transition, which occurs when the thermal energy becomes so low that the system undergoes dynamic arrest and can no longer respond to external stresses. In hydrogen bonded fragile glasses, like the one studied here, this leads to a drastic increase in hydrogen bond times, as there is no longer enough thermal energy to break these contacts. The difficulty in describing the glass transition is, in part, due to the fact that it is not a true phase-transition. Instead, the transition is a purely dynamical phenomenon that is accompanied by no structural signatures. The behavior of both α- and β-relaxation are of particular interest near T_g, where the two relaxation processes tend to diverge as the cooperative rearrangements become hyper sensitive to temperature due to the dynamic arrest process.

This work demonstrates that dynamic heterogeneity of a fragile glass in the supercooled regime extends to the ultrafast timescale, marking the first observation of picosecond dynamic heterogeneity. In addition, the process of dynamic arrest is observed through the picosecond dynamics, and signatures of ultrafast α-like relaxation are observed.

3.2 Dynamic Heterogeneity

The complexity of dynamical phenomena in glass-forming liquids as they approach the glass transition temperature has attracted considerable experimental and theoretical interest.[1-10] Though there are few if any structural signatures, transport properties diverge rapidly as the transition temperature is approached.[1-4,6,7] The dynamical change is accompanied by a growth in dynamical heterogeneity characterized by a broad distribution of relaxation

timescales.[7-10] The increase in dynamically distinct regimes results in a bifurcating of relaxation timescales, where fast β-relaxation results from local fluctuations and slower α-relaxation involves cooperative rearrangement of domains.[11-13] Fragile glasses are materials that display a greater configurational entropy than strong glasses, and, therefore, have an increased propensity for forming dynamically distinct regimes. Dynamical heterogeneity leads to the well characterized non-exponential relaxation of ensemble correlation functions, such as dipole-dipole correlation functions probed by fluorescence anisotropy measurements.[8,14,15]

The difficulty of studying glassy dynamics lies in the spatially heterogeneous distribution of domains displaying unique dynamics and the cooperative motions involved in the reorganization of these domains. Ultrafast nonlinear spectroscopies and single-molecule spectroscopy methods have been used extensively to study glassy dynamics and have proven both indispensible and complementary, despite accessing different time scales.[16-20] There is no doubt that single-molecule techniques can expose heterogeneity directly, but ensemble experiments are also capable of capturing dynamic heterogeneity through non-exponential relaxation of dynamical correlation functions.[8,14] At the single-molecule and ensemble level, fluorescence anisotropy measurements report orientational relaxation times where relaxation can occur on the microsecond timescale and longer.[16,17] Optical Kerr effect experiments have also been able to reproduce many aspects of mode coupling theory of glassy dynamics by observing the ultrafast polarizability dynamics of fragile glass formers.[21,22]

The question remains as to whether it is possible to predict the long time dynamics of glasses based on picosecond measurements, which are substantially more compatible with detailed atomistic simulations. The coupling between short and long time dynamics in glass formers was suggested by Harrowell and coworkers, who used simulations of a two-dimensional glass forming alloy to demonstrate the connection between the Debye-Waller factor (β-like relaxation) and the long-time dynamic propensity (α-like relaxation).[23] In this chapter, we show that it appears to be possible to sense α-type relaxation using ultrafast infrared spectroscopy on the picosecond timescale, indicating that the self-similarity of diffusive dynamics does indeed extend over tens of orders of magnitude in time.

Ultrafast 2DIR spectroscopy has been extensively used to study equilibrium solvation dynamics on ultrafast timescales.[24,25] 2DIR provides a direct means of extracting the frequency-frequency correlation function $C(t)$ of a vibrational transition, where $C(t) = \langle \delta\omega(t)\delta\omega(0) \rangle$ and $\delta\omega(t)$ is the time-dependent fluctuation of the transition frequency ω from its average.[26] The decay of $C(t)$ reveals the solvation dynamics near the probe as well as how these dynamics map to the probed transition. The experimentally observed decay of $C(t)$ is referred to as "spectral diffusion". Using a vibrational probe avoids structural and dynamical perturbations introduced through electronic excitations, and thus allows more direct access to equilibrium dynamics. In earlier studies we demonstrated the correlation between spectral diffusion time scales and solvent viscosity within the Stokes-Einstein regime.[25] Here we present the observation of non-exponential relaxation of $C(t)$ in a fragile glass former, as well as the non-Arrhenius temperature dependence of $C(t)$ that is consistent with observations made of other dynamical properties, such as orientational relaxation, near the glass transition.

The spectral diffusion of a dilute vibrational probe dirhenium decacarbonyl ($Re_2(CO)_{10}$, DRDC) in 1,2-hexanediol was observed as the system was cooled towards its glass transition. DRDC acts as a non-perturbative vibrational probe of the solvent dynamics of 1,2-hexanediol, a fragile glass-former with an accessible T_g at ~279 K. This system was studied at temperatures ranging from 320-283 K, a range that extends from well above the glass transition temperature to only a few degrees removed from the glass transition. The temperature-dependent viscosity of 1,2-hexanediol is known,[27] so we report the spectral dynamics both in terms of temperature and viscosity. Because of the well known super-Arrhenius behavior of viscosity in fragile glasses, presenting the data as a function of viscosity obviates the need to correct for the non-Arrhenius viscosity behavior.

The temperature dependent Fourier transform IR (FTIR) spectra of DRDC in 1,2-hexanediol are shown in **Figure 3.1**. The negligible changes in the FTIR spectrum highlight the limitations of one-dimensional spectroscopy to discern changes in dynamics. That is, from the limited perspective provided by linear spectra, temperature appears to have no effect on the structure or dynamics of the vibrational probe. Previous transient grating and

photon echo experiments on metal carbonyl compounds dissolved in glasses have observed changes to the homogeneous and inhomogeneous dephasing of a metal carbonyl in glassy solvents. Namely, the absorption linewidths were observed to broaden while the

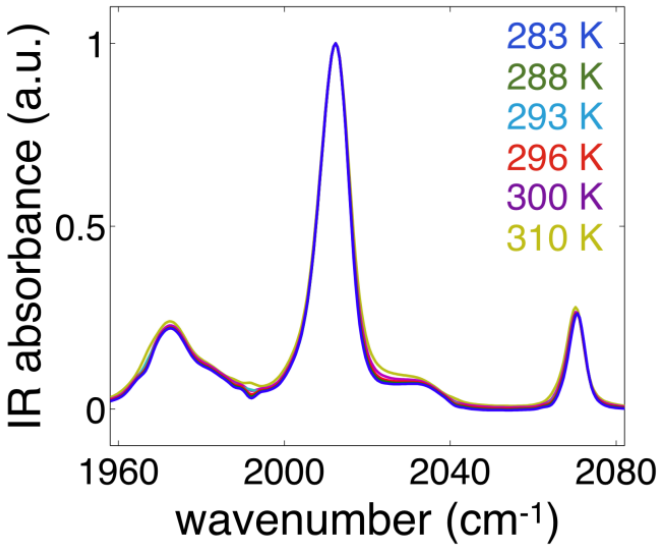

Figure 3.1 Linear FTIR spectra of DRDC in 1,2-hexanediol at six temperatures, ranging from 310 to 283 K. The glass transition temperature of 1,2-hexanediol is roughly 278 K. There is little to no change in the linear spectrum of DRDC as the glass transition is approached.

homogeneous contribution was observed to decrease.[19,20,28] Near T_g both of these observables were seen to be hypersensitive to temperature. Here, the linear spectrum shows no observable change near T_g, suggesting that the total dephasing remains unchanged upon cooling. This difference could be due to the temperature ranges at which the experiments were conducted. In the experiments by Fayer and coworkers, the glass transition temperature was below 200 K, whereas 1,2-hexanediol forms glassy material near room temperature. For the present system, neither the homogeneous nor the inhomogeneous linewidths suggest any significant dynamical consequences associated with the glass transition.

The spectral relaxation observed by 2DIR spectroscopy presents a remarkably different picture. Figure 2A shows $C(t)$ at 296 K for the main vibrational mode located at 2012 cm^{-1}. The plot also shows several functional forms used to fit the data, including single and double exponentials, as well as two different stretched exponentials (where $C(t) =$

$C(0)\exp\left[-\left(t/\tau_{sd}\right)^{\beta}\right]$). For the 296 K data set, both double exponential and stretched exponential ($\beta \approx 0.33$) functions provided good fits to the data, but over the full data set for all temperatures only the $\beta = 0.33$ stretched exponential form fit the data consistently well. The non-exponential relaxation is verified by a plot of ln$C(t)$ (**Figure 3.2**), clearly

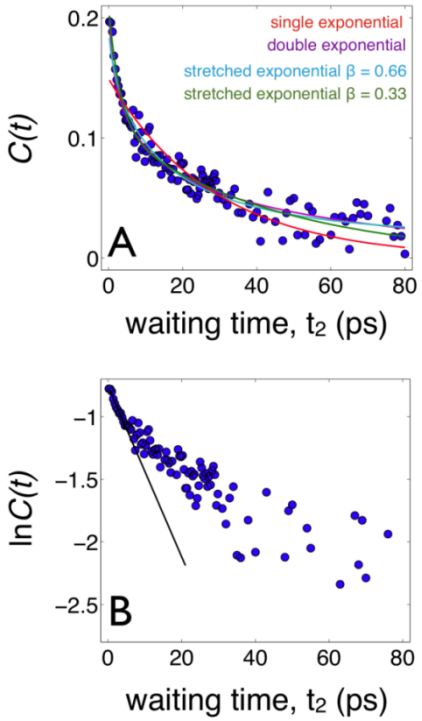

Figure 3.2 Frequency-frequency correlation function of the main vibrational mode of DRDC in 1,2-hexanediol at 296 K. Several fits are shown, demonstrating that the data is best represented by a stretched exponential with a small $\boldsymbol{\beta}$ value of 0.33. (B) Log plot of the correlation function showing non-exponential relaxation. A linear fit is shown of the first 5 ps.

demonstrating that the observed relaxation is not a simple single exponential relaxation. It should also be noted that despite differences in the extracted absolute relaxation times using different functions, the observed temperature dependence described below was retained regardless of the fitting procedures (**Figure 3.2**). For example, single exponential fits and stretched exponential fits with $\beta \sim 0.66$ show the same trend, but with spectral diffusion time constants that are roughly twice as large. By treating the glass transition as a random first order phase transition, the β value can be related to changes in the heat capacity of the system.[29]

3.3 Cooperative Fluctuations and Dynamic Arrest

Glasses typically exhibit two universal relaxation mechanisms, β-relaxation, which are fast, interwell fluctuations on the energy landscape, and α-relaxation, which is the result of cooperative domain rearrangements that become pronounced near T_g.[2,12] The two relaxation processes occurring in glasses can be distinguished by their behavior near T_g. The small scale motions typically associated with β-relaxation display a simple Arrhenius temperature dependence that is maintained through the glass transition temperature. In contrast, α-relaxation processes have a strong viscosity dependence and are sensitive to intermolecular couplings that do not generally influence β-type relaxation. In particular, when diffusive motion becomes a coordinated effort,[2] for instance in crowded environments or in highly viscous liquids, the observed temperature dependence diverges from simple Arrhenius behavior. The partitioning into α and β processes reflects the heterogeneity in the ruggedness of the energy landscape, and since the fundamental dynamics is diffusive, it should be possible to sense the influence of both regimes using dynamical probes operating at any timescale.

The temperature-dependent stretched-exponential spectral diffusion time constants display a marked slowdown near the glass transition, despite showing almost no changes at temperatures far from the transition. To better align this work with our previous studies of a nearly identical vibrational probe in a series of linear alcohols, we consider the spectral diffusion as a function of viscosity.[25] Away from T_g, the spectral diffusion shows no viscosity dependence, with a stretched-exponential decay time constant of ~9-10 ps over a viscosity range of 20-80 cP ($\Delta\eta$ = 60 cp). It is not unexpected for a dynamic quantity to become uncoupled from viscosity at such high values, an effect which has been observed previously in orientational relaxation. Approaching the glass transition, however, the spectral diffusion recovers its viscosity dependence and nearly triples over a viscosity range of 80-140 cP ($\Delta\eta$ = 60 cp).

To avoid any bias introduced by adopting specific fitting functions, we also employ an analysis that operates directly on the measured data.[21,22] The correlation functions can be

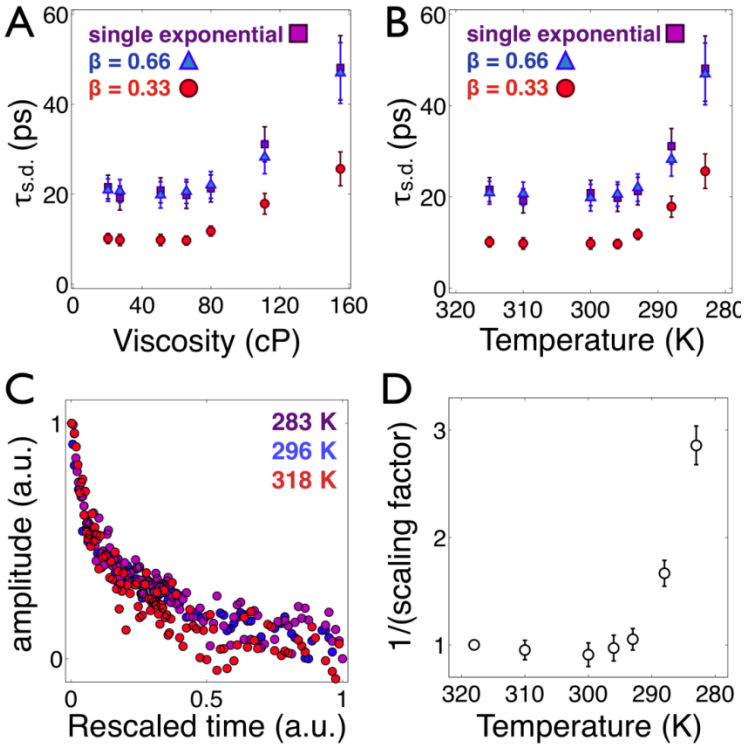

Figure 3.3 Spectral diffusion time constants plotted as a function of viscosity (A) and temperature (B) for three functional fitting forms, single exponential and stretched exponential. It is clear that the observed trend is independent of fitting procedures, despite the absolute time constants obtained from the fitting having a dependence on the fitting function. We also present a master curve approach where the correlation functions are collapsed onto a single curve (C). Three correlation functions are shown as an example and for figure clarity, but all decays can be collapsed onto a single curve. Plotting the inverse of the scaling factor vs temperature it is seen that the trend is once again reproduced (D).

collapsed onto a master curve by rescaling the amplitude and time axis of the data (**Figure 3.3C**), that is $C(t) \rightarrow \alpha C(t \times \tau_{scale})$. The coincidence of the FFCFs suggests that the decays arise from a similar underlying mechanism over the temperature range studied. The dynamical differences in the correlation functions are contained in the scaling factor (τ_{scale}) needed to collapse the time axis onto the master curve. **Figure 3.3D** shows a plot of τ_{scale}^{-1} vs. temperature, where, again, the pronounced retardation of dynamics is observed. We conclude that the observed slowdown in the spectral dynamics approaching the glass transition temperature is independent of specific fitting functional forms.

To distinguish the observed dynamical changes as being characterized as either α- or β-relaxation, we represent the data in an Arrhenius plot (**Figure 3.4**). Within an Arrhenius law framework, the relaxation times would follow a simple relationship with temperature:

$$\frac{1}{\tau_{sd}} = Aexp\left(-\frac{E_a}{RT}\right) \qquad (3.1)$$

where τ_{sd} is the spectral diffusion time constant. It is clear that the spectral diffusion of this system does not follow simple Arrhenius behavior. The phenomenon of non-Arrhenius behavior of glasses is well established and has been observed for other dynamical or bulk properties, such as orientational relaxation,[6] self-diffusion and viscosity.[1,3] Typically, a Vogel-Fulcher (VF) type equation is applied to temperature dependent glassy dynamics.[1-3]

$$\frac{1}{\tau_{sd}} = Bexp\left(-\frac{E_a}{R(T-T_0)}\right) \qquad (3.2)$$

Here, T_0 is a singularity temperature where dynamical and thermodynamical properties diverge. Figure 4 shows a VF fit (solid line), giving a $1/RT_0$ value of 1.86 $(kcal/mol)^{-1}$, or 277 K. The robustness of this fit, even for the small temperature range, suggests that the deviation from Arrhenius behavior is significant. Typically, these fits are best used when considering a substantially larger range of temperatures or viscosities; however, here we find that a reasonable fit is obtained even for the limited range of temperatures used. Though we lack a general microscopic theory linking transport properties and ultrafast spectral dynamics, studies have shown that spectral diffusion is primarily sensitive to short range diffusion and density fluctuations within the first and second solvation shells.[24,25] In particular, we have shown that spectral diffusion depends on the bulk viscosity, suggesting that the spectral diffusion is sensitive to more than simply the rapid ballistic motion within the first solvation shell.[25] The decay of $C(t)$ is thus driven by small scale, stochastic molecular motion. Here, we report the first observation of super-Arrhenius behavior of the ultrafast dynamics observed in a fragile glass former near T_g. The observation of ultrafast α-like relaxation using vibrational chromophores can be rationalized by comparing the typical domain size involved in α relaxation to the typical solvation size of the vibrational chromophore. Domain sizes near T_g involved in relaxation are of the order of 4-8 molecules, which is similar in size to what would be expected for the number of 1,2-hexanediol molecules in the solvation shell of a molecule of DRDC.[30] Larger organic dyes commonly

used to study glassy dynamics would have solvation shells that average over several domains and could mask signatures of cooperative rearrangements on the sensed dynamics.

The decoupling between spectral diffusion and viscosity away from the glass transition temperature deserves additional note. There have been three distinct regimes of spectral diffusion observed that depend strongly on the bulk viscosity. Previously, we have observed a monotonic dependence of spectral diffusion on bulk viscosity using a $Mn_2(CO)_{10}$ probe in linear alcohols with viscosities ranging from 1-4 cP, with the onset of decoupling at the highest viscosity of that range.[25] This breakdown of a hydrodynamic (i.e. Stokes-Einstein) description has also been observed in rotational diffusion at elevated viscosities, for

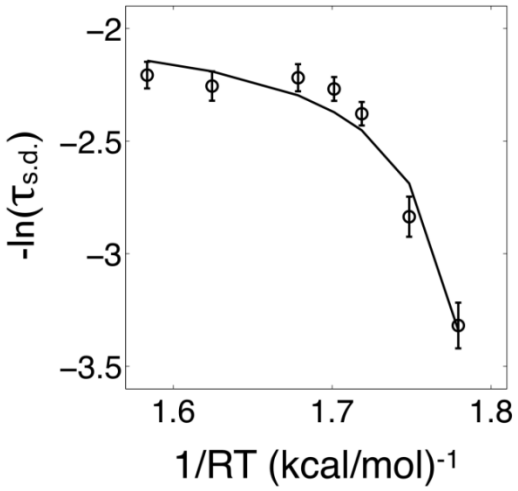

Figure 3.4 Arrhenius plot of the spectral diffusion time constants fit with a stretched exponential ($\boldsymbol{\beta}$ = 0.33), showing strong deviations from Arrhenius behavior near the phase transition. This behavior is consistent with $\boldsymbol{\alpha}$-like relaxation, which is typically considered a process that occurs on significantly longer timescales. Here, signatures of this relaxation process are observed on the ultrafast timescale. The solid line is a VF law fit (Eq. 2) to the data, showing that the non-Arrhenius behavior is well described by an expression typically applied to $\boldsymbol{\alpha}$-like relaxation.

example.[31] The low viscosity (20-80 cP) range of the present study is within the decoupled regime, but there is clearly a second crossover regime near the glass transition where the observed spectral diffusion becomes hypersensitive to the bulk viscosity. The onset of decoupling at high viscosities (but still far removed from T_g) likely is the result of local $\boldsymbol{\beta}$-relaxation decoupling from bulk-solvent fluctuations, an effect that should indeed persist at

all temperatures even absent a glass transition. The second crossover regime observed here near T_g, however, signals the emergence of significant cooperative motion in the liquid.

The universal observation of non-Arrhenius temperature-dependent relaxation on a wide range of timescales warrants further discussion. Experiments measuring translational and orientational diffusion have long been known to capture α-relaxation. Both of these diffusive processes occur with large motion along an effective coordinate of the free energy landscape. The timescale of this motion, however, is relative to the experiment being performed, and due to the fractal-like topology of the energetic landscape, transitions among free energy basins can only be characterized by relative timescales and relative motion along the effective coordinate. For instance, measurements probing glassy dynamics that are sensitive to diffusive motion, such as anisotropy (μs-s),[16,17] solvation dynamics (ps-s)[32] or spectral diffusion (fs-ps), will display the same relaxation phenomena but will manifest these dynamics on timescales that correspond to the measurement details. The self-similarity of the energy landscape allows processes typically associated with slower dynamics to be observed on the ultrafast timescale corresponding to their fundamental molecular origins.

3.4 Conclusions

In this work we have described the direct observation of dynamical heterogeneity on the ultrafast timescale, as well as the observation of picosecond α-like relaxation in a fragile glass forming liquid. Our results show that many of the characteristic phenomena of glassy dynamics—super-Arrhenius and nonexponential relaxation—emerge on the fastest of timescales. Through the use of 2DIR spectroscopy we are able to demonstrate that the FFCF is sensitive to collective molecular motion, a characteristic of fragile glasses near T_g, even when these dynamics are invisible in the linear absorption lineshape. The use of relatively weakly interacting probe molecules that are small compared to the general dimensions of a dynamical domain allow for collective rearrangements to be observed without averaging over the dynamical heterogeneity. Furthermore, the observation of α-relaxation on timescales that cover several orders of magnitude, including the picosecond timescales seen here, is a striking manifestation of the self-similar, or hierarchical, nature of

the free energy landscape. Exploring the ultrafast dynamics of glass formers can aid in eventually understanding the dynamics occurring in other complex or crowded environments found in proteins or inside cells.

References:

(1) Angell, C. A.: Formation of Glasses from Liquids and Biopolymers. *Science* **1995**, *267*, 1924-1935.

(2) Debenedetti, P. G.; Stillinger, F. H.: Supercooled liquids and the glass transition. *Nature* **2001**, *410*, 259-267.

(3) Chandler, D.; Garrahan, J. P.: Dynamics on the Way to Forming Glass: Bubbles in Space-Time. *Annual Review of Physical Chemistry, Vol 61* **2010**, *61*, 191-217.

(4) Angell, C. A.; Ngai, K. L.; McKenna, G. B.; McMillan, P. F.; Martin, S. W.: Relaxation in glassforming liquids and amorphous solids. *Journal of Applied Physics* **2000**, *88*, 3113-3157.

(5) Yang, M.; Richert, R.: Solvation dynamics and probe rotation in glass-forming liquids. *Chemical Physics* **2002**, *284*, 103-114.

(6) Ediger, M. D.; Angell, C. A.; Nagel, S. R.: Supercooled liquids and glasses. *Journal of Physical Chemistry* **1996**, *100*, 13200-13212.

(7) Sastry, S.; Debenedetti, P. G.; Stillinger, F. H.: Signatures of distinct dynamical regimes in the energy landscape of a glass-forming liquid. *Nature* **1998**, *393*, 554-557.

(8) Ediger, M. D.: Spatially heterogeneous dynamics in supercooled liquids. *Annual Review of Physical Chemistry* **2000**, *51*, 99-128.

(9) Richert, R.: Heterogeneous dynamics in liquids: fluctuations in space and time. *Journal of Physics-Condensed Matter* **2002**, *14*, R703-R738.

(10) Fee, R. S.; Milsom, J. A.; Maroncelli, M.: Inhomogeneous Decay Kinetics and Apparent Solvent Relaxation at Low-Temperatures. *Journal of Physical Chemistry* **1991**, *95*, 5170-5181.

(11) Hansen, C.; Stickel, F.; Berger, T.; Richert, R.; Fischer, E. W.: Dynamics of glass-forming liquids .3. Comparing the dielectric alpha- and beta-relaxation of 1-propanol and o-terphenyl. *Journal of Chemical Physics* **1997**, *107*, 1086-1093.

(12) Stillinger, F. H.: A Topographic View of Supercooled Liquids and Glass-Formation. *Science* **1995**, *267*, 1935-1939.

(13) Angell, C. A.: Relaxation in Liquids, Polymers and Plastic Crystals - Strong Fragile Patterns and Problems. *Journal of Non-Crystalline Solids* **1991**, *131*, 13-31.

(14) Bohmer, R.; Ngai, K. L.; Angell, C. A.; Plazek, D. J.: Nonexponential Relaxations in Strong and Fragile Glass Formers. *Journal of Chemical Physics* **1993**, *99*, 4201-4209.

(15) Ito, N.; Richert, R.: Solvation dynamics and electric field relaxation in an imidazolium-PF6 ionic liquid: From room temperature to the glass transition. *Journal of Physical Chemistry B* **2007**, *111*, 5016-5022.

(16) Zondervan, R.; Kulzer, F.; Berkhout, G. C. G.; Orrit, M.: Local viscosity of supercooled glycerol near T-g probed by rotational diffusion of ensembles and single dye

molecules. *Proceedings of the National Academy of Sciences of the United States of America* **2007**, *104*, 12628-12633.

(17) Mackowiak, S. A.; Herman, T. K.; Kaufman, L. J.: Spatial and temporal heterogeneity in supercooled glycerol: Evidence from wide field single molecule imaging. *Journal of Chemical Physics* **2009**, *131*.

(18) Mackowiak, S. A.; Kaufman, L. J.: When the Heterogeneous Appears Homogeneous: Discrepant Measures of Heterogeneity in Single-Molecule Observables. *Journal of Physical Chemistry Letters* **2011**, *2*, 438-442.

(19) Tokmakoff, A.; Zimdars, D.; Urdahl, R. S.; Francis, R. S.; Kwok, A. S.; Fayer, M. D.: Infrared Vibrational Photon-Echo Experiments in Liquids and Glasses. *Journal of Physical Chemistry* **1995**, *99*, 13310-13320.

(20) Tokmakoff, A.; Fayer, M. D.: Homogeneous Vibrational Dynamics and Inhomogeneous Broadening in Glass-Forming Liquids - Infrared Photon-Echo Experiments from Room-Temperature to 10 K. *Journal of Chemical Physics* **1995**, *103*, 2810-2826.

(21) Torre, R.; Bartolini, P.; Ricci, M.; Pick, R. M.: Time-resolved optical Kerr effect on a fragile glass-forming liquid: Test of different mode coupling theory aspects. *Europhysics Letters* **2000**, *52*, 324-329.

(22) Torre, R.; Bartolini, P.; Righini, R.: Structural relaxation in supercooled water by time-resolved spectroscopy. *Nature* **2004**, *428*, 296-299.

(23) Widmer-Cooper, A.; Harrowell, P.: Predicting the long-time dynamic heterogeneity in a supercooled liquid on the basis of short-time heterogeneities. *Physical Review Letters* **2006**, *96*.

(24) Kuroda, D. G.; Vorobyev, D. Y.; Hochstrasser, R. M.: Ultrafast relaxation and 2D IR of the aqueous trifluorocarboxylate ion. *Journal of Chemical Physics* **2010**, *132*.

(25) King, J. T.; Baiz, C. R.; Kubarych, K. J.: Solvent-Dependent Spectral Diffusion in a Hydrogen Bonded "Vibrational Aggregate". *Journal of Physical Chemistry A* **2010**, *114*, 10590-10604.

(26) Roberts, S. T.; Loparo, J. J.; Tokmakoff, A.: Characterization of spectral diffusion from two-dimensional line shapes. *Journal of Chemical Physics* **2006**, *125*.

(27) Jadzyn, J.; Czechowski, G.; Stefaniak, T.: Viscosity of a series of 1,2-alkanediols. *Journal of Chemical and Engineering Data* **2002**, *47*, 978-979.

(28) Walsh, C. A.; Berg, M.; Narasimhan, L. R.; Fayer, M. D.: A Picosecond Photon-Echo Study of a Chromophore in an Organic Glass - Temperature-Dependence and Comparison to Nonphotochemical Hole Burning. *Journal of Chemical Physics* **1987**, *86*, 77-87.

(29) Xia, X. Y.; Wolynes, P. G.: Fragilities of liquids predicted from the random first order transition theory of glasses. *Proceedings of the National Academy of Sciences of the United States of America* **2000**, *97*, 2990-2994.

(30) Stevenson, J. D.; Schmalian, J.; Wolynes, P. G.: The shapes of cooperatively rearranging regions in glass-forming liquids. *Nature Physics* **2006**, *2*, 268-274.

(31) Lee, M.; Bain, A. J.; McCarthy, P. J.; Han, C. H.; Haseltine, J. N.; Smith, A. B.; Hochstrasser, R. M.: Picosecond Photoisomerization and Rotational Reorientation Dynamics in Solution. *Journal of Chemical Physics* **1986**, *85*, 4341-4347.

(32) Richert, R.; Stickel, F.; Fee, R. S.; Maroncelli, M.: Solvation Dynamics and the Dielectric Response in a Glass-Forming Solvent - from Picoseconds to Seconds. *Chemical Physics Letters* **1994**, *229*, 302-308.

Chapter 4

Dynamics of Bulk Water

Part of the work presented in this chapter has been published in the following paper:

J. T. King, M. R. Ross, K. J. Kubarych "*Water-Assisted Vibrational Relaxation of a Metal Carbonyl Complex Studied with 2D-IR Spectroscopy*" Journal of Physical Chemistry B, 116, 2012, 3754-3759.

4.1 Introduction

This chapter initiates our efforts in applying 2DIR studies to biological systems, beginning with the characterization of pure H_2O and D_2O. Our initial studies relied heavily on the vibrational lifetime of metal carbonyl probes in bulk water, which were found to be extremely sensitive to the presence of water. The lifetimes for particular probes measured in water were found to be faster than the lifetimes in organic solvents by an order of magnitude or more. The enhanced vibrational relaxation, termed water-assisted relaxation, is shown to be the result of waters ability to significantly increase the dynamic coupling of internal vibrational modes of the probe. Vibrational probes with many internal degrees of freedom are shown to be extremely sensitive to the presence of water, while probes that are only weakly coupled with internal degrees of freedom show only modest water-assisted relaxation. This is demonstrated by a comparative study between two metal carbonyl vibrational probes,

where the probe coupled to many degrees of freedom (CORM-2) shows a sub-5 ps relaxation time in D_2O, while the probe weakly coupled to other internal modes (CORM-4) shows a relaxation time upwards of 30 ps. We also report the isotope-dependent relaxation of the two metal carbonyl probes in H_2O and D_2O, showing first that the 30% difference in reorientation time between the two solvents can be reproduced in the vibrational lifetimes of the probe with sub-5 ps relaxation. Additionally, the bend+libration combination band is degenerate with the CO vibrational modes of the probes, and opens an intermolecular relaxation pathway through direct energy transfer. While CORM-2 relaxes too fast for this pathway to contribute (hence the isotope difference reproduces what is expected due to the dynamical difference), the CORM-4 relaxation is slow enough for the resonant pathway to significantly contribute. While a 30% isotope difference is measured in CORM-2, a 60% isotope difference is measured in CORM-4, where the additional 30% faster relaxation is the result of resonant energy transfer present only in H_2O.

4.2 Water-Assisted Vibrational Relaxation

The relaxation of a vibrationally excited species is of central importance to chemical dynamics and has been a topic of research for many years.[1-4] The extensive role that the solvent can play in relaxation processes is still being explored, and a complete description that would allow predictions of relaxation rates is not available. One aspect of vibrational relaxation that appears to be essentially universal is that water facilitates rapid relaxation in solutes by typically an order of magnitude over than similarly polar solvents. Several anions have been studied using ultrafast IR pump-probe spectroscopy including CN^-,[5,6] SCN^-,[7,8] $SeCN^-$,[9] and N_3^-.[10-12] Likewise, the peptide amide-I band is also found to relax more rapidly in water than in, for example, DMSO.[13,14] The use of ultrafast spectroscopies have greatly enhanced our understanding of the complex dynamics of liquid water, including the timescales of hydrogen bond rearranging and the mechanism by which hydrogen bond partners switch. For a relaxing molecule, the hydrogen bonding dynamics, together with the large dipole moment of water, endow water with dynamics that result in rapid modulations of the local electric fields which have significant influences on the relaxation rates of excited molecules.

Here, we present an experimental study demonstrating the significant role that water can play in dictating the vibrational dynamics of a small ruthenium carbonyl dimer ($[RuCl_2(CO)_3]_2$, denoted "CORM-2"), where the observed relaxation of the coupled CO vibrational modes is shown to be significantly accelerated by water. For molecular excitations that result in only small perturbations to the solvation environment, the relaxation of the excited molecule back into an equilibrium state is related to the equilibrium fluctuations of the solvent, as described by the fluctuation-dissipation theorem and quantified by linear response theory. Thus, the accelerated vibrational relaxation in water reflects the equilibrium dynamics of water.

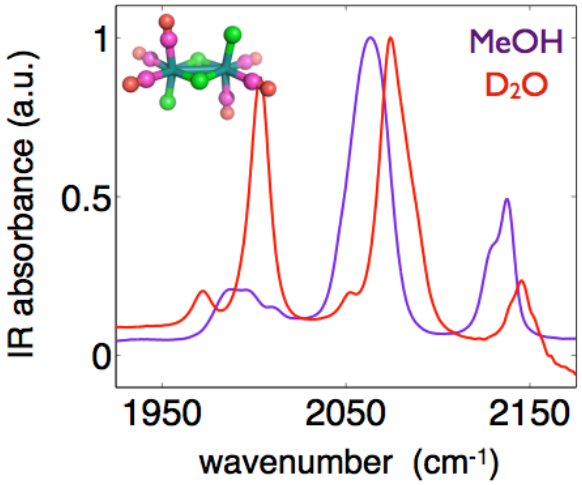

Figure 4.1 Linear FTIR spectra of CORM-2 (structure shown in inset) in methanol (black) and D_2O (red). The low frequency vibrational mode of CORM-2 (2000 cm^{-1}) was analyzed for vibrational lifetime throughout this study.

The linear Fourier Transform IR (FTIR) spectra of CORM-2 in methanol and D_2O are shown in **Figure 4.1** (Fits of the FTIR spectra are presented in the Supporting Information). The modes located at 2003 cm^{-1} and 2073 cm^{-1} in D_2O (and H_2O) are analyzed due to their strong signals and easily accessible frequencies. For the 2DIR experiments in D_2O, spectral overlap with the OD stretch at 2400 cm^{-1} prohibits analysis of the high-frequency band. These vibrational modes are shifted to 1997 cm^{-1} and 2068 cm^{-1} in methanol. That these modes do not simply shift, and indeed exhibit blue shifts in some cases, indicates that water influences the coupling between the CO local units, possibly serving to localize the vibrational modes.

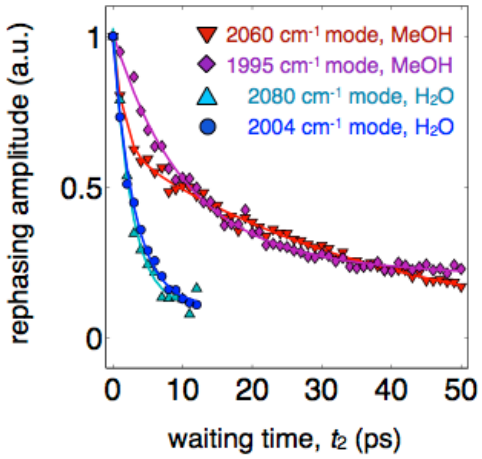

Figure 4.2 Relaxation of the low frequency (modes centered around 2000 cm^{-1}) and mid frequency (modes centered around 2060 cm^{-1}) vibrational modes of CORM-2 in methanol and in H_2O, showing an order of magnitude acceleration in relaxation in water.

The vibrational lifetime is extracted by measuring the time dependent amplitude of absolute-magnitude rephasing 2DIR spectra. In contrast to transient absorption or absorptive 2DIR spectra, using rephasing spectra for lifetime information may have complications arising from differences in the decay rates of excited state absorption and ground state bleach. Nevertheless, we find that the extremely low solubility (~1 mM) of metal carbonyls in aqueous environments leads to pump-probe signals that are below our detection limit. The background-free Fourier transform 2DIR signal is significantly stronger, however, and the error that is introduced through the excited state absorption and ground state bleach not being resolved is overshadowed by the higher signal-to-noise ratios achievable with the more intense signal. **Figure 4.2** shows the vibrational relaxation extracted from 2DIR rephasing spectra of CORM-2 in H_2O (2003 and 2073 cm^{-1} modes, ~1 mM) and in methanol (1997 and 2068 cm^{-1} modes, ~5 mM), indicating significantly different relaxation timescales. The low frequency mode of CORM-2 in methanol has a fast relaxation time of 6.16±1.2 ps followed by a slow relaxation time of 47.36±4 ps. The 2068 cm^{-1} mode of CORM-2 in methanol shows a similar rate of slow relaxation as the low frequency mode (42.25±3 ps), but its initial decay is significantly faster (2.49±0.5 ps). The fast component of the decay is due to intramolecular vibrational redistribution, a process that can be influenced by the solvent.

While IVR rates are difficult to predict based on the molecular structure and the solvent, we have recently observed in the metal carbonyl complex $Mn_2(CO)_{10}$ that IVR rates are sensitive to the degree of hydrogen bonding between the solute and the solvent. In a series of linear alcohols, we found that the presence of hydrogen bonds acts to hinder the IVR among energetically neighboring modes.[15] In the present case, it is possible that the 1997 cm^{-1} band is more delocalized than is the 2058 cm^{-1} band. The delocalized modes would have greater hydrogen bonding opportunities, possibly resulting in slower IVR due to the hydrogen bond defect-induced vibrational exciton trapping found in $Mn_2(CO)_{10}$. The localized vibrational modes, however, would not have as extensive of hydrogen bonding opportunities, allowing the IVR process to proceed with limited interference from the solvent. Although a detailed examination of IVR is beyond the scope of the present

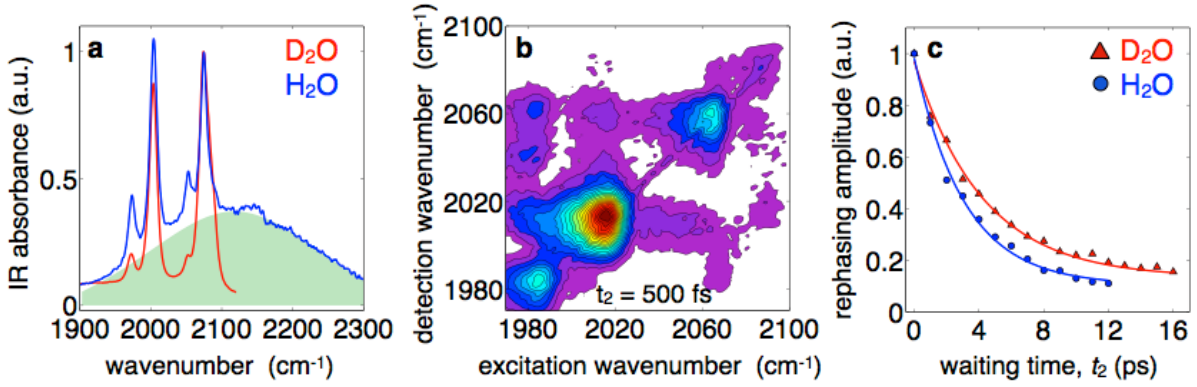

Figure 4.3 Linear FTIR spectra of CORM-2 in D_2O and H_2O (a), where the combination band of water is shadowed with a green filling. This band is centered at 2150 cm^{-1} for H_2O, but is red shifted to 1550 cm^{-1} for D_2O. The 2D-IR spectrum of CORM-2 in D_2O (b) shows a dominant feature at 2003 cm^{-1}. Because the IR pulses used in this experiment have a bandwidth of roughly 100 cm^{-1} that is centered at 2000 cm^{-1}, the higher frequency bands appear with significantly less signal amplitude. (c) The vibrational lifetimes of CORM-2 in D_2O (4.27±0.27 ps) and H_2O (3.12±0.29 ps) of the 2003 cm^{-1} mode show sub 5-ps relaxation, however relaxation in H_2O occurs 30% faster than in D_2O. The vibrational relaxation data are also shown with confidence bounds of one and two standard deviations of the fit.

manuscript, work is underway to examine this issue fully, including accurate quantum chemical calculations of this somewhat challenging, flexible complex.

The vibrational relaxation of CORM-2 in methanol occurs on the 40-50 ps timescale for the two modes studied here. The relaxation of these modes in aqueous solvents, however, are found to be an order of magnitude faster. The relaxation of the low frequency mode in H_2O shows a relaxation time that is an order of magnitude faster at 3.12±0.29 ps. Likewise,

the relaxation of the 2073 cm^{-1} mode of CORM-2 in H_2O shows an identical relaxation rate as found for the 2003 cm^{-1} mode.

In addition, we observe an isotope effect on the relaxation in water and in heavy water. The linear FTIR spectra of CORM-2 in H_2O and D_2O are shown in **Figure 4.3a**, where the broad feature centered at 2150 cm^{-1} in the H_2O spectrum is due to the bend+libration combination band of H_2O.[16] This band is red-shifted to 1550 cm^{-1} in D_2O. The relaxation of CORM-2 in H_2O and D_2O is found to be 3.12±0.29 ps and 4.27±0.27 ps respectively, showing a 30% acceleration of vibrational relaxation in H_2O relative to D_2O. Similar isotope effect trends have been reported in previous relaxation studies of small molecule anions in aqueous solution. The mechanism for this observed effect, as well as the possible role that resonant energy relaxation plays in the case of H_2O, will be discussed below.

The observation of ultrafast vibrational relaxation in water demonstrates an extreme example of solvent-assisted relaxation, where the solvent enhances the internal couplings of the modes available for relaxation. CORM-2 has a large number (3×18–6 = 48) of internal degrees of freedom, many of which may be coupled to the relaxing mode, serving as a bath of accepting modes to enhance the intramolecular relaxation. These internal modes play a dominant role in the relaxation pathway of the vibrational energy, though their full influence is not realized even in the polar solvent methanol due to the relatively weak inherent anharmonic coupling. We have observed slow vibrational relaxation in several metal carbonyl systems even in polar solvents capable of hydrogen bonding. $Mn_2(CO)_{10}$, for example, exhibits ~70 ps vibrational relaxation in linear alcohols, showing little chain-length dependence.[15] Extremely slow, ~20 ps IVR has been observed in organometallic complexes $[C_5H_5Ru(CO)_2]_2$ dimers and the iron analogue, $[C_5H_5Fe(CO)_2]_2$.[17] Similar time scales have been reported for hydrogenase model compounds as well as its photoproducts.[18] A remarkable example of virtually non-existent IVR can be found in $Fe(CO)_5$, where the axial and equatorial modes separated by only 20 cm^{-1} show no measurable IVR, though energy is transferred by chemical exchange through the Berry pseudorotation mechanism.[19]

Several aqueous anions have been studied with ultrafast vibrational spectroscopy. Hamm *et al.* measured vibrational relaxation of CN^- in water to occur between 30-80 ps (depending

on carbon and oxygen isotope),[6] considerably longer than the 3-4 ps timescales found for CORM-2. The significance of additional intramolecular degrees of freedom in facilitating vibrational relaxation is highlighted by the 1-3 ps vibrational lifetime of N_3^-,[10-12,20] which has additional accepting modes as well as a Fermi resonant relaxation channel. The relaxing modes experience enhanced intramolecular coupling in the presence of a rapidly fluctuating local electric field produced by water's large dipole and its fast, abrupt reorientation dynamics. The extensive hydrogen bonding network, which gives rise to many modes of the solvent bath, also provides a large density of low-frequency states capable of accepting energy that has relaxed, intramolecularly, to the lower tiers of the solute molecule.

4.3 Isotope Dependent Relaxation

The observed isotope effect raises questions about the mechanism by which H_2O induces faster vibrational relaxation than D_2O. A feature of the CORM-2/H_2O spectrum that is not present in the CORM-2/D_2O spectrum is the broad bend+libration combination band centered at 2150 cm^{-1}. This combination band is shifted to 1550 cm^{-1} in D_2O. While there is a resonant solvent band present in H_2O, there is also a dynamical difference between the two solvents. In CN^-, where the only pathway for relaxation is via intermolecular energy transfer, the isotope-specific differences in vibrational lifetime are substantially larger than the 30% difference we measure for CORM-2, and the absolute lifetimes are much longer.[6] In

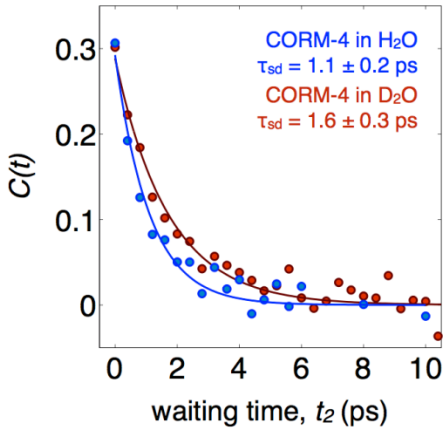

Figure 4.4 Isotope dependent spectral diffusion of CORM-2 in H_2O and D_2O.

particular, $^{13}C^{15}N^-$ has the same IR transition frequency as CORM-2/water (2003 cm^{-1}), yet relaxes with time constants of 31±7 ps (H_2O) and 120±6 ps (D_2O), corresponding to a four-fold enhancement by H_2O. Meuwly *et al.* have used nonequilibrium molecular dynamics simulations of CN^- in water to study the influence of nonbonded interactions on the relaxation rate.[21] By observing the direct excitations of the bend and librational modes after energy is deposited into the CN^- mode, it was concluded that the resonant channel indeed provides an open pathway for energy flow. The slow timescale of relaxation is also similar to the resonant intermolecular relaxation recently reported in SCN^- clusters.[8] It seems, therefore, that the 3-4 ps relaxation of CORM-2 is an order of magnitude too rapid to be attributed to intermolecular, direct resonant energy transfer to the water combination band. This will be discussed further in **Section 4.4**.

4.4 Isotope Dependent Spectral Diffusion

While vibrational lifetimes are often difficult to interpret, the spectral diffusion provides more direct physical insight. Here, we measure the FFCF of CORM-2 in H_2O and D_2O and report an identical 30% faster relaxation in H_2O. Furthermore, the timescales for spectral diffusion reflect the hydrogen bond lifetimes that have been measured in pure H_2O and D_2O of 1 ps and 1.4 ps, respectively.[22-25] This observation once again suggests that the dynamics of a liquid can be accurately measured through the introduction of vibrational probes. Additionally, the observation that CORM-2, a small hydrophobic molecule, measures bulk-like dynamics for water has important implications for hydrophobic hydration that will be discussed in detail in **Section 5.2**.

4.5 Resonant and Nonresonant Relaxation

Resonant energy transfer through a dipole coupling, Förster-like mechanism, is dependent on both the excited state lifetime and the degree of spectral inhomogeneity of both the donor and accepting modes.[8,26] Though the precise inhomogeneity of the water combination band is not yet known directly from 2DIR spectroscopy, there is simulation evidence[27] and indirect experimental indications[28,29] that the 130 cm^{-1} broad band is inhomogeneously broadened. Inhomogeneity limits the efficiency of resonant energy

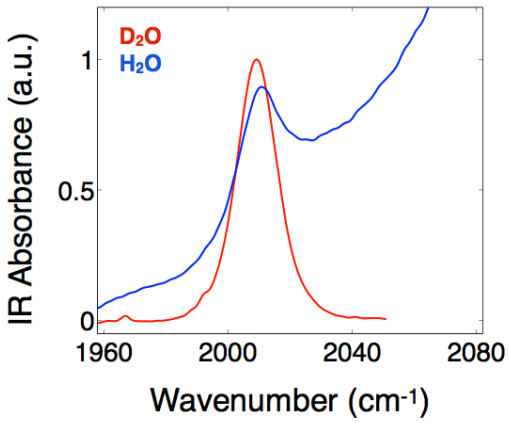

Figure 4.5 FTIR spectrum of CORM-4 in H_2O and D_2O.

transfer due to conformation-specific spectral overlap. On the other hand, spectral diffusion arising from the dynamic sampling of the inhomogenous band, can aid resonant transfer, and taking the ~1 ps time scale for water as a proxy for the combination band dynamics, it is possible that spectral diffusion will be capable of overcoming the transient spectral mismatch between the carbonyl donor and the combination band acceptor. The trouble with this mechanism is that the overall lifetimes are so much shorter than what has been observed in CN^- where there is no competing intramolecular pathway, yet so similar to N_3^- where there are at least two intramolecular channels to relax the vibrationally excited asymmetric stretching mode.

To isolate the pathways of vibrational relaxation we compare the previously discussed results of water-assisted relaxation of CORM-2 in H_2O and D_2O with the relaxation timescales for CORM-4 in H_2O and D_2O (FTIR spectra shown in **Figure 4.5**). The proposed mechanism for the extreme example of water-assisted relaxation observed in CORM-2 is the enhancement of intramolecular couplings due to the presence of a rapidly fluctuating electric field provided by water. CORM-2 has many internal degrees of freedom to couple to the relaxing modes, thus water-assisted vibrational relaxation is extremely rapid. The timescale of relaxation is in fact too slow to allow for resonant energy transfer to the bend+libration combination band of H_2O, thus the isotope dependent relaxation reflects the inherent dynamic difference of the isotopes. To further explore this we measure the isotope dependent relaxation of CORM-4, which has a single metal carbonyl unit, and is only weakly

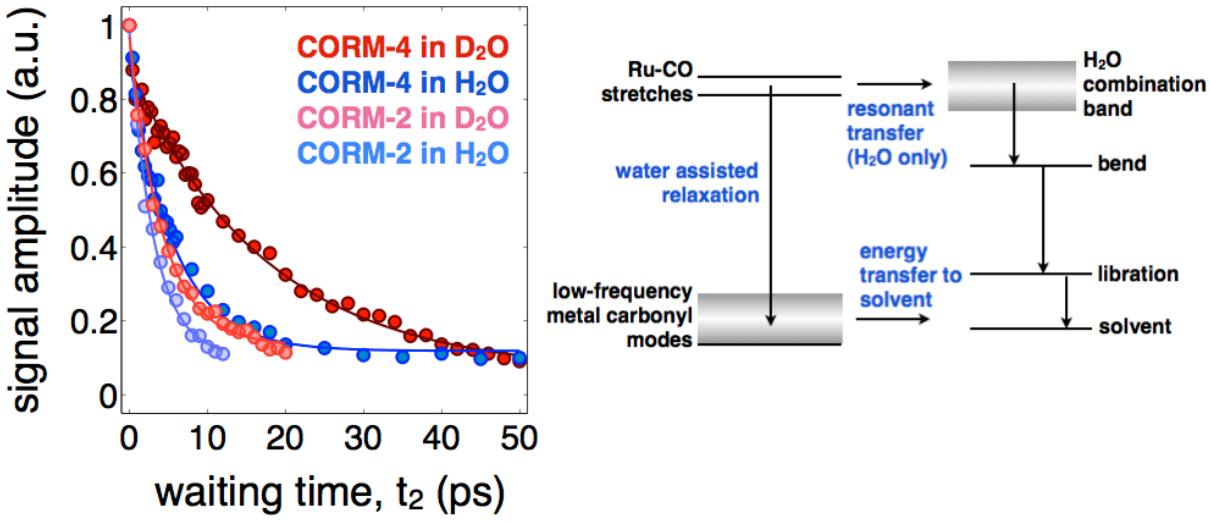

Figure 4.6 (left) Relaxation of the low frequency (modes centered around 2000 cm^{-1}) and mid frequency (modes centered around 2060 cm^{-1}) vibrational modes of CORM-2 in methanol and in H_2O, showing an order of magnitude acceleration in relaxation in water. (right) An energy level depiction of the vibrational relaxation of the CO stretches is also shown. While the water-assisted intramolecular relaxation channel is likely to be the dominant pathway, there is also a resonant relaxation channel from the CO vibrations directly to the $\nu_{bend} + \nu_{libration}$ combination band of H_2O. This pathway is only present in H_2O since the combination band if D_2O is red shifted to 1550 cm^{-1}.

coupled to the other internal modes of the molecule. Given our interpretation of water-assisted relaxation, we would expect a much longer lifetime of CORM-4 in D2O, and a more pronounced isotope effect due to the resonant relaxation pathway that becomes viable with the longer lifetime. Indeed, we find the relaxation time of CORM-4 in D_2O is on the order of 30 ps, and there is a 60% isotope effect between H_2O and D_2O.

The role of non-bonded interactions leading to resonant energy transfer has been identified as a valid relaxation pathway for ions in water, provided the relaxing mode has an extended lifetime. Such relaxation pathways further complicate the interpretation and prediction of vibrational relaxation in the condensed phase. However, the knowledge of resonant relaxation can be applied as a technique to map out the lower frequency liberation spectrum of solvents in cases where there is accidental degeneracy between combination bands and relaxing modes.

4.6 Conclusions

The pronounced difference in vibrational excited state lifetime of excited CO stretching modes in polar organic solvents as opposed to aqueous solution establishes the coupled CO vibrational modes of metal carbonyl complexes as effective water sensors. The ultrafast relaxation observed in water can be explained in terms of the discrete large angular jump dynamics of H_2O, which induce fluctuations in the hydrogen bonding network and produce rapid modulations of the local electric field surrounding the relaxing oscillator. The observed isotope effect is rationalized in terms of the isotope dependence of hydrogen bonding jumping events, which dominate water's dynamics on the picosecond timescale. Since these events involve large displacements of the hydrogen/deuterium atoms, they should be particularly sensitive to the isotope substitution. This ultrafast isotope effect will prove beneficial for studying the disruption of the dynamics of hydrogen bond rearrangements, where the influence of isotope substitution on the relaxation rates can provide insights into the extent to which this subset of water dynamics is perturbed by a solute.

Characterizing the behavior of metal carbonyl complexes in aqueous environments is an important step in using these strong IR absorbers as vibrational probes of more complex systems such as proteins and membranes. The vibrational relaxation of these probes can act as an effective water sensor, and the above results suggest that the isotope dependent relaxation can provide a local window into the angular jump dynamics of hydrating water.

The accidental degeneracy between the carbonyl stretching frequency of the metal carbonyl probes and the bend+libration combination band of water also allows for the role of resonant relaxation to be studied. The competition between internal relaxation and direct relaxation into the solvent was studied using two vibrational probes that have significantly different internal couplings, thus strongly effecting the rate of internal relaxation. It was found that in the case of the weakly coupled vibrational mode the vibrational lifetime was increased and the isotope effect significantly more pronounced, increasing from a 30% difference between H_2O and D_2O to a 60% difference.

References:

(1) Oxtoby, D. W.: Vibrational-Relaxation in Liquids. *Annual Review of Physical Chemistry* **1981**, *32*, 77-101.

(2) Elsaesser, T.; Kaiser, W.: Vibrational and Vibronic Relaxation of Large Polyatomic-Molecules in Liquids. *Annual Review of Physical Chemistry* **1991**, *42*, 83-107.

(3) Owrutsky, J. C.; Raftery, D.; Hochstrasser, R. M.: Vibrational-Relaxation Dynamics in Solutions. *Annual Review of Physical Chemistry* **1994**, *45*, 519-555.

(4) Skinner, J. L.: Vibrational energy relaxation of small molecules and ions in liquids. *Theoretical Chemistry Accounts* **2010**, *128*, 147-155.

(5) Heilweil, E. J.; Doany, F. E.; Moore, R.; Hochstrasser, R. M.: Vibrational-Energy Relaxation of the Cyanide Ion in Aqueous-Solution. *Journal of Chemical Physics* **1982**, *76*, 5632-5634.

(6) Hamm, P.; Lim, M.; Hochstrasser, R. M.: Vibrational energy relaxation of the cyanide ion in water. *Journal of Chemical Physics* **1997**, *107*, 10523-10531.

(7) Ohta, K.; Tominaga, K.: Vibrational population relaxation of thiocyanate ion in polar solvents studied by ultrafast infrared spectroscopy. *Chemical Physics Letters* **2006**, *429*, 136-140.

(8) Bian, H.; Wen, X.; Li, J.; Chen, H.; Han, S.; Sun, X.; Song, J.; Zhuang, W.; Zheng, J.: Ion clustering in aqueous solutions probed with vibrational energy transfer. *Proceedings of the National Academy of Sciences of the United States of America* **2011**, *108*, 4737-4742.

(9) Lenchenkov, V.; She, C.; Lian, T.: Vibrational relaxation of CN stretch of pseudo-halide anions (OCN-, SCN-, and SeCN-) in polar solvents. *Journal of Physical Chemistry B* **2006**, *110*, 19990-19997.

(10) Morita, A.; Kato, S.: Vibrational relaxation of azide ion in water: The role of intramolecular charge fluctuation and solvent-induced vibrational coupling. *Journal of Chemical Physics* **1998**, *109*, 5511-5523.

(11) Hamm, P.; Lim, M.; Hochstrasser, R. M.: Non-Markovian dynamics of the vibrations of ions in water from femtosecond infrared three-pulse photon echoes. *Physical Review Letters* **1998**, *81*, 5326-5329.

(12) Zhong, Q.; Baronavski, A. P.; Owrutsky, J. C.: Vibrational energy relaxation of aqueous azide ion confined in reverse micelles. *Journal of Chemical Physics* **2003**, *118*, 7074-7080.

(13) Rubtsov, I. V.; Wang, J. P.; Hochstrasser, R. M.: Vibrational coupling between amide-I and amide-A modes revealed by femtosecond two color infrared spectroseopy. *Journal of Physical Chemistry A* **2003**, *107*, 3384-3396.

(14) DeFlores, L. P.; Ganim, Z.; Ackley, S. F.; Chung, H. S.; Tokmakoff, A.: The anharmonic vibrational potential and relaxation pathways of the amide I and II modes of N-methylacetamide. *Journal of Physical Chemistry B* **2006**, *110*, 18973-18980.

(15) King, J. T.; Anna, J. M.; Kubarych, K. J.: Solvent-hindered intramolecular vibrational redistribution. *Physical Chemistry Chemical Physics* **2011**, *13*, 5579-5583.

(16) Ratcliffe, C. I.; Irish, D. E.: Vibrational Spectral Studies of Solutions at Elevated-Temperatures and Pressures .5. Raman Studies of Liquid Water up to 300-Degrees-C. *Journal of Physical Chemistry* **1982**, *86*, 4897-4905.

(17) Anna, J. M.; King, J. T.; Kubarych, K. J.: Multiple structures and dynamics of [CpRu(CO)2]2 and [CpFe(CO)2]2 in solution revealed with two-dimensional infrared spectroscopy. *Inorganic chemistry* **2011**, *50*, 9273-83.

(18) Kaziannis, S.; Wright, J. A.; Candelaresi, M.; Kania, R.; Greetham, G. M.; Parker, A. W.; Pickett, C. J.; Hunt, N. T.: The role of CN and CO ligands in the vibrational relaxation dynamics of model compounds of the [FeFe]-hydrogenase enzyme. *Physical Chemistry Chemical Physics* **2011**, *13*, 10295-10305.

(19) Cahoon, J. F.; Sawyer, K. R.; Schlegel, J. P.; Harris, C. B.: Determining transition-state geometries in liquids using 2D-IR. *Science* **2008**, *319*, 1820-1823.

(20) Olschewski, M.; Knop, S.; Lindner, J.; Voehringer, P.: Vibrational relaxation of azide ions in liquid-to-supercritical water. *Journal of Chemical Physics* **2011**, *134*.

(21) Lee, M. W.; Meuwly, M.: On the Role of Nonbonded Interactions in Vibrational Energy Relaxation of Cyanide in Water. *Journal of Physical Chemistry A* **2010**, *115*, 5053-5061.

(22) Loparo, J. J.; Roberts, S. T.; Tokmakoff, A.: Multidimensional infrared spectroscopy of water. I. Vibrational dynamics in two-dimensional IR line shapes. *Journal of Chemical Physics* **2006**, *125*.

(23) Loparo, J. J.; Roberts, S. T.; Tokmakoff, A.: Multidimensional infrared spectroscopy of water. II. Hydrogen bond switching dynamics. *Journal of Chemical Physics* **2006**, *125*.

(24) Nibbering, E. T. J.; Elsaesser, T.: Ultrafast vibrational dynamics of hydrogen bonds in the condensed phase. *Chemical Reviews* **2004**, *104*, 1887-1914.

(25) Moilanen, D. E.; Fenn, E. E.; Lin, Y.-S.; Skinner, J. L.; Bagchi, B.; Fayer, M. D.: Water inertial reorientation: Hydrogen bond strength and the angular potential. *Proceedings of the National Academy of Sciences of the United States of America* **2008**, *105*, 5295-5300.

(26) Woutersen, S.; Bakker, H. J.: Resonant intermolecular transfer of vibrational energy in liquid water. *Nature* **1999**, *402*, 507-509.

(27) Yagasaki, T.; Ono, J.; Saito, S.: Ultrafast energy relaxation and anisotropy decay of the librational motion in liquid water: A molecular dynamics study. *Journal of Chemical Physics* **2009**, *131*.

(28) Chieffo, L. R.; Shattuck, J. T.; Pinnick, E.; Amsden, J. J.; Hong, M. K.; Wang, F.; Erramilli, S.; Ziegler, L. D.: Nitrous oxide vibrational energy relaxation is a probe of interfacial water in lipid bilayers. *Journal of Physical Chemistry B* **2008**, *112*, 12776-12782.

(29) Ingrosso, F.; Rey, R.; Elsaesser, T.; Hynes, J. T.: Ultrafast Energy Transfer from the Intramolecular Bending Vibration to Librations in Liquid Water. *Journal of Physical Chemistry A* **2009**, *113*, 6657-6665.

Chapter 5

Hydrophobic Hydration

The work presented in this chapter has been published in the following papers:

J. T. King, K. J. Kubarych "*Site-Specific Coupling of Hydration Water and Protein Flexibility Studied in Solution with Ultrafast 2D-IR Spectroscopy*" Journal of the American Chemical Society, 134, 2012, 18705-1871.

J. T. King, E. J. Arthur, C. L. Brooks III, K. J. Kubarych "*Site-specific hydration dynamics of globular proteins and the role of constrained water in solvent exchange with amphiphilic cosolvents*" Journal of Physical Chemistry B, 116, 2012, 5604-5611.

5.1 Introduction

Biological processes, from DNA replication to enzyme catalysis, occur in the presence of water. Water's indispensible role in biology has motivated efforts to uncover the degree to which it actively participates in chemical events.[1] As the universal solvent of living organisms, water has a remarkable ability to accommodate both hydrophilic solutes through strong electrostatic interactions, as well as hydrophobic solutes through subtle modifications to the hydrogen bonding network.[2] The hydration of large solutes (> 1 nm), such as membranes and proteins, requires significant rearrangements of the hydrogen bonding

network leading to the sacrifice of hydrogen bonds. Hydration water—water directly solvating the large solute—is thus structurally and dynamically constrained, restricting the configuration space as well as limiting dynamical flexibility. These constraints endow interfacial water with properties that are different from the bulk liquid.[1-17] Whether or not one adopts a picture of protein dynamics as being "slaved" to the solvent, it is nevertheless clear that the preponderance of free energy changes attributable to the solvent arise from the relatively thin hydration layer of water solvating the protein.[18,19]

The interest in studying and characterizing the properties of interfacial water arises from the extensive role that the protein-water interface plays in influencing such processes as small ligand binding,[20,21] protein-protein recognition[15,22,23] and protein-DNA interactions.[24] Studies of orientational and spectral dynamics of water near lipid bilayers,[5] within reverse micelles,[7] or in the presence of small solutes[8,17] indeed support the picture that limiting the configuration space can impose constraints on water's dynamics. Additionally, molecular dynamics simulations have been used extensively to study dynamics that may be difficult to access experimentally, such as in the immediate hydration environments of proteins.[9,25,26] Experimental evidence of water confinement near protein surfaces has been found by studying solvation dynamics of site-specific fluorescent probes of protein surfaces via ultrafast fluorescence upconversion.[11-13] Recently, the combined constraining influence of both protein and lipids has enabled NMR measurements of local water structure and its mobility using reverse micelle-encapsulated ubiquitin.[14,15] THz absorption spectroscopy has also been demonstrated to be a powerful technique for studying the hydration environments of proteins.[27,28] Though these experiments provide evidence for constrained water, it remains unclear precisely which aspects of water's motion are most strongly affected by the interface.

5.2 Water Around Small Hydrophobes

In these experiments the dynamics of water are accessed through the spectral dynamics of metal-carbonyl vibrational probes. We rely on comparisons between two small metal carbonyl molecules, CORM-2 ($[RuCl_2(CO_3)]_2$) and PI-CORM ($[CO]Fe[N_5C_{22}H_{21}]$),[29] that provide a benchmark for bulk-like water dynamics, and hen egg white lysozyme labeled with

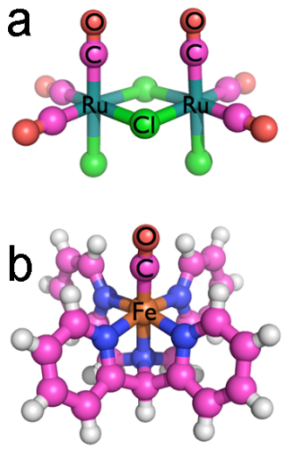

Figure 5.1 Structures of the vibrational chromophores used in this study. CORM-2 and PI-CORM (or CORM-4) are used throughout the study as a model, small molecule metal carbonyl.

a metal-carbonyl vibrational probe (**Figure 5.1**). The FFCFs of CORM-2 and PI-CORM decay completely with time constants of 1.5 ± 0.3 ps and 1.6 ± 0.4 ps, respectively (**Figure 5.2**). This timescale is expected for bulk-like D_2O and reflects the hydrogen bonding dynamics of the hydrating heavy water.[30,31] The complete decay of the correlation function around the small hydrophobic molecules demonstrates that a single, small hydrophobe does not significantly influence the dynamics of the hydrating water.[32] The insensitivity of the spectral diffusion timescales to the chemical structures of the vibrational probes indicates that spectral diffusion measurements in aqueous environments are robust sensors of the surrounding environment. Additionally, the apparent invariance to structure enables direct comparisons between various probe molecules.

There have been many ultrafast experiments that are aimed at studying hydration dynamics around hydrophobic molecules/surfaces directly through the OH/OD stretch. These experiments have provided valuable information regarding the behavior of water in isolated pools or in solutions with high concentrations of hydrophobes.[17,33-35] Studying hydration dynamics through the use of strong vibrational probes provides a complementary view by allowing water to be studied around isolated small molecules or proteins that are in low concentrations, free from possible crowding effects.[32] Studying hydration dynamics at sub-mM solute concentrations provides direct access to the influence of isolated

hydrophobes on the surrounding water, whereas similar studies investigating the water itself are virtually impossible due to the several orders of magnitude imbalance between solvating and bulk water molecules.

5.3 Water Around Extended Protein Surfaces

The binding motif of the vibrational label to the proteins is shown in **Figure 5.3** We also rely on comparisons with the small molecule dichloro-ruthenium(II) dimer (a so-called "carbon monoxide releasing molecule" often denoted CORM-2), which is the precursor to the labeling complex (referred to as CORM-3).[36] Because of the scarcity of water-soluble metal carbonyls we rely on comparisons between the labeled proteins and the CORM-2 complex in both aqueous and organic solvents. While the molecules are clearly different, the comparison between these molecules is both robust and instructive. The crucial properties shared between these molecules are the presence of coupled CO chromophores as well as the presence of numerous low-frequency modes. The anharmonic coupling between the spectroscopic modes and the lower frequency modes of the molecule results in water-assisted relaxation in aqueous environments, a key aspect of the results and interpretations presented here.[37] The side-chains that are in the immediate vicinity of the CO oscillators on HEWL-RC are isoleucine, phenylalanine and alanine residues, which are non-polar residues, as well as an arginine residue. The HuLys-RC probe is mostly exposed to the solvent, though it is neighbored by cysteine, leucine and alanine. While the environment presented by the

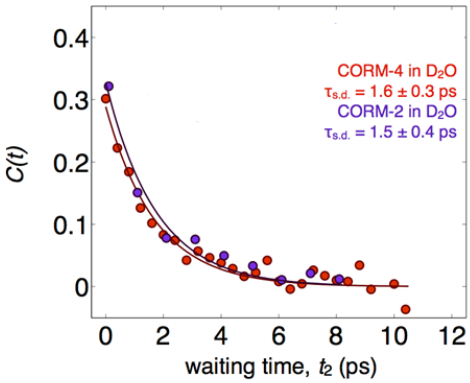

Figure 5.2 Spectral diffusion of CORM-4 and CORM-2 in D_2O, showing identical timescales (1.5 ps) that agree with bulk hydrogen bond dynamics of D_2O.

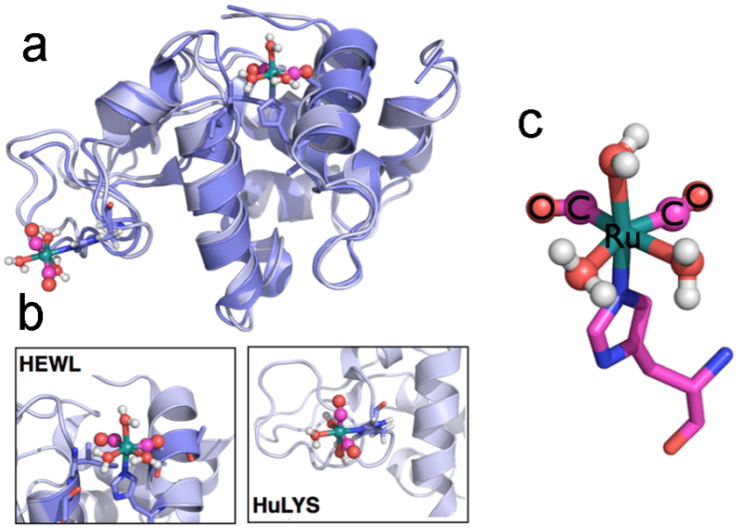

Figure 5.3 (a) Crystal structures of HEWL-RC (PDB code 2XJW) overlaid with the crystal structure of native HuLys (PDB code 2ZIJ). (b) The binding location of the metal-carbonyl on the HEWL protein has been determined by x-ray crystallography. While no crystallographic data is available for the HuLys-RC complex, the binding location is proposed by comparison with the HEWL-RC complex. (c) The vibrational chromophore is covalentely attached to the histidine residue.

protein is an important aspect of the dynamics felt by the vibrational probes, the observed lifetimes are dominated by the hydration water.

Quantitative picture of hydration using vibrational lifetimes. The thermodynamic driving forces for hydrating small and large hydrophobic cavities differ according to the relative significance of enthalpic and entropic contributions. Small hydrophobes and small ions generally sustain water's local hydrogen bonding network through subtle rearrangements, so that free energy gradients arise from changes in entropy.[2,38-41] Conversely, large hydrophobes disrupt hydrogen bonding, leading to driving forces dominated by enthalpic changes.[2,39,41,42] Hence, one expects dynamical perturbations to reflect these distinct underlying free energy landscapes.

Figure 5.4 shows the Fourier transform IR (FT-IR) spectrum of HEWL-RC in H_2O and D_2O. The vibrational probe has two IR active CO modes located at 2004 and 2080 cm^{-1}. We focus on the low frequency mode of both HEWL-RC and HuLys-RC for analysis. Using 2D-IR spectroscopy, the vibrational lifetimes of the CO vibrational modes of HEWL-RC in H_2O and D_2O were extracted for the 2004 cm^{-1} mode, and found to be 3.60±0.18 and

3.73±0.21 ps, respectively. This result is in stark contrast to what has previously been reported for water-assisted vibrational relaxation, where we observed pronounced isotope differences between water and heavy water.[37]

The loss of the isotope effect can be explained in terms of the restraints that large, hydrophobic surfaces place on water's hydrogen bonding structure and dynamics. Comprising a subset of water's fast dynamics are hydrogen bonding switching events, which have been theoretically predicted[43] and experimentally supported[44] as occurring through abrupt angular jumps that involve large scale motion of the hydrogen (or deuterium) atoms of the water. Small molecules at low concentrations do not disrupt hydrogen bonding networks, and, more importantly, do not significantly limit the configuration space available

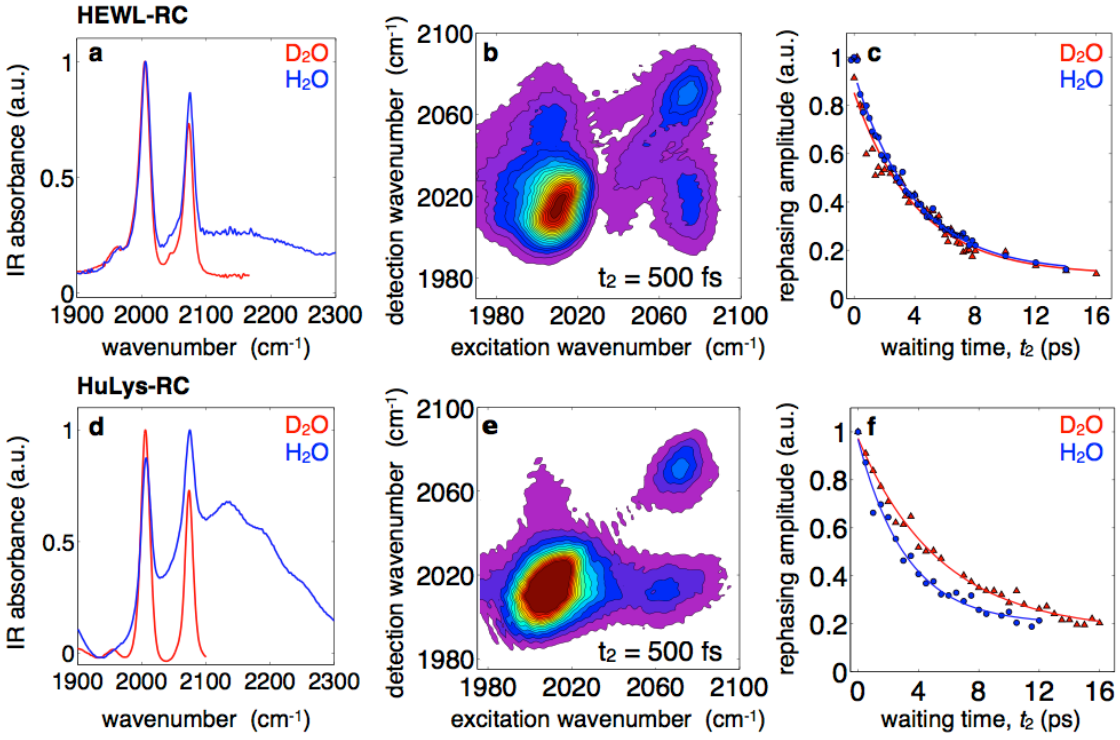

Figure 5.4 Linear FTIR spectra of HEWL-RC (a) and HuLys-RC (d) in D_2O and H_2O. The broad feature in the H_2O spectrum is the bend-libration combination band, centered at 2150 cm^{-1}. The 2D-IR rephasing spectra for HEWL-RC (b) and HuLys-RC (e) in D_2O are shown for a waiting time of t_2 = 500 fs. Monitoring the amplitude of the 2004 cm^{-1} peak as a function of waiting time, t_2, provides the vibrational lifetime of the mode. For HEWL-RC there is no observable isotope effect in the vibrational relaxation between D_2O and H_2O (c) whereas HuLys-RC shows a very clear isotope effect (f). The lack of an isotope effect suggests solvation by slow constrained water, whereas hydration by bulk-like water leads to an observable isotope effect. These results demonstrate the heterogeneous nature of the water dynamics near a protein, where certain regions are hydrated by slow constrained water while other regions are hydrated by bulk-like water.

to hydrogen bond partners, allowing this subset of water's dynamics to occur unperturbed.[10,32,45,46] Because the angular jump dynamics of water involve large displacements of the hydrogen atoms, these dynamics should also be particularly sensitive to isotope substitution. Hence, the solvent fluctuations that drive vibrational relaxation strongly reflect the dynamical differences between H_2O and D_2O. In fact, the water isotope effect on solvation dynamics had been successfully modeled from the perspective of Debye relaxation, which relates the macroscopic dielectric constant of water to the microscopic reorientation dynamics,[47] though the angular jump mechanism had not yet been identified.

The absolute value of the constrained H_2O/D_2O relaxation falls between the values of bulk-like H_2O and D_2O for both CORM-2 as well as HuLys-RC. While the dynamical nature of the solvent can be influential, it is only one component that determines the vibrational lifetime. The electric field generated by the solvent applies the force on the relaxing mode, and is thus an important component of vibrational relaxation that we cannot probe directly. Because hydrophobic hydration is accompanied by dynamical and structural changes, the absolute lifetime observed for the constrained H_2O/D_2O will depend on any structural changes that occur in the hydration layer. Thus, the convergence of the H_2O and D_2O relaxation onto a single lifetime and the absolute value of the vibrational lifetime should be considered somewhat separately.

Magnitude of constrained water slowdown at the protein surface. There is still a considerable debate regarding the origin and magnitude of the slowdown of water near hydrophobic molecules and surfaces. Recent experimental and theoretical studies have suggested that the origin of the hydrophobic effect is the limiting of hydrogen bond switching events near hydrophobic surfaces through an excluded volume effect.[32,48,49] Furthermore, molecular dynamics simulations of HEWL in water have suggested that the magnitude of hydrogen bond switching slowdown is roughly a factor of 2 relative to bulk water for the large majority of hydrating waters.[49] To experimentally compare more quantitatively the dynamics of bulk water and hydrophobic hydration water we use the measured spectral diffusion times of CORM-2 and PI-CORM in D_2O, which were found to

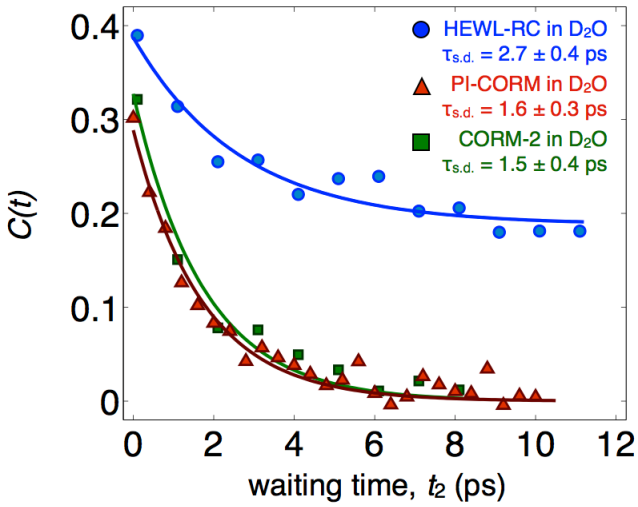

Figure 5.5 Spectral diffusion of HEWL-RC compared to spectral diffusion of CORM-2 and PI-CORM in pure D_2O, showing an experimentally determined slowdown factor of 1.8. This is in excellent agreement with molecular dynamics simulations, which predict a dominant slowdown factor of 2 based on the restriction of hydrogen bond switching events.

be 1.5 ± 0.3 ps and 1.6 ± 0.4 ps, respectively (**Figure 5.5**) as indicative of bulk hydration. In contrast to these small molecule solutes, the correlation function of the HEWL-RC system exhibits two distinct features: an initial decay corresponding to the hydration dynamics, and a static offset corresponding to protein dynamics that are too slow to be sampled during the experimental window. The fast decay time of the FFCF of HEWL-RC in D_2O decays on the order of 2.7 ± 0.4 ps, which is only modestly slower than bulk-like water (measured as roughly 1.5 ps). The experimentally measured slowdown factor of roughly 1.8 is in excellent quantitative agreement with molecular dynamics simulations.[49] The agreement between experiment and simulations lends support not only to the methodology of studying protein hydration with multidimensional spectroscopy, but also to the interpretation of hydrophobic hydration as resulting from hindered hydrogen bond switching events due to excluded volume effects.

The dynamical constraints exerted by extended hydrophobic surfaces on the surrounding water arise from the restrictions imposed on the hydrogen bonding network by the surface.[50] Extended surfaces limit both the configuration space available for hydrogen bonding as well as the associated dynamics, causing water to adopt geometries that are not favorable for hydrogen bond coordination while impeding switching events.[10] The structured region surrounding the HEWL His15 label is an excellent example of a natural extended biological

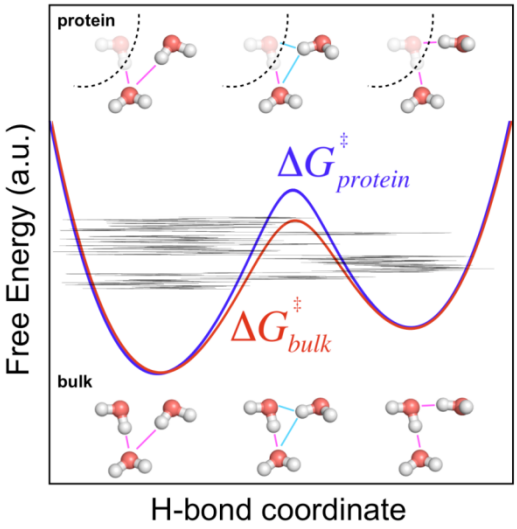

Figure 5.6 Cartoon depicting the free energy surface for hydrogen bond jumps. The transition state has been identified as a bifurcated hydrogen bond with both initial and final donors (shown with cyan hydrogen bonds). In regions of constrained hydration, the protein limits the availability of final donors, raising the free energy barrier by decreasing its entropy. Besides the relatively rare jumping events, the rapid intrawell fluctuations are able to induce enhanced anharmonic coupling, assisting vibrational relaxation for both water isotopes.

surface with low curvature, hence the surface slows down the water dynamics by limiting the available partners for fast hydrogen bond switching, while inhibiting the required coordinated reorientation that accompanies large angular jumps. Because the switching events involve large displacements of the hydrogen atoms, these motions contribute significantly to the measured vibrational relaxation isotope effect, which is only observed when the hydrating water exhibits bulk-like dynamics. This interpretation of "hydrophobic slowing" of water's dynamics is consistent with what has been previously observed for small solutes at high concentrations, where neighboring solutes limit hydrogen bonding switching.[8,17,32]

A cartoon depiction of hydrogen bond switching and its modification by the protein surface is shown in **Figure 5.6** Since successful hydrogen bond switching events proceed through a bifurcated transition state where the switching hydrogen is fleetingly associated with both the initial and final partner O atoms,[43,51] the free energy barrier is necessarily influenced by the availability of such configurations. Relative to the bulk liquid, the protein interface deprives water molecules of potential partners, which reduces the availability of

transition state candidates and lowers the entropy of the transition state. Nevertheless, hydrogen bond jumps are not the only source of environmental fluctuations leading to enhanced anharmonic coupling and the resulting carbonyl vibrational relaxation. The intrawell dynamics comprise the majority of these fluctuations (depicted by the stochastic trajectory in the cartoon), hence resulting in similarly rapid relaxation in both D_2O and H_2O.

5.4 Heterogeneous Hydration Around Proteins

The homologous structures of HEWL and HuLys allow us to investigate the water dynamics near two qualitatively distinct protein-water environments (**Figure 5.3**). We have previously discussed the lack of an observable isotope dependence of the vibrational relaxation of the HEWL-RC complex, where the probe is located on a structured, extended protein surface. In the HuLys-RC complex, however, the probe is located in an unstructured and flexible region of the protein. In contrast to HEWL-RC, the isotope effect is clearly observed in HuLys-RC, where the relaxation time constants for the 2004 cm^{-1} mode are 3.12 ± 0.26 ps and 4.70 ± 0.38 ps in H_2O and D_2O, respectively. Despite being located at the protein surface, the measured solvation dynamics appears more consistent with small molecule hydration. Given that the vibrational probe is attached to a histidine residue in both proteins, the data indicate that some degree of collectivity at each site leads to the protein's heterogeneous influence on the hydrating water, as well as highlighting the role of surface topology on local hydrophobicity.[50]

The water dynamics surrounding the unstructured region of the HuLys-RC complex resemble what was previously observed for a small metal-carbonyl, CORM-2, at low concentrations (~ 2 mM). This similarity suggests that the solvation of the unstructured region of the protein is similar to what is seen for a small molecule, namely that the hydration environment is essentially bulk-like. The picture that emerges from these measurements is that a protein's ability to constrain hydration water dynamics is determined not only by the availability of solvent-exposed side chains capable of forming hydrogen bonds, but also by the presence of a low-curvature surface topology. Though this view is consistent with the prevailing model of hydrophobic solvation,[2] our work shows clearly how

a single, relatively compact globular protein can exhibit both extremes of hydration structure and dynamics.

The heterogeneous nature of the hydration dynamics of a protein raises interesting questions regarding the role, if any, of the dynamically constrained water in biological processes. It has long been speculated that hydrophobic hydration—hydration environments that constrain water—leads to entropic driving forces for surface processes, all of which require protein dehydration as the initial step.[15,21-24,52] A region of hydrophobic hydration can act as a "thermodynamic reservoir," where entropy is created by relaxing constraints on the hydrating water, in turn enabling greater participation in enthalpically favorable hydrogen bonding. We examine hydrophobic assembly below using an amphiphilic alcohol cosolvent.

5.5 Constrained Water as a Driving Force

The tight interplay between protein dynamics and the hydration environment suggests that modulations can significantly impact a protein's dynamics, structure and stability. The properties of a protein can be manipulated by adding small amounts of cosolvents, such as alcohols.[53,54] Low concentrations of 2,2,2-trifluoroethanol (TFE), for example, can stabilize protein secondary structure through a mechanism that is generally attributed to preferential solvation of the protein by TFE, promoting intramolecular hydrogen bonding within the protein by alleviating competition with external hydrogen bonding partners from hydrating water.[53,54] At higher concentrations, however, lacking the driving force of hydrophobicity, the protein becomes unstable and partially denatures into an unfolded state characterized by a loosening of the helix packing even as the helices themselves remain stabilized.[55] Partial unfolding in lysozyme has been observed at TFE concentrations near 15% (v/v). The linear FTIR spectra of HEWL-RC in D_2O/TFE mixtures (shown in the Supporting Information) show no significant changes in either the amide region of the spectrum or in the metal-carbonyl stretch bands.

To investigate the thermodynamic connection between constrained water and the driving force for surface processes such as preferential dehydration, we studied the influence of the amphiphilic cosolvent TFE on the vibrational lifetime of the protein-bound vibrational probe. We have shown that the dominant pathway of vibrational relaxation for the protein-

bound probes is driven by the interfacial water dynamics. Therefore, dehydrating the protein surface surrounding the probe should result in measurable changes to its vibrational lifetime.

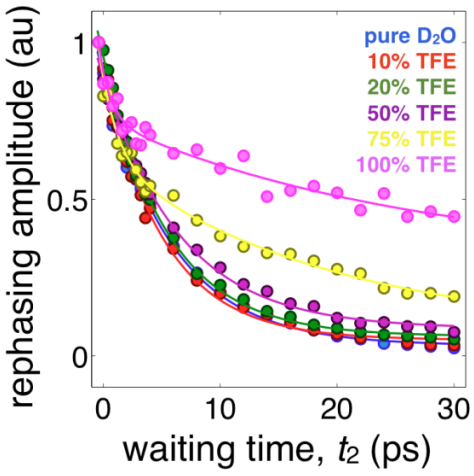

Figure 5.7 Vibrational relaxation of CORM-2 in D_2O/TFE mixtures, demonstrating the lifetime dependence on the cosolvent in the absence of preferential solvation.

As a control experiment, we measured the vibrational lifetimes of CORM-2 in a series of D_2O/TFE mixtures (including pure D_2O, 10,20,50,75 % TFE, and pure TFE). **Figure 5.7** shows the vibrational relaxation of CORM-2 in the D_2O/TFE mixtures. At low concentrations the vibrational lifetime remains dominated by water-assisted vibrational relaxation, only increasing from 4 to 6 ps over a range of 0-50% TFE. At higher concentrations the relaxation becomes dominated by the TFE cosolvent, increasing to 25 ps and 50 ps at 75% and pure TFE, respectively. It is clear that there is a nonlinear dependence of the vibrational lifetime on the solvent composition, likely due to the dominance of water-assisted vibrational relaxation as the most efficient relaxation pathway. Hence, significant changes in the vibrational lifetime are only observed when water is at a very low concentration. These data provide a baseline for vibrational lifetimes in D_2O/TFE mixtures in the absence of preferential solvation which can be applied to the study of HEWL-RC and HuLys-RC in the presence of TFE.

Figure 5.8a shows the vibrational relaxation of HEWL-RC for four different TFE concentrations (0, 10, 15, 20% v/v). In pure D_2O the vibrational lifetime is 3.73±0.21 ps. Upon addition of 10% TFE the vibrational lifetime increases to 32.76±1.15 ps (see

Supporting Information for discussion of fits to the data), suggesting that at low concentrations the alcohol dehydrates the protein near the vibrational probe in exchange for a preferred alcohol environment. Lacking water, the vibrational relaxation becomes significantly slower and resembles relaxation observed in CORM-2 in TFE environments (**Figure 5.8c**). In comparison to the T_1 times for CORM-2 in D_2O/TFE mixtures, the HEWL-RC surface surrounding the vibrational probe has a solvation composition that resembles a solution between 75% TFE and pure TFE, clearly showing there is a lack of water at the protein surface. The vibrational lifetime achieved through only the addition of 10% co-solvent provides clear evidence that the TFE is preferentially drawn to the protein at the hydrophobic region.

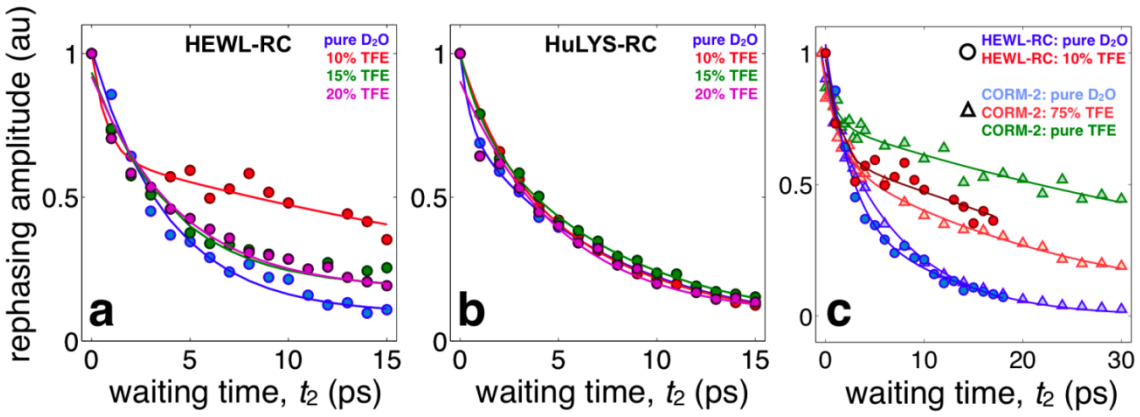

Figure 5.8 Vibrational relaxation for HEWL-RC (a) and HuLys-RC (b) in D_2O/TFE mixtures ranging from 0% to 20% TFE v/v. The addition of small amounts of TFE results in a large increase in the vibrational lifetime of HEWL-RC, followed by a monotonic decrease upon further addition. The increase in lifetime at low concentrations is the result of preferential solvation, and the subsequent decrease in lifetime is the result of the onset of partial protein destabilization. In contrast, HuLys-RC shows no sensitivity to TFE, suggesting this region of the protein resists solvent exchange with TFE and remains hydrated. (c) A comparison of the co-solvent dependent relaxation for HEWL-RC (cirlces) and CORM-2 (triangles) shows that at 10% TFE, HEWL-RC indicates a local solvation environment with nearly no water, with a relaxation timescale similar to other metal carbonyls in alcohol environments.

Further addition of TFE induces a decrease of the vibrational lifetime, resulting in relaxation times that reflect a homogeneous solution of water and TFE (15% TFE T_1 = 3.99 ± 0.60, 20% TFE T_1 = 4.41 ± 0.48 ps). This decrease in vibrational lifetime, which returns to characteristic timescales for water-assisted relaxation by 20% TFE, warrants additional discussion. This experimental observation, that preferential solvation at low TFE concentration is not sustained at higher TFE concentrations, suggests the emergence of structural instability of the protein at TFE concentrations above 10%. Previous reports using

a combination of spectroscopic techniques have shown that TFE concentrations near 15% can promote significant structural changes, including some destabilization of protein tertiary structure. Early work by Dobson using circular dichroism found TFE enhanced the overall helical content of the protein, but at the cost of destabilization of tertiary structure.[55] Our experimental results are consistent with helical portions of the protein being susceptible to dehydration and interactions with the hydrophobic portions of TFE. The decreased lifetime is consistent with the following scenario: As the constrained water is relieved and the protein alters its structure, the solvation environment becomes a mixture of D_2O/TFE as the collective influence of the extended hydrophobic surface is disrupted due to the loosened helix packing.

The mechanism by which small molecules denature proteins has been, and remains, an area of intense research.[54-61] The present data suggest that there is a direct interaction between the protein surface and TFE, leading to the formation of a dehydrated interface between the protein and the cosolvent. This cosolvent shell in turn can modify the limited water dynamics at the surface by supplying hydrogen bonding partners through the alcohol's hydroxyl group. This interpretation would be consistent with a mixed direct[59,62] and indirect[60,61] mechanism, where the cosolvent, directed to regions of constrained water, essentially coats the protein surface, promoting intraprotein hydrogen bonding and stabilizing secondary structure. Cosolvent association destabilizes the tertiary contacts between helices once the protein becomes so dehydrated that it loses the hydrophobic driving force to fold, resulting in partial denaturation, effectively reducing the cooperativity. This picture of TFE-modulated lysozyme stability is consistent with thermodynamic measurements based on calorimetry and structural studies using NMR spectroscopy.[58]

While we observe that the structured region of the HEWL-RC complex leads to constrained water that can drive solvent exchange, the unstructured β-region of HuLys is solvated by bulk-like water, suggesting that this region would not experience substantial solvent exchange. **Figure 5.8b** shows the vibrational relaxation of HuLys-RC in TFE/D_2O solution. Indeed, the vibrational relaxation of the label at this site shows no dependence on TFE, indicating that this location resists preferential dehydration by TFE and shows a

solvation environment that might be expected for a simple mixture of D_2O/TFE (**Figure 5.7**). Comparing the experimental observations of HEWL-RC and HuLys-RC it is clear that the interaction of TFE with the protein depends, to some degree, on the extended properties of the surface and not simply on individual amino acid residues since the vibrational probe is attached to a histidine residue in both cases.

The correlation between constrained water and solvent exchange demonstrates how the release of dynamically constrained water can drive hydrophobic association. It is known, however, that for many association processes the entropic contribution is insufficient to account for the total change in free energy.[63] While the hydrophobic interaction between the protein surface and the hydration environment is indeed the driving force for such processes, its influence is not limited to entropic changes associated with liberating the water's constraints[58] since expelling hydration water affords enthalpic gains by restoring hydrogen bonding that is diminished near extended surfaces.[2] Moreover, since many macromolecular assembly processes are kinetically controlled the time required to allow for the diffusive liberation of constrained water may be too long given that the approaching extended hydrophobic surfaces are both solvated by water with diffusivity that is lower than the bulk.

5.6 Conclusions

The results presented here provide a site-specific probe of heterogeneous hydration dynamics of large proteins in pure H_2O and D_2O, and, more importantly, provide experimental evidence of the mechanism of the hydration slowdown. A key aspect of this work is the study of labeled proteins at μM concentrations, which allows an unobstructed observation of the influence of the protein surface on hydration water. The results indicate that a single lysozyme protein is capable of influencing its hydration environment. This result is to be contrasted to numerous other studies that rely on high concentrations of solute in order to observe slowed water dynamics, where the crowding of multiple solutes can cooperatively constrain the hydration water. Although crowding is a central aspect of *in vivo* chemical biology, it is essential to characterize a single protein's influence over its hydration environment in addition to the specific or nonspecific perturbations induced by crowders.

Evidence for constrained water is found near the large, structured α domain of HEWL (**Figure 5.4**), where the individual amino acid residues act in a cooperative manner to create an extended hydrophobic surface, depriving water of hydrogen bonding partners. In contrast, bulk-like water is found on the unstructured region of HuLys (**Figure 5.4**), where the residues behave as independent solutes with a hydration environment resembling that of a small molecule. Around these individual residues water retains a bulk-like hydrogen bonding network and the dynamics are not suppressed. It is important to note that it is precisely this unstructured and flexible region that acts as a flap over the substrate binding site.

In addition to the heterogeneous nature of hydration dynamics surrounding large globular proteins, this study also reveals the correlation between dynamically constrained water and the driving force for site-specific association at the protein surface. The free energy that is released upon dehydration of constrained water appears to be sufficient to drive the association of small molecules to the protein surface. Using a water sensing vibrational probe, we can distinguish between direct cosolvent-protein association and indirect disruption of the hydration layer. Based on the marked changes in the vibrational lifetime, our data are consistent with direct displacement of water from the protein surface. This view is further buttressed by the subsequent cosolvent-induced destabilization caused by competing out the water to such an extent that the protein's tertiary structure loosens, evidenced by the infiltration of water in the absence of the structured, extended hydrophobic surface. Taken together, our data indicates that the spatially heterogeneous dynamics of hydration water is, to a significant degree, responsible for site-directed hydrophobic association, a perspective that should be helpful in rationalizing and perhaps in guiding the controlled disruption of deleterious protein-protein interactions.

We also observe that the hydration dynamics around small hydrophobic metal-carbonyls reflects bulk-like dynamics, with spectral diffusion timescales measured to be around 1.5 ps. Furthermore, surface labeling of a protein reveals a modest slowdown of roughly a factor of 2 between bulk D_2O and hydrating D_2O, in quantitative agreement with predictions from MD simulations. The retardation is attributed to the collective solvation dynamics becoming

slowed due to the hindering of hydrogen bond switching events by the extended hydrophobic surface of the protein. This study marks the most direct experimental evidence to date on the slowdown of water around hydrophobic proteins, and provides the foundation for extending this methodology into crowded, cellular like environments.

Water's importance in biology cannot be overstated, but ample evidence shows that often only a small amount of water is truly necessary for function. Water-sensitive vibrational probes on the surfaces of proteins will enable an experimental platform to systematically map interactions between proteins and other biomacromolecules including DNA and antibodies, while simultaneously monitoring the role (or lack thereof) played by the thin layer of hydration water.

References:

(1) Ball, P.: Water as an active constituent in cell biology. *Chemical Reviews* **2008**, *108*, 74-108.

(2) Chandler, D.: Interfaces and the driving force of hydrophobic assembly. *Nature* **2005**, *437*, 640-647.

(3) Scatena, L. F.; Brown, M. G.; Richmond, G. L.: Water at hydrophobic surfaces: Weak hydrogen bonding and strong orientation effects. *Science* **2001**, *292*, 908-912.

(4) Bagchi, B.: Water dynamics in the hydration layer around proteins and micelles. *Chemical Reviews* **2005**, *105*, 3197-3219.

(5) Chieffo, L. R.; Shattuck, J. T.; Pinnick, E.; Amsden, J. J.; Hong, M. K.; Wang, F.; Erramilli, S.; Ziegler, L. D.: Nitrous oxide vibrational energy relaxation is a probe of interfacial water in lipid bilayers. *Journal of Physical Chemistry B* **2008**, *112*, 12776-12782.

(6) Fenn, E. E.; Wong, D. B.; Fayer, M. D.: Water dynamics at neutral and ionic interfaces. *Proceedings of the National Academy of Sciences of the United States of America* **2009**, *106*, 15243-15248.

(7) Fayer, M. D.; Levinger, N. E.: Analysis of Water in Confined Geometries and at Interfaces. *Annual Review of Analytical Chemistry, Vol 3* **2010**, *3*, 89-107.

(8) Bakulin, A. A.; Liang, C.; Jansen, T. L. C.; Wiersma, D. A.; Bakker, H. J.; Pshenichnikov, M. S.: Hydrophobic Solvation: A 2D IR Spectroscopic Inquest. *Accounts of Chemical Research* **2009**, *42*, 1229-1238.

(9) Pizzitutti, F.; Marchi, M.; Sterpone, F.; Rossky, P. J.: How protein surfaces induce anomalous dynamics of hydration water. *Journal of Physical Chemistry B* **2007**, *111*, 7584-7590.

(10) Stirnemann, G.; Rossky, P. J.; Hynes, J. T.; Laage, D.: Water reorientation, hydrogen-bond dynamics and 2D-IR spectroscopy next to an extended hydrophobic surface. *Faraday Discussions* **2010**, *146*, 263-281.

(11) Pal, S. K.; Peon, J.; Zewail, A. H.: Biological water at the protein surface: Dynamical solvation probed directly with femtosecond resolution. *Proceedings of the National Academy of Sciences of the United States of America* **2002**, *99*, 1763-1768.

(12) Qiu, W.; Kao, Y.-T.; Zhang, L.; Yang, Y.; Wang, L.; Stites, W. E.; Zhong, D.; Zewail, A. H.: Protein surface hydration mapped by site-specific mutations. *Proceedings of the National Academy of Sciences of the United States of America* **2006**, *103*, 13979-13984.

(13) Zhang, L.; Wang, L.; Kao, Y.-T.; Qiu, W.; Yang, Y.; Okobiah, O.; Zhong, D.: Mapping hydration dynamics around a protein surface. *Proceedings of the National Academy of Sciences of the United States of America* **2007**, *104*, 18461-18466.

(14) Nucci, N. V.; Pometun, M. S.; Wand, A. J.: Site-resolved measurement of water-protein interactions by solution NMR. *Nature Structural & Molecular Biology* **2011**, *18*, 245-U315.

(15) Nucci, N. V.; Pometun, M. S.; Wand, A. J.: Mapping the Hydration Dynamics of Ubiquitin. *Journal of the American Chemical Society* **2011**, *133*, 12326-12329.

(16) Stirnemann, G.; Hynes, J. T.; Laage, D.: Water Hydrogen Bond Dynamics in Aqueous Solutions of Amphiphiles. *Journal of Physical Chemistry B* **2010**, *114*, 3052-3059.

(17) Rezus, Y. L. A.; Bakker, H. J.: Observation of immobilized water molecules around hydrophobic groups. *Physical Review Letters* **2007**, *99*.

(18) Fenimore, P. W.; Frauenfelder, H.; McMahon, B. H.; Young, R. D.: Bulk-solvent and hydration-shell fluctuations, similar to alpha- and beta-fluctuations in glasses, control protein motions and functions. *Proceedings of the National Academy of Sciences of the United States of America* **2004**, *101*, 14408-14413.

(19) Frauenfelder, H.; Chen, G.; Berendzen, J.; Fenimore, P. W.; Jansson, H.; McMahon, B. H.; Stroe, I. R.; Swenson, J.; Young, R. D.: A unified model of protein dynamics. *Proceedings of the National Academy of Sciences of the United States of America* **2009**, *106*, 5129-5134.

(20) Wei, B. Q. Q.; Baase, W. A.; Weaver, L. H.; Matthews, B. W.; Shoichet, B. K.: A model binding site for testing scoring functions in molecular docking. *Journal of Molecular Biology* **2002**, *322*, 339-355.

(21) Halperin, I.; Ma, B. Y.; Wolfson, H.; Nussinov, R.: Principles of docking: An overview of search algorithms and a guide to scoring functions. *Proteins-Structure Function and Genetics* **2002**, *47*, 409-443.

(22) Jones, S.; Thornton, J. M.: Principles of protein-protein interactions. *Proceedings of the National Academy of Sciences of the United States of America* **1996**, *93*, 13-20.

(23) Papoian, G. A.; Ulander, J.; Wolynes, P. G.: Role of water mediated interactions in protein-protein recognition landscapes. *Journal of the American Chemical Society* **2003**, *125*, 9170-9178.

(24) Jayaram, B.; Jain, T.: The role of water in protein-DNA recognition. *Annual Review of Biophysics and Biomolecular Structure* **2004**, *33*, 343-361.

(25) Brooks, C. L.; Karplus, M.: Solvent Effects on Protein Motion and Protein Effects on Solvent Motion - Dynamics of the Active-Site Region of Lysozyme. *Journal of Molecular Biology* **1989**, *208*, 159-181.

(26) Makarov, V.; Pettitt, B. M.; Feig, M.: Solvation and hydration of proteins and mucleic acids: A theoretical view of simulation and experiment. *Accounts of Chemical Research* **2002**, *35*, 376-384.

(27) Heyden, M.; Havenith, M.: Combining THz spectroscopy and MD simulations to study protein-hydration coupling. *Methods* **2010**, *52*, 74-83.

(28) Niehues, G.; Heyden, M.; Schmidt, D. A.; Havenith, M.: Exploring hydrophobicity by THz absorption spectroscopy of solvated amino acids. *Faraday Discussions* **2011**, *150*, 193-207.

(29) Jackson, C. S.; Schmitt, S.; Dou, Q. P.; Kodanko, J. J.: Synthesis, Characterization, and Reactivity of the Stable Iron Carbonyl Complex Fe(CO)(N4Py) (ClO4)(2):

Photoactivated Carbon Monoxide Release, Growth Inhibitory Activity, and Peptide Ligation. *Inorganic Chemistry* **2011**, *50*, 5336-5338.

(30) Loparo, J. J.; Roberts, S. T.; Tokmakoff, A.: Multidimensional infrared spectroscopy of water. I. Vibrational dynamics in two-dimensional IR line shapes. *Journal of Chemical Physics* **2006**, *125*.

(31) Loparo, J. J.; Roberts, S. T.; Tokmakoff, A.: Multidimensional infrared spectroscopy of water. II. Hydrogen bond switching dynamics. *Journal of Chemical Physics* **2006**, *125*.

(32) Laage, D.; Stirnemann, G.; Hynes, J. T.: Why Water Reorientation Slows without Iceberg Formation around Hydrophobic Solutes. *Journal of Physical Chemistry B* **2009**, *113*, 2428-2435.

(33) Fayer, M. D.: Dynamics of Water Interacting with Interfaces, Molecules, and Ions. *Accounts of Chemical Research* **2012**, *45*, 3-14.

(34) Park, S.; Fayer, M. D.: Hydrogen bond dynamics in aqueous NaBr solutions. *Proceedings of the National Academy of Sciences of the United States of America* **2007**, *104*, 16731-16738.

(35) Yang, M.; Szyc, L.; Elsaesser, T.: Decelerated Water Dynamics and Vibrational Couplings of Hydrated DNA Mapped by Two-Dimensional Infrared Spectroscopy. *Journal of Physical Chemistry B* **2011**, *115*, 13093-13100.

(36) Motterlini, R.; Otterbein, L. E.: The therapeutic potential of carbon monoxide. *Nature Reviews Drug Discovery* **2010**, *9*, 728-U24.

(37) King, J. T.; Ross, M. R.; Kubarych, K. J.: Water-Assisted Vibrational Relaxation of a Metal Carbonyl Complex Studied with Ultrafast 2D-IR. *Journal of Physical Chemistry B* **2012**, *116*, 3754-3759.

(38) Stillinger, F. H.: Structure in Aqueous Solutions of Nonpolar Solutes from the Standpoint of Scaled-Particle Theory. *Journal of Solution Chemistry* **1973**, *2*, 141-158.

(39) Lum, K.; Chandler, D.; Weeks, J. D.: Hydrophobicity at small and large length scales. *Journal of Physical Chemistry B* **1999**, *103*, 4570-4577.

(40) Smith, J. D.; Saykally, R. J.; Geissler, P. L.: The effects of dissolved halide anions on hydrogen bonding in liquid water. *Journal of the American Chemical Society* **2007**, *129*, 13847-13856.

(41) Li, I. T. S.; Walker, G. C.: Signature of hydrophobic hydration in a single polymer. *Proceedings of the National Academy of Sciences of the United States of America* **2011**, *108*, 16527-16532.

(42) Lee, C. Y.; McCammon, J. A.; Rossky, P. J.: The Structure of Liquid Water at an Extended Hydrophobic Surface. *Journal of Chemical Physics* **1984**, *80*, 4448-4455.

(43) Laage, D.; Hynes, J. T.: A molecular jump mechanism of water reorientation. *Science* **2006**, *311*, 832-835.

(44) Ji, M.; Odelius, M.; Gaffney, K. J.: Large Angular Jump Mechanism Observed for Hydrogen Bond Exchange in Aqueous Perchlorate Solution. *Science* **2010**, *328*, 1003-1005.

(45) Moilanen, D. E.; Wong, D.; Rosenfeld, D. E.; Fenn, E. E.; Fayer, M. D.: Ion-water hydrogen-bond switching observed with 2D IR vibrational echo chemical exchange spectroscopy. *Proceedings of the National Academy of Sciences of the United States of America* **2009**, *106*, 375-380.

(46) Stirnemann, G.; Sterpone, F.; Laage, D.: Dynamics of Water in Concentrated Solutions of Amphiphiles: Key Roles of Local Structure and Aggregation. *Journal of Physical Chemistry B* **2011**, *115*, 3254-3262.

(47) Schwartz, B. J.; Rossky, P. J.: The isotope effect in solvation dynamics and nonadiabatic relaxation: A quantum simulation study of the photoexcited solvated electron in D2O. *Journal of Chemical Physics* **1996**, *105*, 6997-7010.

(48) King, J. T.; Arthur, E. J.; Brooks, C. L. I.; Kubarych, K. J.: Site-specific hydration dynamics of globular proteins and the role of constrained water in solvent exchange with amphiphilic cosolvents. *Journal of Physical Chemistry B* **2012**, *116*, 5604-5611.

(49) Sterpone, F.; Stirnemann, G.; Laage, D.: Magnitude and Molecular Origin of Water Slowdown Next to a Protein. *Journal of the American Chemical Society* **2012**, *134*, 4116-4119.

(50) Nicholls, A.; Sharp, K. A.; Honig, B.: Protein Folding and Association - Insights from the Interfacial and Thermodynamic Properties of Hydrocarbons. *Proteins-Structure Function and Genetics* **1991**, *11*, 281-296.

(51) Eaves, J. D.; Loparo, J. J.; Fecko, C. J.; Roberts, S. T.; Tokmakoff, A.; Geissler, P. L.: Hydrogen bonds in liquid water are broken only fleetingly. *Proceedings of the National Academy of Sciences of the United States of America* **2005**, *102*, 13019-13022.

(52) Wei, T.; Carignano, M. A.; Szleifer, I.: Lysozyme Adsorption on Polyethylene Surfaces: Why Are Long Simulations Needed? *Langmuir* **2011**, *27*, 12074-12081.

(53) Cammers-Goodwin, A.; Allen, T. J.; Oslick, S. L.; McClure, K. F.; Lee, J. H.; Kemp, D. S.: Mechanism of stabilization of helical conformations of polypeptides by water containing trifluoroethanol. *Journal of the American Chemical Society* **1996**, *118*, 3082-3090.

(54) Roccatano, D.; Colombo, G.; Fioroni, M.; Mark, A. E.: Mechanism by which 2,2,2-trifluoroethanol/water mixtures stabilize secondary-structure formation in peptides: A molecular dynamics study. *Proceedings of the National Academy of Sciences of the United States of America* **2002**, *99*, 12179-12184.

(55) Povey, J. F.; Smales, C. M.; Hassard, S. J.; Howard, M. J.: Comparison of the effects of 2,2,2-trifluoroethanol on peptide and protein structure and function. *Journal of Structural Biology* **2007**, *157*, 329-338.

(56) Schellman, J. A.: Protein stability in mixed solvents: A balance of contact interaction and excluded volume. *Biophysical Journal* **2003**, *85*, 108-125.

(57) Sharp, K. A.; Vanderkooi, J. M.: Water in the Half Shell: Structure of Water, Focusing on Angular Structure and Solvation. *Accounts of Chemical Research* **2010**, *43*, 231-239.

(58) Tanford, C.: Interfacial Free-Energy and the Hydrophobic Effect. *Proceedings of the National Academy of Sciences of the United States of America* **1979**, *76*, 4175-4176.

(59) Hua, L.; Zhou, R.; Thirumalai, D.; Berne, B. J.: Urea denaturation by stronger dispersion interactions with proteins than water implies a 2-stage unfolding. *Proceedings of the National Academy of Sciences of the United States of America* **2008**, *105*, 16928-16933.

(60) Frank, H. S.; Franks, F.: Structural Approach to Solvent Power of Water for Hydrocarbons - Urea as a Structure Breaker. *Journal of Chemical Physics* **1968**, *48*, 4746-&.

(61) Bennion, B. J.; Daggett, V.: The molecular basis for the chemical denaturation of proteins by urea. *Proceedings of the National Academy of Sciences of the United States of America* **2003**, *100*, 5142-5147.

(62) Tanford, C.: Protein denaturation. C. Theoretical models for the mechanism of denaturation. *Advances in protein chemistry* **1970**, *24*, 1-95.

(63) Ross, P. D.; Subramanian, S.: Thermodynamics of Protein Association Reactions - Forces Contributing to Stability. *Biochemistry* **1981**, *20*, 3096-3102.

Chapter 6

Protein and Hydration Dynamics in Crowded Environments

Part of the work presented in this chapter has been published in the following paper:

J. T. King, K. J. Kubarych "*Site-Specific Coupling of Hydration Water and Protein Flexibility Studied in Solution with Ultrafast 2D-IR Spectroscopy*" Journal of the American Chemical Society, 134, 2012, 18705-1871.

6.1 Introduction

There is considerable evidence for the slaving of biomolecular dynamics to the motions of the surrounding solvent environment, but to-date there have been few direct experimental measurements capable of site selectively probing both the dynamics of the water and the protein with ultrafast time resolution. Here, 2DIR is used to study the ultrafast hydration and protein dynamics sensed by a metal carbonyl vibrational probe covalently attached to the surface of hen egg white lysozyme dissolved in D_2O/glycerol solutions. Surface labeling provides direct access to the dynamics at the protein-water interface, where both the hydration and the protein dynamics can be observed simultaneously through the vibrational probe's frequency-frequency correlation function. In pure D_2O, the correlation function

shows a fast initial 3 ps decay corresponding to fluctuations of the hydration water, followed by a significant static offset attributed to fluctuations of the protein that are not sampled within the <20 ps experimental window. Adding glycerol increases the bulk solvent viscosity while leaving the protein structurally intact and hydrated. The hydration dynamics exhibit a greater than three-fold slowdown between 0 and 80% glycerol (v/v), and the contribution from the protein's dynamics is found to slow in a nearly identical fashion. In addition, the magnitude of the dynamic slowdown associated with hydrophobic hydration is directly measured and shows quantitative agreement with predictions from molecular dynamics simulations.

In addition, protein-hydration dynamics of HEWL-RC are observed in the presence of macromolecular crowding agents. While experiments performed on isolated proteins in simple environments has provided important insight into the design and function of biological macromolecules, there is increasing interest in studying the behavior of these molecules in more complex, cell-like environments.[1-11] It has been estimated that proteins fold and function in cellular environments that can contain up to 400 mg/mL if macromolecules.[12] Crowding of proteins by macromolecules is traditionally considered from an energetic standpoint, where macromolecules induce hard-core repulsive interactions, which tend to stabilize more compact forms of proteins, and weak attractive interactions, which tend to induce more disordered structures.[13] The extent to which repulsive and attractive forces contribute in crowded environments is a still a debated topic.[4 11] PEG400 is used as a polymer crowding agent that, similar to glycerol, preserves the structure of HEWL and leaves the protein hydrated. We study HEWL-RC in D_2O/PEG400 mixtures ranging up to 80% PEG400 v/v. An unexpected transition is observed at roughly 50% PEG400 were the protein-hydration dynamics drastically slow down. The protein-hydration dynamics are only mildly coupled to the PEG400 concentration before and after the transition. The dynamical transition is attributed to a percolation-like transition occurring when the macromolecules are close enough for collective hydration. Much like HEWL, PEG400 is a larger hydrophobic molecule capable of perturbing the dynamics of the surrounding waters,

and thus both macromolecules have extensive hydration environments. The overlap of these hydration shells is the suspected source of the observed dynamical transition.

To further support the results and interpretation of protein crowding with PEG400 we performed a similar experiment using unlabeled lysozyme as the crowding agent. A 20 mg/mL solution of HEWL-RC was crowded with up to 140 mg/mL of unlabeled human lysozyme. Similar to the observations made using PEG400 a sharp transition is observed between 100 and 120 mg/mL. Using the well-defined shape of lysozyme we are able to estimate that the protein-protein distance at this concentration is roughly 30-40 Å, suggesting that lysozyme has a hydration environment that extends upwards of 15-20 Å before "bulk-like" water is observed. Such an extended hydration environment provides insight into crowded environments, were the extended influence of the macromolecules needs to be considered for crowded conditions.

6.2 Small Molecule Crowders

To further expand this method of studying the hydration environments of proteins with site-specific resolution, we attempt to modulate and further constrain the hydration water around HEWL using a kosmotropic co-solvent, glycerol. It is known from neutron scattering experiments[14-16] and thermodynamic data[17,18] that glycerol is preferentially excluded from the protein surface at nearly all concentrations. As a result the protein structure and first hydration shell are preserved in the presence of glycerol, which acts to increase the viscosity of the bulk solvent without altering the chemical environment. This co-solvent approach provides an excellent platform for studying the coupling of protein and hydration dynamics to the bulk solvent.

Solvent Dependent Linewidths and Vibrational Relaxation. The 2D-IR spectra and linear FTIR spectrum of HEWL-RC in D_2O/glycerol mixtures are shown in **Figure 6.1** and **Figure 6.2a**, respectively. Because of the stronger signal strength in the 2D-IR spectrum the low-frequency mode is analyzed. From the linear spectrum the center frequency and the peak width (FWHM) of the low-frequency transition were determined. Using the linear and 2D-IR spectrum together the homogeneous and inhomogeneous contributions to the total

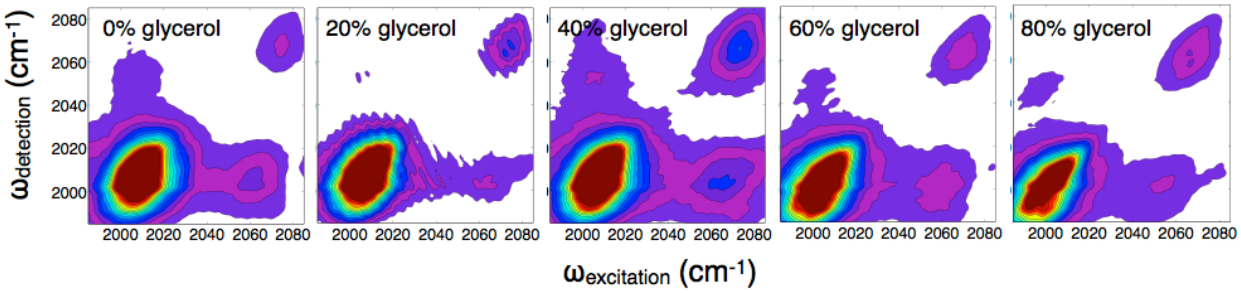

Figure 6.1 2DIR absolute value rephasing spectra of HEWL-RC in D2O/glycerol mixtures. The waiting time between pump pulses and probe pulses, t_2, is 500 fs for all spectra.

linewidth were extracted using a procedure introduced by Kwak et al.[19] The homogeneous linewidth shows a sharp increase at low glycerol concentrations, followed by a steady decrease. The decrease in linewidths corresponds to slower dephasing times, which reflects an increase in local viscosity induced by higher concentrations of glycerol. The inhomogeneous contribution is found to increase only slightly over the entire range of mixtures. The increase in inhomogeneous broadening of the CO transitions reflects a larger configurational space being sampled by the local region of the protein surrounding the vibrational chromophore.

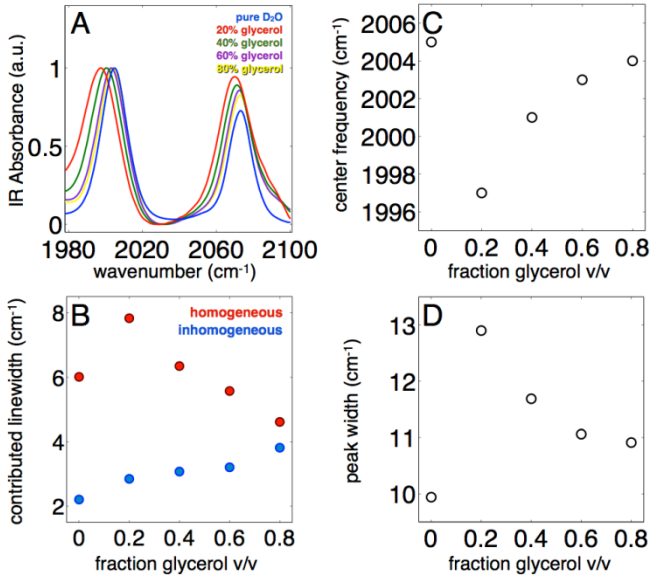

Figure 6.2 (A) FTIR spectra of HEWL-RC in pure D_2O and D_2O/glycerol mixtures. The main observations in the linear spectrum are the center frequencies of the low frequency mode (C) and the peak widths of the low frequency mode (D). The peak width measured in linear FTIR spectroscopy contain contributions from homogeneous and inhomogeneous broadening. 2D-IR spectroscopy allows these contributions to be separated using the FWHM of the linear spectrum and the *C(t=0)* value of the FFCF (B).

2D-IR spectra were recorded for HEWL-RC in pure D_2O as well as in D_2O/glycerol mixtures (20, 40, 60, 80% glycerol by volume) for t_2 waiting times of 0 to 11 ps with 1 ps steps. The previously reported sub-5 ps relaxation of the CO vibrations in water and heavy water limits the observational window.[20,21] Our previous work on HEWL-RC in mixtures of D_2O and 2,2,2-trifluoroethanol (TFE) found that the dehydration of the protein surface results in a pronounced increase in the carbonyl label's vibrational lifetime.[20] In the solvent

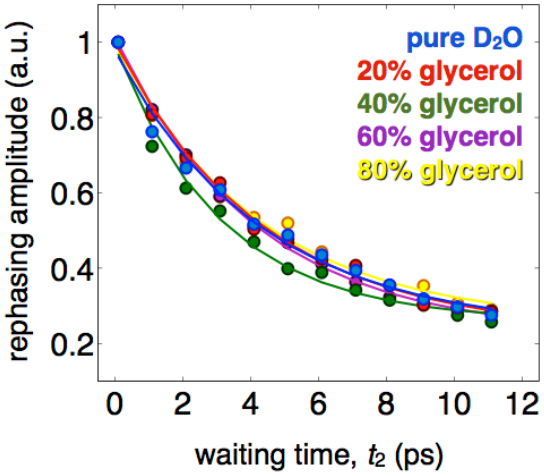

Figure 6.3 (A) Vibrational relaxation of the low frequency mode extracted from the rephasing spectrum. The vibrational lifetimes are faster than 5 ps for all solvent compositions, suggesting that the region of the vibrational probe remains largely hydrated despite the presence of the cosolvent.

mixtures, the vibrational lifetime of the 2004 cm^{-1} mode was found to be insensitive to the addition of glycerol, which provides consistent, yet novel, confirmation that glycerol is indeed preferentially excluded from the protein surface (**Figure 6.3**), and that the protein remains solvated by water.

Spectral Dynamics of HEWL-RC in D_2O/glycerol mixtures. The FFCF for the 2004 cm^{-1} mode of HEWL-RC in pure D_2O is shown in **Figure 6.4a**. The two distinguishing features in the correlation function are a fast initial decay and a significant static offset. Again, the fast decay occurs on a 2.7 ps timescale, corresponding to the hydration dynamics. The static offset of the correlation function results from inhomogeneities arising from

protein conformations that fluctuate on the timescale of tens of picoseconds or longer, and hence appear static on the timescale accessible within the vibrational lifetime of the probe.[22-

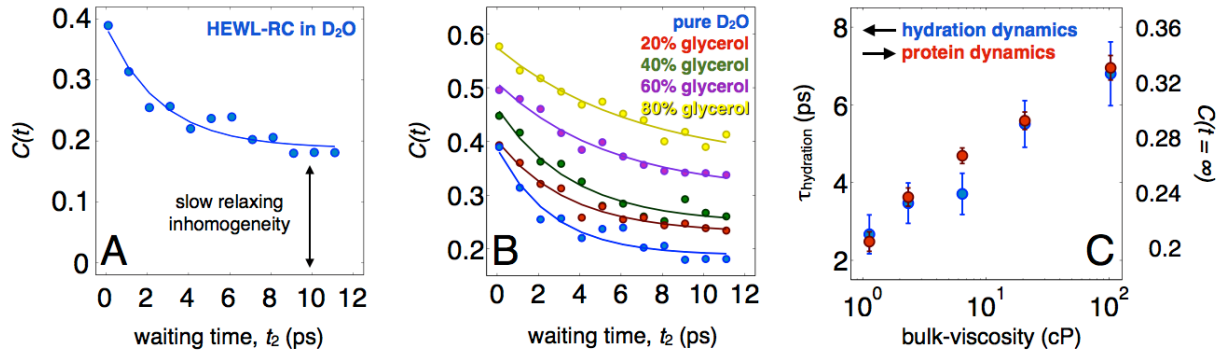

Figure 6.4 (A) FFCF of HEWL-RC in pure D_2O, highlighting the initial decay due to hydration dynamics and the static offset of the correlation function corresponding to the protein dynamics. (B) Correlation functions for each solvent composition, ranging from pure D_2O to 80% glycerol by volume. From the data it is clear that there is a marked slowing in the hydration dynamics as well as in the protein dynamics (C).

[24] Although the protein contribution is not time resolved and appears only as a static offset, the large difference in timescales between the hydration dynamics and the protein conformational dynamics allows both to be measured simultaneously. While the observed vibrational lifetimes suggest that glycerol does not directly interact with the protein surface, the measured spectral diffusion shows pronounced changes upon the addition of glycerol (**Figure 6.4b**). The timescale of the fast decay as a function of bulk solvent viscosity is shown in **Figure 6.4c**. The viscosity of D_2O/glycerol mixtures was calculated using a kinematic model, and follows a similar viscosity trend as H_2O/glycerol mixtures that have been measured experimentally. This observation shows that glycerol indirectly influences the hydration dynamics without leading to dehydration of the protein surface. Furthermore, the protein flexibility is clearly hindered in a nearly identical manner (**Figure 6.4c**).

Despite evidence that there is little mixing between the hydration water and the bulk-solvent, both the protein and hydration water are linked to the dynamics of the bulk solvent. The timescales of the spectral diffusion caused by the hydration environment increase more than three-fold, ranging from 2 to 7 ps over a bulk viscosity range of 1 to 120 cP. We note that previous studies observing spectral diffusion in a small metal carbonyl complex in alcohol solvents yielded a similar change in spectral diffusion timescales, but required a

much smaller viscosity range (1-4 cP).[25] The relatively weak coupling of the hydration dynamics to the bulk viscosity is not unexpected given the inhomogeneous nature of the solvation environment, which gradually transitions from pure water at the protein surface to a homogeneous bulk solution. In addition, dynamical decoupling from solvent dynamics can become accentuated at sufficiently high viscosities, which has been observed with molecular reorientation[26] as well as dynamics in fragile glasses.[27]

Side-chain motions are often observed in proteins as a decay of the FFCF on the timescale of tens of picoseconds.[28,29] Here we do not observe any indication of side-chain motions contributing to the decay of the correlation functions, which are accurately fit using a single exponential decay and a static offset. Recent NMR relaxation results have found that the side chains of HEWL show unusually rigid dynamics[30] as compared to what is more traditionally observed in protein backbone[31] and side-chain motions.[32] The rigidity of side-chain dynamic of HEWL is also suggested from thermodynamic data.[33] The rigidity of HEWL could certainly limit the contribution of side-chain dynamics to the FFCF. In addition, the crystal structure of HEWL-RC shows that the CO oscillators are in the immediate vicinity of isoleucine, phenylalanine and alanine residues, which are non-polar side-chains that likely do not significantly influence the transition frequency of the CO vibrational modes. Furthermore, we have shown here, as well as in previous studies, that the vibrational relaxation is dominated by the hydration water, and in fact we have shown that the protein makes only minor contributions to the vibrational relaxation. It is not surprising that the hydration water would also dominate the spectral dynamics as it does the vibrational relaxation.

Calorimetric data has shown that lysozyme undergoes only modest changes in conformational entropy over the glycerol range studied here. Significant changes to the structural ensemble are only induced at higher concentrations, where the structures converge to a narrower ensemble.[18] The observed trend in the static component of the correlation function is thus attributed mostly to a dynamical effect, where the timescales for sampling conformational substates within an ensemble of configurations is modulated by the addition

of glycerol. This picture is supported by the nearly constant inhomogeneous spectral width at all glycerol concentrations (**Figure 6.2**).

Without the aid of molecular dynamics simulations it is difficult to assign the protein motions that are being influenced by the presence of the cosolvent, but in general, protein motion is known to occur on several timescales. Because the protein's contribution is so sensitive to glycerol concentration, it is probable that the motions most susceptible to the solvent occur on timescales just outside the experimental window, and thus can have a significant influence on the FFCF. The hinge-like modes of lysozyme, for instance, are characterized by frequencies of a few wavenumbers, corresponding to periods of 10-30 ps.[34,35] These motions can significantly modulate the frequency of the vibrational probe, which is located at an interface between domains that exhibit opposite displacements when viewed as normal modes.

Site-Specificity and Normal Mode Analysis Suggests protein-solvent coupling "Susceptibility." The His15-bound probe is located at the interface between two helical domains that for some of the low-frequency modes exhibit displacements corresponding to an opening-and-closing of the tertiary contact (**Figure 6.5**). From the results of an elastic network normal mode analysis (NMA),[36] we analyzed the relative motions of the α-carbons

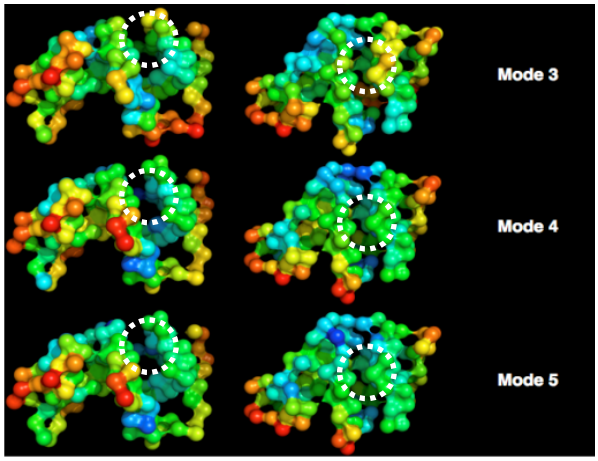

Figure 6.5 HEWL-RC from PDB file 2XJW showing the magnitude of motion of the α-carbonrs for low-frequency modes.

in each of the first five normal modes using the α-carbon of His15 as an origin. The NMA output consists of a set of coordinates for the α-carbons displaced along the normal mode from the initial structure, so taking the difference between the final and initial positions for α-carbon *j* results in a net displacement vector $\vec{d}_j$. In addition to the amplitude of motion given by the magnitude of this vector, it is possible to use the set of displacement vectors to map the relative displacement "overlap" as follows. We assign the orientational overlap between α-carbon *j* and His15 as:

$$\sigma_{j,His15} = \vec{d}_j \cdot \vec{d}_{His15} \qquad (6.1)$$

which can range from -1 to 1 since we first normalize all of the displacement vectors. A

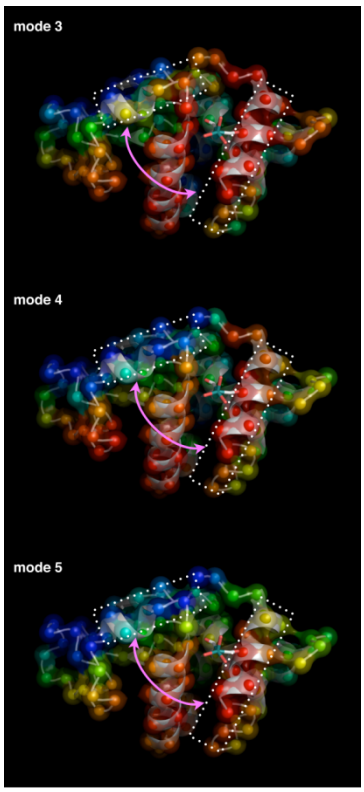

Figure 6.6 HEWL-RC from PDB file 2XJW showing the metal carbonyl label, color-coded according to the orientational overlap defined in the text. Red corresponds to motion in the same direction as that of His15, and blue is in the opposite direction, and other colors are intermediate overlaps. The three modes that have the most pronounced opening-and-closing character at the His15 label site are shown. Dotted areas correspond to the domains that open and close.

value, for example, of -1 indicates that the residue moves in precisely the opposite direction to that of the motion of His15. This analysis loses the magnitude of motion, but that information is apparent from the magnitude. The map is shown in **Figure 6.6** for modes 3, 4 and 5, which showed the largest His15 displacements. The color coding in the map ranges from blue (-1) to red (+1). The displacement overlap maps show that for these three modes, the probe is located between two helices that exhibit considerable hinging motion.

The coupling of hydration and protein dynamics suggests that protein motion most susceptible to the solvent involves significant changes in the surface topology since these are necessarily accompanied by solvent reorganization. Hence, the larger amplitude motions, such as those associated with the collective, low-frequency modes, are most susceptible to solvent slaving. On the other hand, local side-chain motion unimpeded by solvent reorganization may show only a modest solvent dependence, if any. Side chains not capable of hydrogen bonding with the hydration water are likely to be particularly *insensitive* to changes in the hydration dynamics because of the limited coupling. Hence, the motions of the enzyme most susceptible to slaving are precisely those most influential to the catalytic function, including substrate binding and release. Active site slaving has already been observed in numerous rebinding and 2DIR studies using heme proteins as models.[37-40] In most heme proteins, where the binding site is buried within the interior of the protein, 2DIR studies of bound CO ligands show bulk solvent viscosity dependent spectral dynamics. Lysozyme, like many enzymes, has a surface accessible catalytic cleft, in addition to a well-studied hinging motion that becomes perturbed upon inhibitor binding.[30] Hence, lysozyme, unlike myoglobin, is a more appropriate model system to investigate the specific link between protein dynamics and catalysis, and how both are slaved to the environment. There is already significant evidence that functionally relevant protein motions occur in the absence of substrate,[41] and the present study offers a promising approach to investigate directly the fundamental picosecond dynamics that underlie these intrinsic dynamics. Since the solvent-coupling of the hinging motions of lysozyme is inherently a surface process, where the coupling of the protein dynamics to the solvent is transmitted by the hydration reorganization that is required for the protein motion, surface specific probes are required to

access the dynamics that can influence such protein motions. In the future, the use of surface probes together with probes on the interior, or at the active site, will be able to provide a more complete picture of protein-solvent coupling.

6.3 Polymer Crowding

The coupling of protein dynamics and hydration dynamics was demonstrated using glycerol

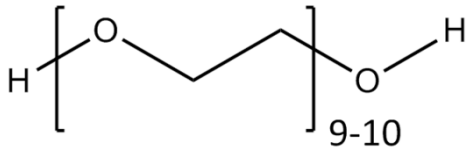

Figure 6.7 Structure of PEG 400 which was used in the polymer crowding experiments.

as a cosolvent, where a continuous and gradual slowdown of the protein-hydration dynamics as the viscosity of the bulk solvent increased was observed. Here, we use a larger polymeric cosolvent, PEG400, capable of playing a similar role as glycerol to systematically crowd HEWL-RC. The majority of experimental[10] and theoretical work on protein structure, function and dynamics in crowded environments has focused on an excluded volume picture, where crowding effects are intimately linked to changes in volume between different structural states.[1-6,8-10] The dynamical consequences of macromolecular crowding are more

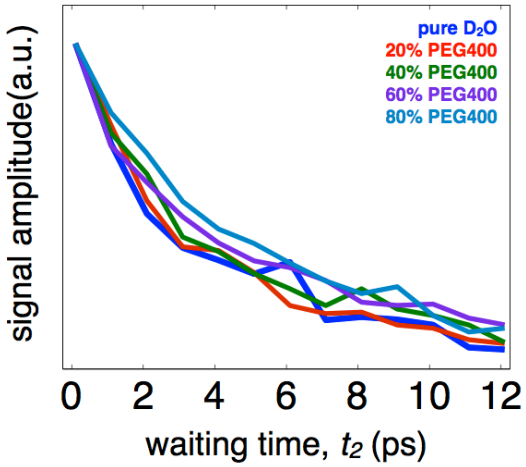

Figure 6.8 Vibrational lifetimes of HEWL-RC in ranging concentrations of PEG400.

seldom considered.[7] Using HEWL-RC crowded by PEG400 we are able to observe novel dynamical behavior of proteins under crowded conditions that are fundamentally different from the dynamical behavior in the presence of smaller cosolvents.

Polyethylene glycol 400 (PEG400) is a polyalcohol that averages a chain length of 9-10 units (**Figure 6.7**). The structure is largely hydrophobic, and in dilute solutions it has been shown to collapse in water to form a highly compact structure. PEG400 is a widely used crowding agent that has been shown to have a thermodynamically stabilizing effect of proteins, similar to what has been shown for glycerol.[42-44] We study a 1 mg/mL solution of HEWL-RC in D_2O with PEG400 concentrations ranging from 0-80% by volume. Similar to the glycerol studies, we find no evidence for protein dehydration, evidenced by no substantial increase in the vibrational lifetime (**Figure 6.8**). Observing the FFCF, however, we find an unexpected transition that occurs around 40% water composition (**Figure 6.9**). From 100% water to 60% water we find only a modest dependence of the protein-hydration dynamics on the PEG400 concentration, though the coupling is still apparent. From 60% water to 40% water, however, there is a drastic increase in both the hydration timescales, which nearly quadruple, as well as the protein fluctuations. After this transition the dependence of the dynamics on PEG400 composition becomes weak once again.

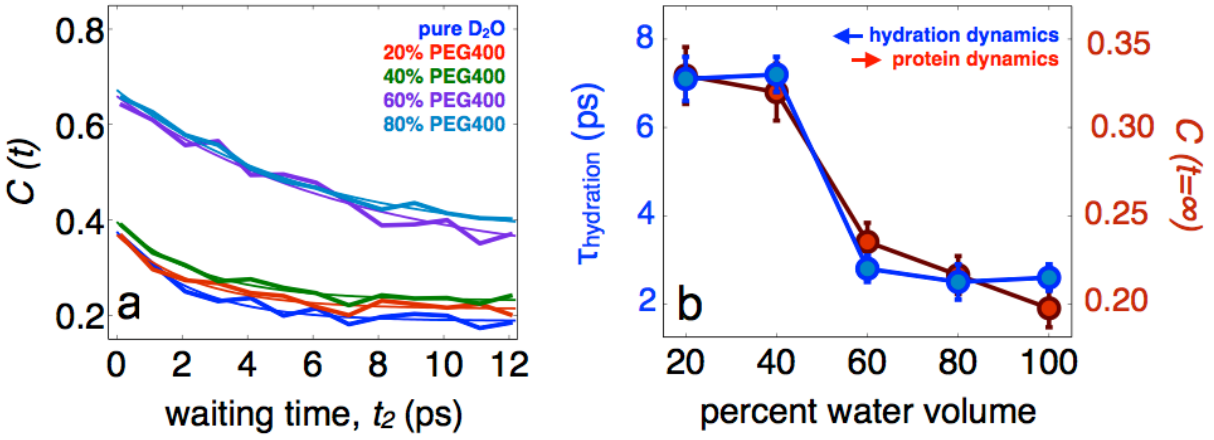

Figure 6.9 (left) FFCFs for HEWL-RC in D_2O/PEG mixtures, ranging from pure D_2O to 80% PEG by volume. (right) Hydration timescale, obtained by the initial decay of the correlation function, and the protein dynamics, estimated by the static offset of the correlation function, plotted as a function of solvent composition. A strong coupling is clear from the data, with both the hydration and protein dynamics slowing down as glycerol is added to the system. There is also a sharp dynamic transition occurring at roughly around 60% PEG. This transition is suggested to be the result of the extended protein hydration environment and the PEG hydration environment overlapping.

The transition observed in the polymer crowding experiments is attributed to the hydration shell overlap of neighboring macromolecules. Unlike glycerol, PEG400 is a larger hydrophobic molecule that collapse into a compact structure in water, similar in size to a small to medium sized proteins (such as lysozyme). The collapse into a compact structure leads to PEG400 forming a hydrophobic interface and thus an extended hydrophobic solvation environment, similar to what we see in proteins. When in a dilute solution with the protein, the macromolecules seem to remain isotropic with large distances between

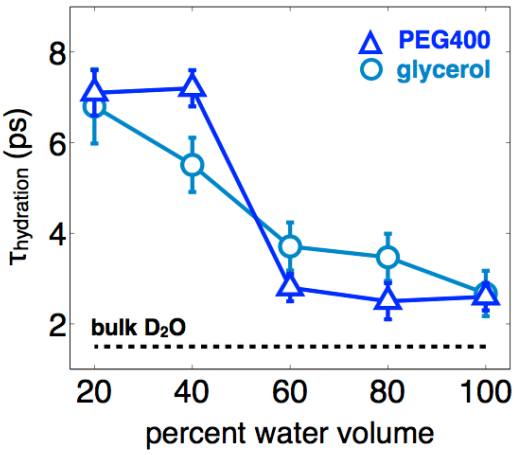

Figure 6.10 Comparison of interfacial water dynamics of HEWL-RC in solutions of glycerol and PEG400. While the magnitude of slowdown induced by each cosolvent is similar at high concentrations, the dynamic transition is observed only in the macromolecular crowding agent.

structures, thus there is only a weak coupling of the protein-hydration dynamics to PEG400 concentration in the low limit. At sufficiently high concentrations, however, the hydration environments are forced to overlap and cooperative hydration is induced. The overlapping of the effective hydration environments, which is the amount of hydration water that is dynamically distinct from bulk water, leads to the sudden slowing of the protein-hydration dynamics (**Figure 6.9**).

While the structure of PEG400 in water at low concentrations is thought to collapse into a compact structure,[45-48] it is unclear what structure is adopted at higher concentrations. Due to the complications of applying scattering techniques to concentrated solutions there is little literature regarding the structure and topology of PEG400 in water at concentrations upwards to 80% PEG by volume. Given the uncertainty in the structure of PEG400 in

concentrated solutions it is not clear how to estimate the distances at which the transition occurs. In addition, it is possible that a structural change of the polymer is the cause of the observed transition, however, complimentary results of lysozyme self-crowding suggests that this transition is a general property of crowding (**see Section 6.4**).

6.4 Self-Crowding

The spectral dynamics of HEWL-RC were systematically studied in concentrated solutions of lysozyme (HuLys used as a crowder). A solution of 1 mg/mL of HEWL-RC in D_2O was used as the initial solution, then HuLys was added up to 160 mg/mL to act as a macromolecular crowding agent. Again, no sign of protein dehydration was observed through the vibrational lifetime (**Figure 6.11**), suggesting that the solution remains isotropic with no aggregate of lysozyme at elevated concentrations. The FFCFs again show evidence for a dynamic transition upon macromolecular crowding, with the transition occurring around 80-100 mg/mL of crowding agent. At this concentration the hydration water slows by a factor of nearly 8, with the protein dynamics staying strongly coupled to the hydration water fluctuations (**Figure 6.12**).

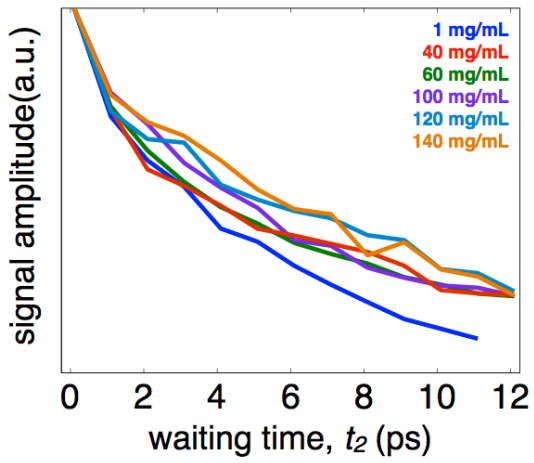

Figure 6.11 Vibrational lifetimes of HEWL-RC in ranging concentrations of HuLys.

The well-defined structure of lysozyme allows us to estimate the protein-protein distance assuming an isotropic mixture. By doing so, we estimate that the dynamical transition occurs when the proteins are forced within 30-40 Å of their nearest neighbor, suggesting a 15-20 Å

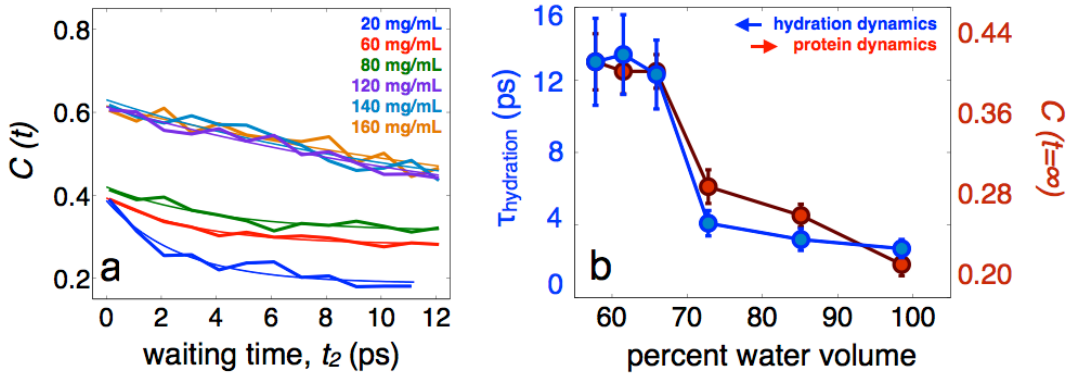

Figure 6.12 (a) FFCFs for HEWL-RC in self-crowding conditions, ranging from 1 mg/mL to 160 mg/mL. (b) Hydration timescale, obtained by the initial decay of the correlation function, and the protein dynamics, estimated by the static offset of the correlation function, plotted as a function of solvent composition. A strong coupling is clear from the data, with both the hydration and protein dynamics slowing down as glycerol is added to the system. An apparent dynamic transition occurs around 60% water, where there is an abrupt slowing in both the hydration and protein dynamics.

dynamical hydration shell around each protein (**Figure 6.13**). Such an extended hydration environment is both surprising and noteworthy. Work using THz absorption spectroscopy has suggested an extended hydration shell of proteins,[7] but the systematic results presented here are the clearest demonstration of extended, cooperative hydration of proteins in crowded environments. Indeed, the distance over which the hydration water is influenced by the protein roughly estimates the size of the protein.

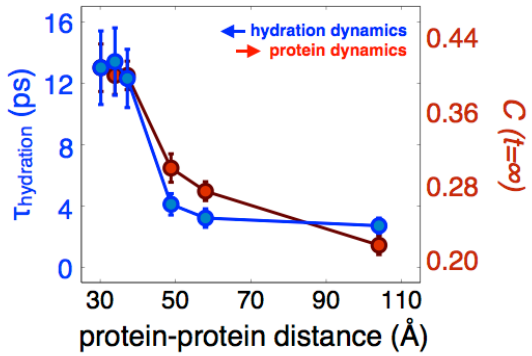

Figure 6.13 The self-crowding data can be used to estimate the protein-protein distance at which collective hydration is induced .Assuming a spherical shape for proteins and an isotropic mixture the concentration at which this transition occurs coincides with a protein-protein distance of roughly 30-40 Å, suggesting that each protein can modulate the surrounding waters up to 15-20 Å away from the protein surface.

The observed results that the hydration water around proteins is only modestly constrained by the presence of the protein (retardation factor of 2), together with the experimental result that the dynamical hydration layer is extended, highlights the remarkable cooperativity seen in the hydrogen bonding of water. Indeed, cooperative hydration has been observed in the hydration of cations and anions in concentrated salt solutions. The results presented here further demonstrates the high level of connectivity and cooperation in water, and provides a physical interpretation of what "crowded" systems are.

6.5 Simulations

MD simulations were performed to support the experiment results of a crowding induced percolation-like transition. Two simulations were carried out, one of which consisted of two proteins separated by a variable distance, the second consisted of four proteins arranged in a tetrahedral separated by a variable distance. In each case the hydrogen bond autocorrelation function was analyzed for bridging waters at each protein-protein distance. In both simulations evidence for a percolation-like transition of the water dynamics was observed. For the two protein simulation this transition occurred around 10-15 Å, while the four protein simulation shows a transition between 25-30 Å (**Figure 6.13**). The simulation results are consistent with experimental observations of an abrupt slowing of water dynamics upon crowding, but also suggest that the location of this transition (that is, the distance at which it occurs) is strongly dependent on the specific nature of the crowding and the number of crowding agents participating.

6.6 Conclusions

In the work presented in this chapter, we observe that the hydration dynamics around small hydrophobic metal-carbonyls reflects bulk-like dynamics, with spectral diffusion timescales measured to be around 1.5 ps. Furthermore, surface labeling of a protein reveals a modest slowdown of roughly a factor of 2 between bulk D_2O and hydrating D_2O, in quantitative agreement with predictions from MD simulations. The retardation is attributed to the collective solvation dynamics becoming slowed due to the hindering of hydrogen bond switching events by the extended hydrophobic surface of the protein. In addition, as

glycerol is added to modulate the hydration and protein dynamics, a 100-fold increase in bulk viscosity (0-80% glycerol) induces only a modest three-fold slowdown in the hydration dynamics. Accompanying the hydration retardation is a complimentary slowdown of the protein dynamics. The results demonstrate a weak coupling between the hydration water and the bulk solvent, but strong coupling between the protein and water dynamics.

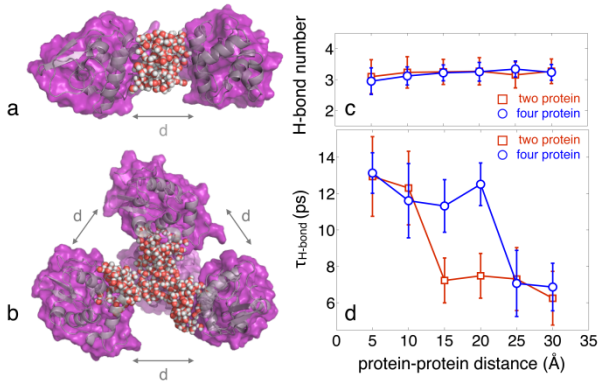

Figure 6.14 Example of the simulation analysis where (a) two proteins are separated by a set distance and the bridging water is selected for analysis and (b) four proteins arranged in a tetrahedral. (c)Hydrogen bond correlation times for water crowded by the proteins as a function of protein-protein distance. The occurrence of a dynamic transition is found between 10-15 Å for two proteins and 20-25 Å for the four protein simulation. The hydrogen bonding number does not undergo any observable transition, suggesting that the observed transition is purely dynamical.

The thermodynamic role of glycerol and other glassy solvents as stabilizing osmolytes originates from creating unfavorable protein backbone-solvent interactions, where the protein preferentially excludes glycerol and other kosmotropes from the protein surface. The dynamic consequence is a modest coupling of the protein dynamics to the bulk solvent mediated by the hydration water, which can act to constrain the space of conformational substates and prevent partial unfolding.[14] Limits imposed by the environment on protein motion can have significant implications on processes such as amyloid fibril formation, which often require partial protein denaturation to nucleate.

Determining factors that influence the structure and dynamics of biological catalysts, in particular the role that crowded, inhomogeneous and complex environments may play, is an active area of research. The development of experimental techniques that provide time-resolved, site-specific information about the dynamics occurring at the surface of biomolecules will be crucial in elucidating the couplings and dynamics that may contribute to protein structure and function. In this initial work using a vibrational site label of a dilute enzyme in solution, we have found that a region at the interface of two helical domains of HEWL is susceptible to solvent slaving, and that the hydration water is also slaved to the bulk solution. Since our earlier study of site-specific hydration revealed that hydration water

dynamics is itself heterogeneous, here, with only a single site we are able to propose that solvent-protein coupling is also heterogeneous. The combination of surface labeling and 2DIR spectroscopy, augmented by site-directed mutagenesis, will allow for a detailed mapping of protein-water interfacial dynamics, including a quantitative analysis of the susceptibility of different regions of the protein to solvent fluctuations and slaving. Because this methodology requires mutations to native proteins structural analysis will be required to characterize any possible structural changes induced by the mutagenesis and labeling procedures. The sensitivity of vibrational chromophores to solvent environments, in particular aqueous environments, makes this approach well suited for describing protein-protein interfaces crucial for protein recognition as well as protein-water-protein encounters central to aggregation and protein-water-lipid assemblies fundamental to membrane association.

Studying the coupled protein-hydration dynamics in crowded environments furthered our understanding of hydrophobic hydration, and gave a physical picture to what it means for a system to be "crowded." Using a macromolecular polymer (PEG400) as a crowding agent we observe a sharp transition around a solvent composition of 40% water and 60% PEG by volume, where the hydration dynamics timescale more than tripled from a 60-40% water volume, while being fairly uncoupled before and after the transition. This result is in contrast to the glycerol results, which showed a gradual slowdown of the protein-hydration dynamics as a function of solvent composition. Likewise, a transition is observed in the self-crowding experiments, where the hydration dynamics slow by a factor of seven from 60 to 100 mg/mL of protein. In both crowding environments (polymer and protein) the coupling between the hydration dynamics and the protein dynamics remains robust.

The occurrence of a crowding induced transition is attributed to extended hydration shells around the hydrophobic macromolecules. The cooperative nature of hydrogen bonding in water allows structural and dynamical perturbations to be carried over extensive distances, and allows for a percolation type transition to occur during collective hydration. Using the well-defined shape of lysozyme and assuming an isotropic mixture, we can estimate that the transition occurs when there is only 30-40 Å of water between neighboring

proteins, suggesting a hydration shell upwards of 15-20 Å. An extended hydration shell, where "hydration water" is dynamically distinct from bulk water for up to 15-20 Å, is remarkable considering the magnitude of dynamic constraining measured around lysozyme (retardation factor of 2). The transmitting of such a modest constraining across many solvation shells highlights the connectivity and cooperativity in hydrogen bond dynamics, where small dynamic perturbations can influence an extended region of water.

The dynamical aspects of macromolecular crowding are not often considered, though we present results here that suggest a significant slowing in the protein-hydration dynamics upon crowding. In general, the influence of crowding on protein structure and function are considered in terms of energetics, where hard-core repulsive interactions result in entropic contributions through an excluded volume effect, and weak attractive forces result in enthalpic contributions.[11,13] While the majority of work has focused on energetics, we suggest that there is a significant dynamical contribution to crowding.

References:

(1) Minton, A. P.: The Effect of Volume Occupancy Upon the Thermodynamic Activity of Proteins - Some Biochemical Consequences. *Molecular and Cellular Biochemistry* 1983, *55*, 119-140.

(2) Minton, A. P.: The influence of macromolecular crowding and macromolecular confinement on biochemical reactions in physiological media. *Journal of Biological Chemistry* 2001, *276*, 10577-10580.

(3) Minton, A. P.: Models for excluded volume interaction between an unfolded protein and rigid macromolecular cosolutes: Macromolecular crowding and protein stability revisited. *Biophysical Journal* 2005, *88*, 971-985.

(4) Cheung, M. S.; Klimov, D.; Thirumalai, D.: Molecular crowding enhances native state stability and refolding rates of globular proteins. *Proceedings of the National Academy of Sciences of the United States of America* 2005, *102*, 4753-4758.

(5) Minton, A. P.: How can biochemical reactions within cells differ from those in test tubes? *Journal of Cell Science* 2006, *119*, 2863-2869.

(6) Minton, A. P.: Influence of macromolecular crowding upon the stability and state of association of proteins: Predictions and observations. *Journal of Pharmaceutical Sciences* 2005, *94*, 1668-1675.

(7) Ebbinghaus, S.; Kim, S. J.; Heyden, M.; Yu, X.; Heugen, U.; Gruebele, M.; Leitner, D. M.; Havenith, M.: An extended dynamical hydration shell around proteins. *Proceedings of the National Academy of Sciences of the United States of America* 2007, *104*, 20749-20752.

(8) Goins, A. B.; Sanabria, H.; Waxham, M. N.: Macromolecular Crowding and Size Effects on Probe Microviscosity. *Biophysical Journal* 2008, *95*, 5362-5373.

(9) Homouz, D.; Perham, M.; Samiotakis, A.; Cheung, M. S.; Wittung-Stafshede, P.: Crowded, cell-like environment induces shape changes in aspherical protein. *Proceedings of the National Academy of Sciences of the United States of America* 2008, *105*, 11754-11759.

(10) Dhar, A.; Samiotakis, A.; Ebbinghaus, S.; Nienhaus, L.; Homouz, D.; Gruebele, M.; Cheung, M. S.: Structure, function, and folding of phosphoglycerate kinase are strongly perturbed by macromolecular crowding. *Proceedings of the National Academy of Sciences of the United States of America* 2010, *107*, 17586-17591.

(11) Wang, Y.; Sarkar, M.; Smith, A. E.; Krois, A. S.; Pielak, G. J.: Macromolecular Crowding and Protein Stability. *Journal of the American Chemical Society* 2012, *134*, 16614-16618.

(12) Rivas, G.; Ferrone, F.; Herzfeld, J.: Life in a crowded world. Workshop on the Biological Implications of Macromolecular Crowding. *EMBO Reports* 2004, *5*, 23-27.

(13) McGuffee, S. R.; Elcock, A. H.: Diffusion, Crowding & Protein Stability in a Dynamic Molecular Model of the Bacterial Cytoplasm. *Plos Computational Biology* 2010, *6*.

(14) Tsai, A. M.; Neumann, D. A.; Bell, L. N.: Molecular dynamics of solid-state lysozyme as affected by glycerol and water: A neutron scattering study. *Biophysical Journal* 2000, *79*, 2728-2732.

(15) Sinibaldi, R.; Ortore, M. G.; Spinozzi, F.; Carsughi, F.; Frielinghaus, H.; Cinelli, S.; Onori, G.; Mariani, P.: Preferential hydration of lysozyme in water/glycerol mixtures: A small-angle neutron scattering study. *Journal of Chemical Physics* 2007, *126*.

(16) Vagenende, V.; Yap, M. G. S.; Trout, B. L.: Mechanisms of Protein Stabilization and Prevention of Protein Aggregation by Glycerol. *Biochemistry* 2009, *48*, 11084-11096.

(17) Gekko, K.; Timasheff, S. N.: Mechanism of Protein Stabalization Stabilization by Glycerol - Preferential Hydration in Gylcerol-Water Mixtures. *Biochemistry* 1981, *20*, 4667-4676.

(18) Spinozzi, F.; Ortore, M. G.; Sinibaldi, R.; Mariani, P.; Esposito, A.; Cinelli, S.; Onori, G.: Microcalorimetric study of thermal unfolding of lysozyme in water/glycerol mixtures: An analysis by solvent exchange model. *Journal of Chemical Physics* 2008, *129*.

(19) Kwak, K.; Park, S.; Finkelstein, I. J.; Fayer, M. D.: Frequency-frequency correlation functions and apodization in two-dimensional infrared vibrational echo spectroscopy: A new approach. *Journal of Chemical Physics* 2007, *127*.

(20) King, J. T.; Arthur, E. J.; Brooks, C. L. I.; Kubarych, K. J.: Site-specific hydration dynamics of globular proteins and the role of constrained water in solvent exchange with amphiphilic cosolvents. *Journal of Physical Chemistry B* 2012, *116*, 5604-5611.

(21) King, J. T.; Ross, M. R.; Kubarych, K. J.: Water-Assisted Vibrational Relaxation of a Metal Carbonyl Complex Studied with Ultrafast 2D-IR. *Journal of Physical Chemistry B* 2012, *116*, 3754-3759.

(22) Chung, J. K.; Thielges, M. C.; Fayer, M. D.: Dynamics of the folded and unfolded villin headpiece (HP35) measured with ultrafast 2D IR vibrational echo spectroscopy. *Proceedings of the National Academy of Sciences of the United States of America* 2011, *108*, 3578-3583.

(23) Ghosh, A.; Qiu, J.; DeGrado, W. F.; Hochstrasser, R. M.: Tidal surge in the M2 proton channel, sensed by 2D IR spectroscopy. *Proceedings of the National Academy of Sciences of the United States of America* 2011, *108*, 6115-6120.

(24) Bandaria, J. N.; Dutta, S.; Nydegger, M. W.; Rock, W.; Kohen, A.; Cheatum, C. M.: Characterizing the dynamics of functionally relevant complexes of formate dehydrogenase. *Proceedings of the National Academy of Sciences of the United States of America* 2010, *107*, 17974-17979.

(25) King, J. T.; Baiz, C. R.; Kubarych, K. J.: Solvent-Dependent Spectral Diffusion in a Hydrogen Bonded "Vibrational Aggregate". *Journal of Physical Chemistry A* 2010, *114*, 10590-10604.

(26) Lee, M.; Bain, A. J.; McCarthy, P. J.; Han, C. H.; Haseltine, J. N.; Smith, A. B.; Hochstrasser, R. M.: Picosecond Photoisomerization and Rotational Reorientation Dynamics in Solution. *Journal of Chemical Physics* 1986, *85*, 4341-4347.

(27) King, J. T.; Ross, M. R.; Kubarych, K. J.: Ultrafast alpha-Like Relaxation of a Fragile Glass-Forming Liquid Measured Using Two-Dimensional Infrared Spectroscopy. *Physical Review Letters* 2012, *108*, 7401-7401.

(28) Thielges, M. C.; Chung, J. K.; Fayer, M. D.: Protein Dynamics in Cytochrome P450 Molecular Recognition and Substrate Specificity Using 2D IR Vibrational Echo Spectroscopy. *Journal of the American Chemical Society* 2011, *133*, 3995-4004.

(29) Urbanek, D. C.; Vorobyev, D. Y.; Serrano, A. L.; Gai, F.; Hochstrasser, R. M.: The Two-Dimensional Vibrational Echo of a Nitrile Probe of the Villin HP35 Protein. *Journal of Physical Chemistry Letters* 2010, *1*, 3311-3315.

(30) Moorman, V. R.; Valentine, K. G.; Wand, A. J.: The dynamical response of hen egg white lysozyme to the binding of a carbohydrate ligand. *Protein Science* 2012, *21*, 1066-1073.

(31) Jarymowycz, V. A.; Stone, M. J.: Fast time scale dynamics of protein backbones: NMR relaxation methods, applications, and functional consequences. *Chemical Reviews* 2006, *106*, 1624-1671.

(32) Igumenova, T. I.; Frederick, K. K.; Wand, A. J.: Characterization of the fast dynamics of protein amino acid side chains using NMR relaxation in solution. *Chemical Reviews* 2006, *106*, 1672-1699.

(33) Garcia-Hernandez, E.; Zubillaga, R. A.; Chavelas-Adame, E. A.; Vazquez-Contreras, E.; Rojo-Dominguez, A.; Costas, M.: Structural energetics of protein-carbohydrate interactions: Insights derived from the study of lysozyme binding to its natural saccharide inhibitors. *Protein Science* 2003, *12*, 135-142.

(34) McCammon, J. A.; Gelin, B. R.; Karplus, M.; Wolynes, P. G.: HINGE-BENDING MODE IN LYSOZYME. *Nature* 1976, *262*, 325-326.

(35) Brooks, B.; Karplus, M.: Normal-Modes for Specific Motions of Macromolecules - Application to the Hinge-Bending Mode of Lysozyme. *Proceedings of the National Academy of Sciences of the United States of America* 1985, *82*, 4995-4999.

(36) Tirion, M. M.: Large amplitude elastic motions in proteins from a single-parameter, atomic analysis. *Physical Review Letters* 1996, *77*, 1905-1908.

(37) Austin, R. H.; Beeson, K. W.; Eisenstein, L.; Frauenfelder, H.; Gunsalus, I. C.: Dynamics of Ligand-Binding to Myoglobin. *Biochemistry* 1975, *14*, 5355-5373.

(38) Ansari, A.; Jones, C. M.; Henry, E. R.; Hofrichter, J.; Eaton, W. A.: The Role of Solvent Viscosity in the Dynamics of Protein Conformational-Changes. *Science* 1992, *256*, 1796-1798.

(39) Rector, K. D.; Jiang, J. W.; Berg, M. A.; Fayer, M. D.: Effects of solvent viscosity on protein dynamics: Infrared vibrational echo experiments and theory. *Journal of Physical Chemistry B* 2001, *105*, 1081-1092.

(40) Finkelstein, I. J.; Massari, A. M.; Fayer, M. D.: Viscosity-dependent protein dynamics. *Biophysical Journal* 2007, *92*, 3652-3662.

(41) Henzler-Wildman, K.; Kern, D.: Dynamic personalities of proteins. *Nature* 2007, *450*, 964-972.

(42) Atha, D. H.; Ingham, K. C.: Mechanism of Precipitation of Proteins by Polyethylene Glycols - Analysis in Terms of Excluded Volume. *Journal of Biological Chemistry* 1981, *256*, 2108-2117.

(43) Arakawa, T.; Timasheff, S. N.: Mechanism of Poly(Ethylene Glycol) Interaction with Proteins. *Biochemistry* 1985, *24*, 6756-6762.

(44) Kulkarni, A. M.; Chatterjee, A. P.; Schweizer, K. S.; Zukoski, C. F.: Effects of polyethylene glycol on protein interactions. *Journal of Chemical Physics* 2000, *113*, 9863-9873.

(45) Leneveu, D. M.; Rand, R. P.; Parsegian, V. A.: Measurement of Forces Between Lecithin Bilayers. *Nature* 1976, *259*, 601-603.

(46) Pochylski, M.; Aliotta, F.; Ponterio, R. C.; Saija, F.; Gapinski, J.: Some Evidence of Scaling Behavior in the Relaxation Dynamics of Aqueous Polymer Solutions. *Journal of Physical Chemistry B* 2010, *114*, 1614-1620.

(47) Chen, J.: Molecular recognition in terms of a dimensionless index. 2. Thermodynamic patterns of intermolecular interactions of PEG and its alcohol substrates. *Journal of Physical Chemistry B* 2008, *112*, 1706-1711.

(48) Xu, Q.; Mi, J.; Zhong, C.: Structure of poly(ethylene glycol)-water mixture studied by polymer reference interaction site model theory. *Journal of Chemical Physics* 2010, *133*.

Chapter 7

Conclusion

7.1 General Conclusions

The work presented in this thesis has followed two themes: **1.** exploring hydrogen bonding dynamics in bulk water, room temperature alcohols and the heterogeneous environments found in fragile glasses. (**Chapters 2-4**) **2.** studying the hydrogen bond dynamics associated with hydrophobic hydration, including small hydrophobes, isolated proteins and crowded proteins (**Chapters 5,6**). Ultrafast infrared spectroscopy has been an extremely valuable tool for studying the hydrogen bond dynamics of water in many environments, including of course bulk water.[1-4] Due to experimental complications, however, it has proven difficult to come to a unified picture of hydration dynamics of small molecules,[5-9] as well as biological molecules, such as proteins[9-12] and DNA,[13] by studying the –OH stretch of water directly.

The work provides a comprehensive picture of using strong IR vibrational probes (metal carbonyls) to probe hydrogen bonding dynamics. We first demonstrate that the use of vibrational probes is capable of preserving and reporting on the equilibrium hydrogen bonding dynamics in both alcohols and water. We observed a strong correlation between spectral diffusion time and solvent viscosity, which is a relationship well understood for rotational and translational motion through the

Stokes-Einstein equation, though no such theory is currently available to predict spectral diffusion timescales. While in the low viscosity range there is a strong correlation between spectral dynamics and viscosity, in fragile glass forming liquids the dependence can become more complicated. Using 1,2-hexanediol, we first characterized dynamic heterogeneity, observed through non-exponential relaxation of the FFCF, and super-Arrhenius behavior when the liquid is in the supercooled state. The work raises questions about super-Arrhenius behavior of fast, local fluctuations when there is a high degree of connectivity, and thus the possibility of cooperative fluctuations.

We also develop a novel approach to studying hydrophobic hydration, which is a field plagued with inconsistent experimental results. While many ultrafast studies have relied on studying the -OH stretch of water in solutions of hydrophobic molecules, this approach is inadequate for studying hydrophobic hydration of isolated hydrophobes and provides only a "crowded" view of hydration.[5-8,13] The previous results using this method have largely reported on the hydration of concentrated solutions of small hydrophobes, where cooperative effects can give misleading results regarding dynamics around isolated hydrophobes.

With this approach we were able to first demonstrate that water surrounding small hydrophobic molecules (small being molecules with diameter < 1 nm) is not constrained to any measurable degree, but instead demonstrates bulk-like dynamics.[9] This result is in agreement with MD simulations,[14] but starkly contrasts most experiments that rely on concentrated solutions and suggest retardation factors of up to an order of magnitude.[5,7,8] Our approach supplies a view of hydrophobic hydration that is free from crowding effects and truly represents an isolated scenario.

We then extended this approach to the hydration environments of proteins through the use of metal-carbonyl surface labels, which we found to be sensitive to both the hydration water dynamics as well as the protein dynamics. The strong transitions allowed the proteins to be studied at concentrations on the order of 1 mg/mL, which assures that the proteins are isolated with excess water between

structures. Leveraging vibrational lifetimes we were able to observe heterogeneous hydration that correlated with protein structure, where flat structured regions of the protein lead to constrained hydration dynamics, while loose flexible regions of the protein lead to bulk-like hydration. Additionally, the magnitude of the slowdown of hydration water around the hydrophobic protein surface was measured to be roughly a factor of 2, which agrees quantitatively with molecular dynamics simulations.[15]

The observation of the modest slowdown around isolated proteins provided an excellent picture of nature hydrophobic interfaces perturbing the dynamics of neighboring waters, but it also provided a starting point for studying how the hydration dynamics can be further enhanced in more complex environments. Using a series of additives, including 2,2,2-trifluoroehtanol (TFE), glycerol, PEG400 as well as excess lysozyme, we observed the dynamics of the interfacial water as the bulk solvent became more complex. Using TFE, a commonly used protein denaturant, we were able to observe site-specific protein dehydration at regions of the protein rich in α-helices. This set of experiments also showed unambiguously that TFE interacts with proteins through a direct interaction that includes protein dehydration.

Glycerol, PEG400 and excess lysozyme were used as small and large crowding agents, to study the protein dynamics and interfacial water dynamics in cell-like environments. Using these crowding agents we can explore the dependence on the macromolecular nature of the crowding agent, as well as the relative importance of chemical differences between crowding agents. In the glycerol experiments, we observed a monotonic slowing in the protein and hydration dynamics, as well as a strong coupling between protein flexibility and hydration water. We observed fundamentally different results in the case of PEG400, a polymeric analogue of glycerol. In the case of a macromolecular crowding agent, a distinct dynamic transition occurs that is attributed to independent to collective hydration. This leads to an abrupt slowing in the hydration dynamics, as well as the low-frequency fluctuations of the protein. Similar behavior was seen when the system was crowded with excess lysozyme, suggesting that the chemical nature of the crowding agent is

less influential than the macromolecular nature. The dynamic transition was found to occur at protein-protein distances of 30-40 Å, suggesting extended hydration of macrostructures over extended distances. The collective hydration water was measured to be significantly slower than bulk water (factor of 5 slower for PEG400, factor of 10 for lysozyme crowding).

From this work we were able to present a coherent, unified picture of hydration dynamics around hydrophobes of different sizes, as well as a picture of collective hydration of macromolecular structures over extended lengths. Such experimental data is crucial to gain an understanding of the role of water in biology, and the properties of water inside of cells where it is likely that very little bulk-like water exists.

7.2 Future Outlooks

The work presented here provides a strong foundation for future studies that will push the developed methodology to study protein-hydration dynamics in cellular like environments, upon the binding of substrates, and the role of surface slaving in modulating active site dynamics. Efforts will be put into mapping protein slaving through surface and active site labeling, focusing on the magnitude of coupling at the protein-water interface and within the active site. Because many binding locations and active sites are located on the surface of the protein (as is the case with lysozyme), the demonstration of protein slaving at the surface can certainly strongly influence the catalytic performance. The role of protein slaving in the catalytic performance of proteins is an open field that this methodology provides an excellent opportunity to explore.

To further explore crowding effects on protein-hydration dynamics, experiments using crowding agents that more accurately represent the interior of cells should be performed. NMR experiments, for instance, have studied protein dynamics in *E. coli* lystate, which provides an excellent proxy for cellular environments.[16] Through the use of careful protein labeling and cell-injection, it may

be possible to perform ultrafast vibrational spectroscopy studies of proteins in living, functioning cells, much like what has been done with NMR spectroscopy.[17-20]

Focusing on equilibrium dynamics we were able to characterize and interpret dynamic observables available in 2D IR spectroscopy (lifetimes, IVR, spectral diffusion), which can now be extended to nonequilibrium protein dynamics. Many spectroscopic techniques, including 2D IR[21-23] and time-resolved FRET,[24,25] use high power non-resonant laser pulses to jump the temperature of a sample and to trigger thermal unfolding of proteins. The refolding process can then be monitored using various forms of spectroscopy. The current temperature jump 2D IR experiments rely on analyzing congested 2D spectra of the amide region of the vibrational spectrum. Secondary structures and couplings are then extracted from the position of diagonal and off-diagonal peaks. By coupling temperature jumps with the work presented above it would be possible to map not only the presence/exclusion of water during the folding process, but also the evolution of protein-hydration dynamics as the protein folds into a compact state. Such experiments could provide unparalleled information regarding the role of the hydrophobic effect in driving protein folding.

References:

(1) Eaves, J. D.; Loparo, J. J.; Fecko, C. J.; Roberts, S. T.; Tokmakoff, A.; Geissler, P. L.: Hydrogen bonds in liquid water are broken only fleetingly. *Proceedings of the National Academy of Sciences of the United States of America* **2005**, *102*, 13019-13022.

(2) Fecko, C. J.; Loparo, J. J.; Roberts, S. T.; Tokmakoff, A.: Local hydrogen bonding dynamics and collective reorganization in water: Ultrafast infrared spectroscopy of HOD/D2O. *Journal of Chemical Physics* **2005**, *122*.

(3) Loparo, J. J.; Roberts, S. T.; Tokmakoff, A.: Multidimensional infrared spectroscopy of water. II. Hydrogen bond switching dynamics. *Journal of Chemical Physics* **2006**, *125*.

(4) Nicodemus, R. A.; Ramasesha, K.; Roberts, S. T.; Tokmakoff, A.: Hydrogen Bond Rearrangements in Water Probed with Temperature-Dependent 2D IR. *Journal of Physical Chemistry Letters* **2010**, *1*, 1068-1072.

(5) Rezus, Y. L. A.; Bakker, H. J.: Observation of immobilized water molecules around hydrophobic groups. *Physical Review Letters* **2007**, *99*.

(6) Park, S.; Fayer, M. D.: Hydrogen bond dynamics in aqueous NaBr solutions. *Proceedings of the National Academy of Sciences of the United States of America* **2007**, *104*, 16731-16738.

(7) Bakulin, A. A.; Liang, C.; Jansen, T. L. C.; Wiersma, D. A.; Bakker, H. J.; Pshenichnikov, M. S.: Hydrophobic Solvation: A 2D IR Spectroscopic Inquest. *Accounts of Chemical Research* **2009**, *42*, 1229-1238.

(8) Bakulin, A. A.; Pshenichnikov, M. S.; Bakker, H. J.; Petersen, C.: Hydrophobic Molecules Slow Down the Hydrogen-Bond Dynamics of Water. *Journal of Physical Chemistry A* **2011**, *115*, 1821-1829.

(9) King, J. T.; Kubarych, K. J.: Site-Specific Coupling of Hydration Water and Protein Flexibility Studied in Solution with Ultrafast 2D-IR Spectroscopy. *Journal of the American Chemical Society* **2012**, *134*, 18705-12.

(10) Ghosh, A.; Hochstrasser, R. M.: A peptide's perspective of water dynamics. *Chemical Physics* **2011**, *390*, 1-13.

(11) Tucker, M. J.; Gai, X. S.; Fenlon, E. E.; Brewer, S. H.; Hochstrasser, R. M.: 2D IR photon echo of azido-probes for biomolecular dynamics. *Physical Chemistry Chemical Physics* **2011**, *13*, 2237-2241.

(12) King, J. T.; Arthur, E. J.; Brooks, C. L. I.; Kubarych, K. J.: Site-specific hydration dynamics of globular proteins and the role of constrained water in solvent exchange with amphiphilic cosolvents. *Journal of Physical Chemistry B* **2012**, *116*, 5604-5611.

(13) Yang, M.; Szyc, L.; Elsaesser, T.: Decelerated Water Dynamics and Vibrational Couplings of Hydrated DNA Mapped by Two-Dimensional Infrared Spectroscopy. *Journal of Physical Chemistry B* **2011**, *115*, 13093-13100.

(14) Laage, D.; Stirnemann, G.; Hynes, J. T.: Why Water Reorientation Slows without Iceberg Formation around Hydrophobic Solutes. *Journal of Physical Chemistry B* **2009**, *113*, 2428-2435.

(15) Sterpone, F.; Stirnemann, G.; Laage, D.: Magnitude and Molecular Origin of Water Slowdown Next to a Protein. *Journal of the American Chemical Society* **2012**, *134*, 4116-4119.

(16) Latham, M. P.; Kay, L. E.: Is Buffer a Good Proxy for a Crowded Cell-Like Environment? A Comparative NMR Study of Calmodulin Side-Chain Dynamics in Buffer and E. coli Lysate. *Plos One* **2012**, *7*.

(17) Serber, Z.; Keatinge-Clay, A. T.; Ledwidge, R.; Kelly, A. E.; Miller, S. M.; Dotsch, V.: High-resolution macromolecular NMR spectroscopy inside living cells. *Journal of the American Chemical Society* **2001**, *123*, 2446-2447.

(18) Serber, Z.; Selenko, P.; Haensel, R.; Reckel, S.; Loehr, F.; Ferrell, J. E., Jr.; Wagner, G.; Doetsch, V.: Investigating macromolecules inside cultured and injected cells by in-cell NMR spectroscopy. *Nature Protocols* **2006**, *1*, 2701-2709.

(19) Inomata, K.; Ohno, A.; Tochio, H.; Isogai, S.; Tenno, T.; Nakase, I.; Takeuchi, T.; Futaki, S.; Ito, Y.; Hiroaki, H.; Shirakawa, M.: High-resolution multi-dimensional NMR spectroscopy of proteins in human cells. *Nature* **2009**, *458*, 106-U11.

(20) Ikeya, T.; Sasaki, A.; Sakakibara, D.; Shigemitsu, Y.; Hamatsu, J.; Hanashima, T.; Mishima, M.; Yoshimasu, M.; Hayashi, N.; Mikawa, T.; Nietlispach, D.; Waelchli, M.; Smith, B. O.; Shirakawa, M.; Guentert, P.; Ito, Y.: NMR protein structure determination in living E. coli cells using nonlinear sampling. *Nature Protocols* **2010**, *5*, 1051-1060.

(21) Smith, A. W.; Lessing, J.; Ganim, Z.; Peng, C. S.; Tokmakoff, A.; Roy, S.; Jansen, T. L. C.; Knoester, J.: Melting of a beta-Hairpin Peptide Using Isotope-Edited 2D IR Spectroscopy and Simulations. *Journal of Physical Chemistry B* **2010**, *114*, 10913-10924.

(22) Jones, K. C.; Ganim, Z.; Peng, C. S.; Tokmakoff, A.: Transient two-dimensional spectroscopy with linear absorption corrections applied to temperature-jump two-dimensional infrared. *Journal of the Optical Society of America B-Optical Physics* **2012**, *29*, 118-129.

(23) Baiz, C.; Peng, C.; Reppert, M.; Jones, K.; Tokmakoff, A.: Investigating protein structure and folding with temperature-jump multidimensional infrared spectroscopy. *Protein Science* **2012**, *21*, 90-91.

(24) Dhar, A.; Girdhar, K.; Singh, D.; Gelman, H.; Ebbinghaus, S.; Gruebele, M.: Protein Stability and Folding Kinetics in the Nucleus and Endoplasmic Reticulum of Eucaryotic Cells. *Biophysical Journal* **2011**, *101*, 421-430.

(25) Guo, M.; Xu, Y.; Gruebele, M.: Temperature dependence of protein folding kinetics in living cells. *Proceedings of the National Academy of Sciences of the United States of America* **2012**, *109*, 17863-17867.